TÉCNICO LISBOA

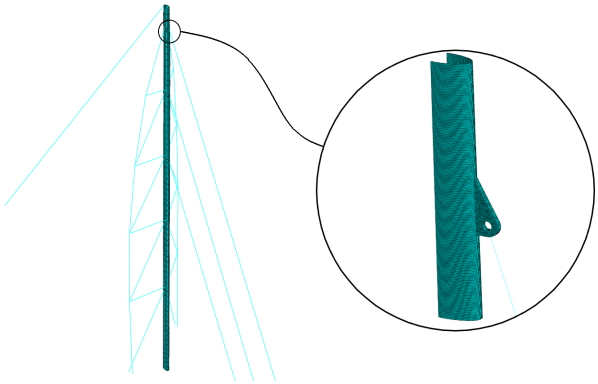

Numerical Structural Analysis of a Sailing Yacht Mast

Gabriel Alejandro Herrat Vieira

Thesis to obtain the Master of Science Degree in

Naval Architecture and Ocean Engineering

Supervisor(s): Prof. Yordan Ivanov Garbatov
Eng. Marco Nawijn

Examination Committee

Chairperson: Prof. Ângelo Manuel Palos Teixeira
Supervisor: Prof. Yordan Ivanov Garbatov
Member of the Committee: Prof. Baiqiao Chen

May 2022

Dedicado aos que estiveram presentes neste percurso académico
e aos os que contribuiram para as experiências que aqui me trouxeram.

Acknowledgments

Ao finalizar esta longa caminhada no Instituto Superior Técnico, cheia de aprendizagem e experiência, resta-me agredecer a todos os docentes pelos conhecimentos transmitidos. Um especial agradecimento ao Professor Yordan Garbatov pela sua compreensão e apoio na realização desta tese e ao Engenheiro Marco Nawijn pela sua disponibilidade e suporte.

Como bolseiro, quero transmitir o meu profundo agradecimento à família Soares dos Santos pelo apoio incondicional e por todas as oportunidades que me foram dadas ao longo deste percurso académico.

Finalmente, um obrigado a todos os meus amigos e familiares que de alguma forma contribuíram para tornar estes anos inesquecíveis.

Finalizing this learning journey at Instituto Superior Técnico, filled with knowledge acquired, I can only express my gratitude to my professors for the transmitted knowledge. A special acknowledgement to Professor Yordan Garbatov for his comprehension and support during the chapter of my dissertation, and to Engineer Marco Nawijn for the availability and support.

As a fellow from the scholarship funded by family Soares dos Santos, I want to transmit my profound gratitude for the unconditional support and the opportunities that were created for me during this academic journey.

Finally, an appreciation to all my friends and family that, in a certain way contributed to make these years unforgettable.

Resumo

Devido à complexidade de um mastro e ao seu sistema estrutural, o mesmo deve ser projetado com precisão para garantir a sua confiabilidade e alto desempenho. Seguindo esse raciocínio, esta investigação utiliza a técnica de Submodeling em Análises de Elementos Finitos, ao modelar o comportamento de um mastro de um veleiro produzido em fibra de carbono e os elementros estruturais que os complementam, acompanhado de um estudo local para analisar uma zona específica do mastro. Do ponto de vista técnico e como resultado da parametrização efetuada, concluiu-se que a utilização de camadas finas de fibra de carbono laminado no reforço estrutural pode ser benéfico para a distribuição de tensão obtida na zona próxima da conexão entre o mastro e o estai de proa. Como parte fundamental do projeto apresentado, o contributo teórico e prático fornecido pela empresa de mastreação de veleiros Rondal foi de uma importância vital.

A aplicação do método de análise estrutural desenvolvida nesta dissertação promove uma análise local que pode ser elaborada em diversas componentes críticas de um mastro, permitindo criar uma refinação na malha de elementos finitos na região de interesse para analisar localmente a distribuição de tensão e outras possíveis aplicações.

Adicionalmente, este método permite simular soluções diferentes de desenho de componentes como uma forma de otimização. A metodologia aplicada pode ser considerada de grande interesse para o processo de design presente na indústria de produção de mastros.

Palavras-chave: Mastro, Submodelação, FEM, Aparelho Fixo, Análise Estrutural

Abstract

Due to the complexity of the mast and its structural system, it must be designed with attention to guarantee structural integrity and high performance. To fulfill those criteria, this research makes use of the Sub modelling Technique in the Finite Element Method, analysing the behaviour of a sailing yacht mast made of carbon fibre and the structural elements that support it, along with a local strength approach, examining a specific region of the mast. From the technical point of view and as a result of the applied parametric study, it was concluded that the usage of thinner layers of stacked carbon fibre plies for the ply drop-off of the reinforcement patch can be beneficial for the stress distribution in the mast-forestay region. As a fundamental part of this project, the theoretical and engineering aid provided by the yacht spars company Rondal was of vital.

The structural analysis employed in this thesis promotes a detailed analysis that can be applied in several critical regions of the mast, allowing to create mesh refinement in the region of interest to analyse local strength.

Furthermore, this method enables simulating different design solutions for different structural components for optimisation. The methodology applied can be considered of great interest for the design process of the mast design industry.

Keywords: Mast, Submodeling, FEM, Rigging, Structural Analysis

Contents

List of Tables

List of Figures

Nomenclature

Greek symbols

ν	Poisson Ratio for isotropic material
ν_{12}	Poisson Ratio in axis 1 and 2
ν_{13}	Poisson Ratio in axis 1 and 3
ν_{23}	Poisson Ratio in axis 2 and 3

Subscripts

E	Elastic Modulus for isotropic material
E_{xx}	Elastic Modulus in *x* axis
E_{yy}	Elastic Modulus in *y* axis
E_{zz}	Elastic Modulus in *z* axis
G_{12}	Shear Modulus in axis 1 and 2
G_{13}	Shear Modulus in axis 1 and 3
G_{23}	Shear Modulus in axis 2 and 3
i, j, k	Computational indexes
dof	Degree of freedom

Chapter 1

Introduction

The objective of the dissertation is to create a structural analysis of a sailing yacht mast through the application of the Finite Element Method and, more precisely, the implementation of the sub modeling technique available in the commercial software Abaqus.

A sailing yacht mast and all structural components that support it, commonly called standing rigging, are constantly subjected to a complex load throughout their entire operational life. This structure can be simultaneously loaded throughout its lifetime, either by the aerodynamic loads generated by the wind while sailing, by the inertial loads as a consequence of the hull's motion in the water or by the load present on the rigging system caused by the standing rigging on the mast.

By employing the Finite Element Method in this type of analysis, several outcomes may be achieved depending on the analysis that is targeted. In this thesis, the sub modeling technique is explored firstly in the preliminary study cases to get a profound understanding of the subject and applied afterwards on a mast with 57 m in length allowing to perform a global strength analysis of the structure and a local analysis on a critical region that is normally subjected to stress concentration by the own operating nature of the rigging system. It is worth noticing the theoretical and practical contributions that were provided by ”Rondal” located in Vollenhove, Netherlands. This support was given by a professional expert in the field.

1.1 Motivation

Given the complexity that's inherent to the mast and its structural system, it must be precisely designed to ensure a reliable functioning of the principal mean of propulsion of sailing vessels. In addition, a good level of performance is many times desired by those passionate about sailing, making the design cycle of such structures a constant research to find an equilibrium between stiff and very resilient structural solutions and the optimization of components to reduce the weight as much as possible.

The application of numerical simulations in the design process becomes of extreme importance when an optimized structural solution is targeted, by employing of Finite Element Analysis (FEA) several types of structural analysis can be performed. Either at an initial stage of design to assess the global strength

with simplified models using beam elements, or to elaborate on more complex and detailed analysis in critical regions of the mast and its structural components.

Several studies related to the structural analysis of rigging systems implemented the Finite Element Method for different purposes. However, the most common implementation is by using beam elements with equivalent stiffness to assess the global strength and verify the compliance with the classification society requirements. More detailed analyses are not worth it for many manufacturers since it can be time consuming and empiricism plays a more present role in many stages of design.

1.2 Topic Overview

This dissertation aims to establish a productive methodology to perform accurate analyses of global and local models by using the sub modeling technique in FEA.

This type of approach allows defining a connection between global and local models, creating a rational way to apply a mesh refinement in the region of interest. From the engineering point of view, this method is functional to compare different design solutions for key components of the structure.

1.3 Objectives and Deliverables

Using the aforementioned technique as a mean of obtaining results for the structural analysis, the present research allowed to formulate as a global objective, the modelling of the behaviour of a sailing yacht mast and the structural elements that support it. Based on the global objective, the following specific objectives were planned: design the reinforcement of the connection between the mast and the forestay performing a parametric study, analyse the results obtained for the different design solutions and compare the implications of parameters that varied in the design.

1.4 Thesis Outline

The present thesis, includes five chapters structured to complement the subjects inherent to the research. The first chapter, contains the introduction where an overview is presented, a motivation for the research, an overview of the topic developed and the objectives of the dissertation.

In the second chapter, the theoretical and practical backgrounds are presented. Followed by that, chapter three is introduced, presenting study cases related to the sub modeling technique. Subsequently, the fourth chapter was formulated, composed of the structural analysis of a mast applying the sub modeling technique and presenting results and observations.

Finally, chapter five presents the general conclusions of the analysis, the achievements and recommendations for future work.

Chapter 2

Background

The present chapter contains the background and theoretical support that allowed to elaborate the thesis. Several topics are developed related to the engineering present in sailing yachts design and the methodology implemented for the structural analysis.

2.1 Sails and Rig System Interaction

When a sailing yacht is considered, it involves a complex system due to aerodynamic and hydrodynamic forces that constitute the equilibrium state and generate the propulsion of these vessels in different sailing conditions. Despite the complexity involved in this type of propulsion, it is possible to observe it as a simplified concept by considering that, under equilibrium conditions, the hull creates a resistance force when moving in the water that is balanced by the forces generated by the sails. These lifting surfaces can create enough lift to overcome the drag of the hull, nevertheless, the same force generated by the sails has a lateral component (perpendicular to the sails) that must be compensated by the righting moment of the hull. The righting moment is generated by the contributions of the hull and keel's weight, and the buoyancy when the yacht has a leeway heeling angle. This lateral force equilibrium also has the ability to reduce the sway motion of the yacht. Figures 2.1 and 2.2 represent graphically the elementary forces present in the hull and sails that generate propulsion in a sailing boat, with its respective components. It's also possible to observe in Figure 2.1 the apparent wind direction, which is the resultant wind direction accounting for the yacht speed.

It is worth noting that the explanation aforementioned is a simplification of the loading condition created in real sailing conditions, still, it is the most predominant. Forces and moments generated by other effects are being neglected at this stage such as inertial forces, wave induced loads, as well as internal forces inherent to the rigs and sails trim systems.

With regards to the rig system, it can be described as a structure composed by beams and cables that support the loads generated by the sails. The mast, as the principal vertical structural component, is subjected to axial, longitudinal and transverse loads therefore, it is balanced and supported by the shrouds and stays. In simultaneous, the spreaders can reduce the unsupported length of the mast and

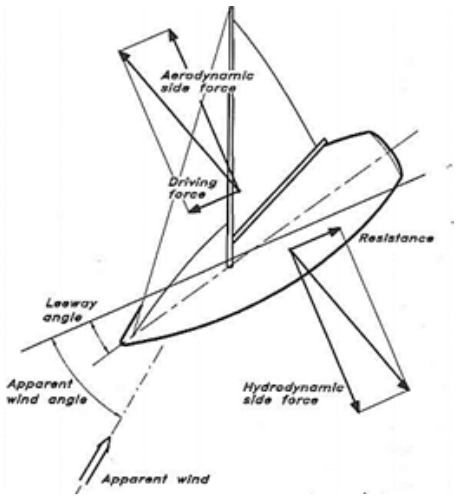

Figure 2.1: Elementary forces on a sailing yacht (upwind). [1]

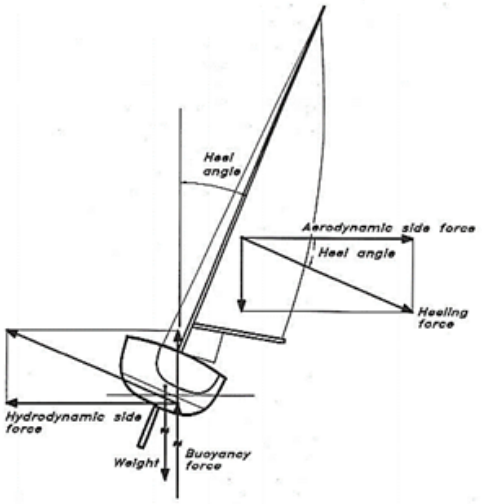

Figure 2.2: Transverse equilibrium of forces. [1]

increase its transverse stability. Added to that, there are the fore and back stays (or runners) which counteract the bending effect of spreaders and longitudinal deflection of the mast.

Different sailing conditions generate different loads that should be considered, nevertheless, upwind reaching and broaching situations are the ones considered to generate the biggest loads on the rig. Also, the loads of sail sheets and halyards must be taken into consideration, which is dependent on the tension applied on the leech and luff of the sails and have a considerable influence on the tension state of the mast. As the fluid-structure interaction problem that sail systems are, the acting loads are dependent on the structural deformation, making it complicated to analyse and simulate. With the technological innovations that had appear in sailing yacht design and construction, the rigging systems have also evolved, making the work of riggers and sail-makers more and more involved with high-tech in cooperation with skilled aerodynamicists and material scientists.

When it comes to strength stability, it has been observed that the limit states of rigging systems are mainly governed by the buckling phenomenon due to its slenderness. Despite that, ultimate strength, yielding and fatigue (e.g., in welded or bonded zones, turnbuckles, toggles, terminals and others) may also be considered. Since these structures are essential for sailing yachts and its performance, the assessment of structural ability to deform in a controllable way is crucial.

2.2 Rigging System

2.2.1 Mast

To describe a rigging system of a sailing yacht, several structural components may be considered, being the mast one of the principals. This slender piece must support high levels of stress and sustain the main sail and its tunning systems. In the case of large yachts, this component should be carefully thought out and produced, from a design perspective, since its weight can correspond to up to thirty per

cent of the total load that the rigs support in sailing conditions [2]. For that matter, masts tend to have a decreasing sectional area in the upper part, reducing the moment generated when the yacht sails with a heeling angle and making it more flexible which can be beneficial for sail tunning purposes.

Even though masts have an apparent similitude with a beam, these components behave in a more complex way and have several peculiarities such as holes, connections with other structural components and changes in the section geometry as well as mechanical properties. All these factors and their non-linear behaviour make the analysis of such structure more complex to achieve an optimized design.

Regarding the mechanical requirements, the mast must be able to support the compression induced by stays and shrouds as a consequence of rig tunning as well as the aerodynamic loads. Hence, for the mast not to break or permanently bend, it must have enough transverse and longitudinal stiffness, i.e. enough transverse and longitudinal moment of inertia. One factor that contributes for the resultant stiffness is the place in which the mast step is situated. By letting the mast go through the deck and be stepped on the keel, the required moment of inertia can be reduced by 35% [1].

Moreover, from the perspective of aerodynamics, the mast can interfere with the air flow near the leading edge of the main sail which can reduce its efficiency. Therefore, mast sections must have the cross-section area as reduced as possible, while still complying with the mechanical and stability requirements.

Keel Stepped Mast and Deck Stepped Mast

The mast can be either stepped on the deck or stepped on the keel and both of these alternatives can have its attributes and drawbacks.

In the case of the keel stepped mast, which is the better solution in terms of structural integrity, the mast is supported by the hull structure, normally on the longitudinal reinforcements near the hull centreline, resulting in a better distribution of the compressive loads applied on the mast which comes in great hands specially for large yachts.

Besides that, the passage of the mast through the deck creates an extra point of support, when compared to deck-stepped masts, which increases the mast stability and stiffens the whole structure since it adds a constraint at the deck height. For that purpose, the mast opening in the deck must be reinforced transversally and longitudinally to ensure a good support of the mast and deck integrity.

In addition, the keel stepped mast allows the usage of a hydraulic mast jack to apply the pretension on the rigging system. In general, this solution is preferable, since it can provide higher resistance for bending, compression and buckling.

As a drawback, in this type of mast stepping there is the space below the deck that is occupied by the mast. This might be a concern from the interiors design point of view, which can be important in some cases. Also, the deck opening, if not well sealed, can let water leak inside the hull.

Regarding deck stepped masts, these are normally positioned on a metal support and are well constrained through bolts to ensure a good attachment of the mast and a good distribution of compressive loads. Besides that, hull reinforcements should be allocated in that region such as a rigid bulkhead or a pillar. The absence of the mast below deck is one good aspect of deck-stepped masts since it implies

more space available to determine the cabin layout with less obstruction and can create a more spacious sensation for the interior's design.

From what was stated previously, it might seem obvious that the solution of a keel-stepped mast is still preferable, even though that deck-stepped masts eliminate the possibility of water entering inside the hull through the deck and signifies having more space below the deck.

In addition, one important goal of the standing rigging is sail trim, besides supporting the mast. From that perspective, deck-stepped masts tend to be more flexible and easier to bend, meaning that the mast is more easily adjustable to obtain optimum performance in diverse wind and sea conditions. For that reason, deck-stepped masts are preferable for racing yachts, where achieving the limits of the vessels is a goal to generate as much speed as possible from the wind.

For example, when the yacht is sailing upwind, the longitudinal rigs such as backstay, runners and check stay can be tensioned, bending the mast towards the aft and tensioning the forestay, giving the yacht more weather helm, i.e. more control and pointing ability with stronger wind. In opposition to that, when sailing downwind the longitudinal rigs are intentionally slackened, easing the forestay and giving the yacht more leeward helm. These technical adjustments are very important in a racing context where small adjustments can make the difference. With that said, it is understandable why deck stepped masts might be a good option for racing yachts.

In the case of the study developed for this dissertation, a keel-stepped mast is analysed. Since the mast under consideration belongs to a superyacht, the keel stepped solution is the most reliable for this type of vessel due to the height of the mast, ensuring more structural integrity and ease to tune.

Mast Pretension

Apart from the tension generated by sails, the application of pretension on a sailing yacht rig system has great relevance when it comes to structural stability and safety, also for racing performance reasons this is a subject of paramount importance. By increasing the stiffness of the rig system when applying tension, the structure is more prevented from large displacements, keeping the structure stable but also significantly improving the sails aerodynamic performance.

Despite that, it is quite complex to understand each rig system and how it should be tunned since each yacht is unique, principally when it comes to larger yachts. Most of the time, this is executed by an iterative process based on practical knowledge and Finite Element Simulations with the purpose of finding the right tension that should be applied in each rig and mast jack displacement.

That is one of the main causes of the lack of existence of specific dock tuning procedures and guidelines from the classification societies, since it is extremely difficult to define a procedure that can fit every kind of rig system due to its variation in size, materials, structural components and other factors. Consequently, each rig company end up having its methods that normally suit the best with their experience and the engineering solutions that each company develops. For that matter, the majority of that knowledge is not commonly found in the open literature, especially for large yachts.

2.2.2 Shrouds and Stays

As supportive structural elements, shrouds and stays from one perspective, allow a distribution of the stress applied on the mast, making the rig system stiffer and well supported. On the other hand, they also allow the application of the desired tension on the mast to achieve the desired mast curvature to obtain its best performance and ensure the safety of the structure, making these key components for the rig structure.

The rigs are attached to the mast at different heights, depending on the rigging system configuration and are fixed to the hull structure in reinforced points with chainplates. The shrouds and stays' tension are adjustable using turnbuckles, and in the case of large yachts, a mast jack is also used to push the mast step upwards, increasing the mast compression generated by the rigs. These structural components are pre-tensioned to avoid excessive deformations when the rig is under load, as mentioned previously, whilst permitting the structure to have slight flexibility for trimming purposes. The main principle of the pretension is that only when the structure is fully subjected to load, the leeward shrouds should just begin to slacken. In effect, in [3] it is provided, as a standard for rig scantlings, that the mast pretension must be performed to avoid slack in the leeward cap shrouds with an appropriate safety factor to avoid slack when sailing at angles equal to or lower than the Safety Working Angle, which is generally 30º.

It is noteworthy to state that stays and shrouds, due to their working nature, are designed specifically to support tension loads, thus these are made of materials with adequate properties for that purpose such as stainless steel beams or wire ropes and composite materials with predominant axial oriented fibres. Having that said, it is expected that stays and shrouds have much more tensile strength than compressive strength and can even be damaged if they are maintained with slack due to fatigue and repeated shocks.

Between these two main types of rigs, several nomenclatures that exist to specify each one of the variants, having as the main principle that every type of stay belongs to the longitudinal rigging and every type of shroud belongs to the transverse rigging. The following topics explain the different types of rigs that are commonly used.

Longitudinal Rigging

Constituted by different types of stays that interact with each other, the longitudinal rigging allows to control of the longitudinal bending of the mast for safety reasons and to optimize the yacht's performance by tunning it according to the sailing condition.

Forestay: Stay that carries the genoa and jib and the closest to the bow. It supports the top of the mast not to move aft and its tension is affected by the backstay, cap shrouds (in the case of a rig system with swept spreaders), runners and the mainsail sheet.

Cutter stay: Stay that carries the staysail and is attached lower than the forestay on the mast and aft to the forestay. Its tension normally can be adjusted by the backstay or runners.

Inner forestay: This stay, despite not being a sail-carrying stay, provides control on the mast deformation

at a mid-height in conjunction with the checkstays.

Baby stay: Attached near the height of the lower spreaders, this stay is intended to support the lower panel of the mast and controlling its bending.

Backstay: Sustains the top of the mast to prevent it to move forward. Normally this stay is adjustable, depending on the sailing condition, using a sheet tunning system or hydraulics. The tunning of this stay ends up affecting the bending of the mast and forestay tension.

Runners: Most commonly found on fractional rigs (rig system with forestay attached to the mast below the masthead) where they adjust the forestay tension. These rigs are connected laterally to the mast and are adjustable since the windward runner must be the one under tension and the leeward runner slack to not interfere with the boom and mainsail. Depending on their longitudinal attachment to the hull, these can affect both lateral and longitudinal rigging.

Check stays: As stated previously, these stays interact with the inner forestay to stabilise the mast bending at a mid-height, preventing uncontrolled bending.

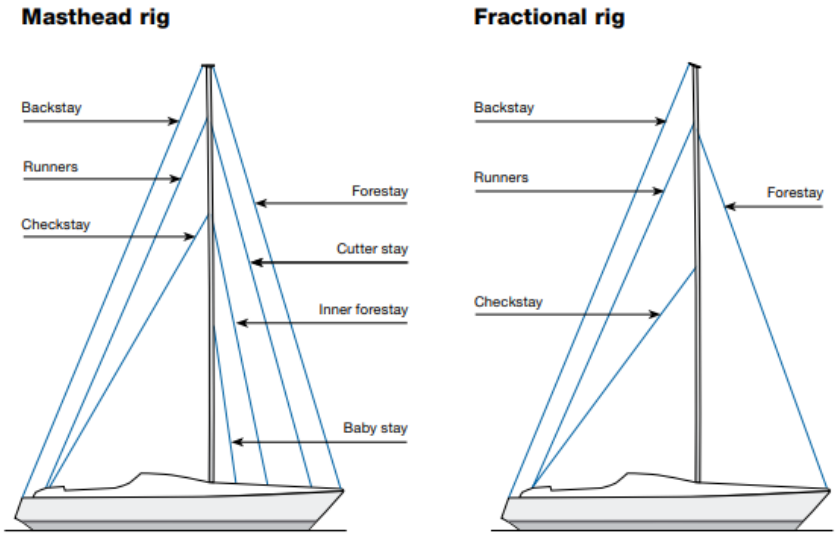

Figure 2.3: Different types of longitudinal rigs. [4]

Lateral Rigging

Cap shrouds: (V1-V3, D4 in Figure 2.4) These shrouds sustain the mast against athwartship loads. Normally attached to the mast near the masthead, connected with the spreaders and to the hull by chainplates.

Intermediate shrouds: (D2-D3 in Figure 2.4) Attached in the upper spreaders region of the mast and are normally fitted with links in the lower spreader tips. These shrouds support the free length of the mast between the upper spreaders and reduce athwartship deformation.

Lower shrouds: (D1F and D1A in Figure 2.4) Attached to the mast near the lower spreaders, the lower shrouds have the same function as the intermediate shrouds. Frequently these are fitted as fore and aft lower shrouds by adding a longitudinal inclination, which also stabilises the longitudinal deformation of the mast.

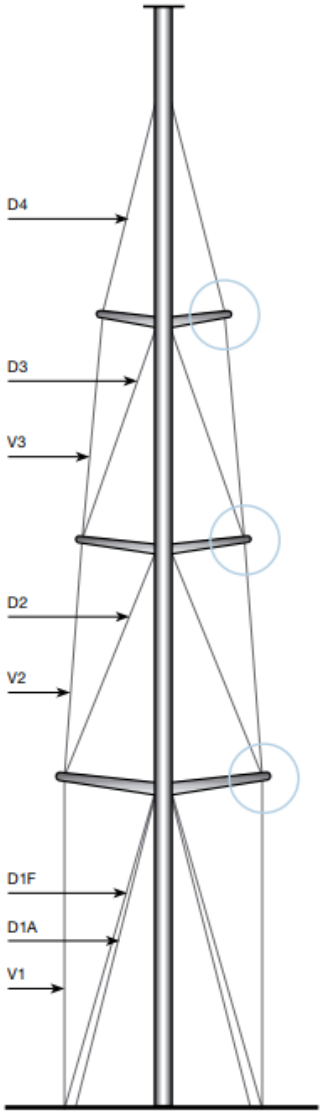

Figure 2.4: Lateral rigging of a three spreader mast. [4]

2.2.3 Spreaders

The spreaders have the important role of reducing the unsupported length of the mast and increasing its transverse stability along with the shrouds. They also are useful to obtain a longitudinal pre-bend of the mast, which is achieved by the aft swept spreaders (that creates a force pointing forward) together with the backstay, this configuration benefits the aerodynamical performance and balances the load generated by the sails.

These structural elements are mainly loaded by compression created by the shrouds and are normally fitted in the mast allowing the rotation around the y axis, as shown in Figure 2.5 to avoid having a bending moment acting on them, while the rotation around the z-axis is blocked to prevent the mast to change its curvature longitudinally. This effect can be provoked by strong pitch movements, which can create high buckling loads on the mast and put at risk the structure's safety.

As it is expected, the spreader's dimension and configuration relative to the mast have significant

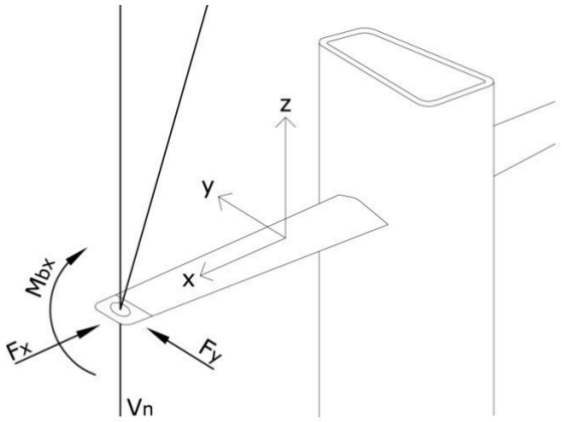

Figure 2.5: Shrouds and spreader connection with force and moment vector diagram. [5]

implications on its behaviour. By having spreaders higher in length, the leverage to support the transverse bending of the mast becomes higher, making the structure safer and permitting to have a mast with lower inertia, thus reducing its weight.

Another aspect to be considered in the spreader's design is the angle of sweep, which is commonly used due to its beneficial impact, as mentioned previously. By pushing the mast forward, the spreaders bring up another longitudinal support besides the stays. On the other hand, the resultant stress on the back face of the mast is increased by this effect, therefore the mast section should withstand this extra load.

2.3 State of the Art

Due to the complexity and peculiarity of the subject, a big share of masts and rigging systems design has been substantially based on empiric design criteria. Indeed, as mentioned in [6] large uncertainties still affect the design loads applied and most of them are empirical. Only high-level competitions such as the America's Cup and unique projects for large yachts can afford the computation time and cost involved in a profound investigation that a sailing system requires.

On the other hand, there is an analytical method that has prevailed through time which is the well-known Skene's method, based on the analysis of the transverse stability of the yacht. This method is based on the assumption of mast stability in compression, from which the mast cross-section characteristics can be calculated. With further studies developed on this subject this method has been approached by researchers to account for other effects such as distributed forces from sails, longitudinal forces applied on the mast by the stays and halyard forces.

Additionally, the implementation of numerical simulations for rigging systems in diverse contexts has become more frequent and convenient, remarking the importance and reliability of Finite Element Analysis implementation. Moreover, it has become a requirement in [3].

In literature [6], a study case focused on the structural design of mast and rigging of sailing yachts from a practical point of view, it is stated how the equilibrium of yachts is traditionally analysed in a quasi-

static state, considering that the aerodynamic forces equilibrate the vessel's righting moment. Therefore, aerodynamic forces are computed by assuming that these act as tensile on the rigs and various load distributions on the mast are considered. Furthermore, longitudinal loads on the mast relative to stays, halyards and sheets are empirically estimated and considered for the loading of the rigging system, revealing the importance of empiric knowledge to elaborate the load cases in different sailing conditions.

It is also worth mentioning that inertial forces due to ship motions are not explicitly considered in analytical procedures of design, which is a subject that has significant importance, principally in large sailing yachts. All the uncertainties around the determination of actions and their effect on the rig as well as their distribution make the designers work with high safety factors (around 3.0 compared with breaking loads). Furthermore, with yachts getting bigger and bigger, the inertial effect and weight become more significant.

It was underlined in [7] that despite the evolution of the aerodynamic and hydrodynamic fields thanks to prestigious investigations developed for international competitions, some problems remain with a question mark, such as the behaviour of rigging under wind gusts, the dynamic loading on the mast due to inertial loads caused by rough sea state and the pretension loads induced by the rig tunning. These topics cause, the beforementioned consequence of having to work with high safety factors which can lead to creating a very safe rig but not as optimized as desired for performance.

Moreover, in [8] can be found information regarding rig tunning procedures. It reviewed the application of pretension on a sailing yacht rig system, presenting a numerical validation while comparing with experimental results of the dock tunning of a 67 m mast. It was also demonstrated the importance of predicting the nonlinear behaviour of the structure with accuracy, emphasizing the fact that the sequence of the procedure taken to trim the mast has great relevance in its behaviour and evidencing practical tricks and drawbacks that can be useful for designers and sailmakers.

Regarding the implementation of nonlinear FE analysis in this work [8], it is shown that in this type of problem, the principle of superposition is not verified, meaning that the response of the system is not only dependent of the sum of the individual loads applied but also influences of the sequence of applications. Also, the existence of large displacements makes this type of problem impossible to be solved assuming a linear behaviour. In the specifications given for the FE analysis, considerations taken in terms of the element type, boundary conditions and load application were presented, and a numerical comparison was established for the different simulations that were performed, corroborating the initial idea of the study.

Furthermore, in [2], a work developed with the TU-Berlin University research sailing yacht called "Dyna", it was investigated the measurements taken from force transducers to compare with the results of a FE analysis.

Since the mast deformation has an important contribution to the performance of sailing yachts, predicting the loads and deformation of rigs is crucial for design purposes. Thus, the forces present in the rigs were measured with 20 separate force transducers in the mast, shrouds, stays and sheets. Besides that, a global FE model of the rig was created. The load cases considered in the computations were the dock pretension applied on the rig and sailing upwind with a 30º heel angle.

By introducing Finite Element Analysis, it is possible to predict the deformation of the rigging system when loaded by the sail forces or trim equipment, which is quite important for the sail design as well as the performance of the yacht. Also, FE allows to introduce other alternatives in the design.

It is correctly expressed that, although the application of FE for rigging systems design is a great advantage to predict deformation and stress distribution, this tool does not directly allow to find the most suitable cross section properties of the mast and standing rigging but allows to create an iterative process until desired safety factors for aspects such as global and local buckling are achieved.

The specifications given for the FE allow understanding the method used to make the simulations as realistic as possible since topics such as boundary conditions and loads applied on the rig system were extensively detailed. Finally, satisfactory results were presented when compared with the measurements performed.

While most of the literature that uses FE to approach rig systems, elaborate global models, with one dimensional elements such as beam and truss, in [9], a more profound evaluation of a mast deformation was elaborated, considering the governing limit states and the typical behaviour of these slender structures. More precisely, a dynamic buckling analysis was carried out for the bottom panel of a large sailing yacht, aiming to provide a different perspective for scantling assessment of sail systems, compared with the most commonly found approaches.

Although FE nonlinear analysis can be quite demanding, Classification Societies requirements are not that strict regarding this topic. As an example, according to [10], the reigning limit state which is global buckling can be simulated using the Euler eigenmode method on FEA with models composed of one-dimensional elements. With that said, the beforementioned type of analysis can be sufficient for normal scantling assessment procedures but it might not be the case for performance analysis, which requires the dynamic behaviour of the structure. To create such a detailed assessment, accurate information about the loads should be known for different sailing conditions. Besides that, inertial loads on the mast caused by the hull should also be accounted for as well as the self-weight of the rigs, in the case of larger yachts.

As referred in [9] inertial effects due to ship motions can be intensified by the rigs' pre tension since it generates a certain stress state on the mast when considering a quasi-static condition. Added to that, there is the effect of motions like the pitching in waves that generate a momentaneous longitudinal bending of the mast and can make the shrouds and stays become slack while halyards and running rigging also load the mast. All these sudden changes in stress state induce a huge amount of the energy that must be absorbed by the mast.

Two other phenomena, referred in [9], that are of concern too are the appearance of high-intensity wind gusts and their effect on the apparent wind speed, increasing the force generated by sails, and decelerations caused by slamming on waves. During all these dynamic effects, the load imposed by mast tunning can be transferred to other components due to large deformations and even be loaded beyond its limits.

In this research that aimed to study the dynamic buckling of the mast panel, a quasi-static collapse analysis was performed firstly to identify the mast collapse behaviour and its post-buckling response.

Afterwards, several sinusoidal axial compressive loads are applied in different simulations to create the dynamic loading condition, progressively increasing the amplitude of the impulse. This approach showed its potential to assess the influence of inertial effects due to ship motions, which can be implemented when optimising a column-like structure such as the mast when subjected to uniaxial compressive loads.

Indeed, in the approach made in [6] for the different procedures that are applicable to mast and rigging design, it is pointed out several methods and considerations such as the importance of studying global buckling and the computation of yielding and collapse through the generation of different loading conditions. Nevertheless, for a local analysis (local buckling and deformation), it is stated that more detailed models should be developed with shell or three-dimensional elements. Also, for a more detailed analysis, it may be considered the correct allocation of forces such as those caused by the halyards (acting on the sheave axles), outhaul and Cunningham besides those prevenient from the sails.

The conclusions taken from the latter mentioned study demonstrate how the global analysis of mast deformation can be useful to obtain results of its behaviour in non-linear conditions, helping in mast tuning and sails design while local models are convenient to analyse any specific region or component leading to conclude how different types of analysis can be achieved by different types of models.

2.4 Finite Element Method Principles

To analyse structural components, the finite element method is crucial and has brought an unmeasurable positive impact due to its capabilities of transforming very complex problems, many times impossible to solve analytically, into many simple problems, assembling a discretized solutions altogether to obtain a final response, not only for structural problems but also for a large variety of scientific fields.

As referred to in [11], this computational technique is used to obtain approximate solutions to boundary value problems, which are the mathematical representation of a physical structure, obtained through the geometrical discretization of the structure. This discretization, also called finite element mesh, allows to generating simple geometries that approximate the analysed structure while making it possible to calculate numerically its dependent variables since these are governed by ordinary differential equations and boundary conditions. The finite element mesh is defined by nodes, which are the geometrical locations where the variables are to be explicitly calculated.

There are many different types of elements to discretize in FEM, which make the selection to be following the problem that's being studied. In this thesis, more specifically, the most suitable element is the shell element to define the mast surface in the global model due to its good capabilities of defining thin surfaces while representing better displacement, stress and shear patterns three-dimensionally. As for the other structural components such as rigs and spreaders, the beam element is the most suitable due to its geometrical and mechanical characteristics. Moreover, solid elements are also implemented in submodels to assess the response variation throughout the material's thickness in the mast and its reinforcements.

2.5 Approach to Structural Analysis

As it is known, the complexity of some structural components, when put under loading conditions, the stress distribution results can be uneven. The regions with stress concentrations often act as critical locations from where damage can initiate and/or propagate. When seeking reliability and efficiency in structural analysis, the trade-off between reducing the computation time and obtaining accurate results becomes one of the main priorities. To approach problems with Finite Elements, many industrial sectors, including yacht design implement reduced-order element types in many cases, such as beams, plates and shells since these produce more computationally efficient models.

Despite that, there are always situations where models contain complex regions in geometry, loading or material behaviour, making the usage of higher-order element types important for this matter since to capture critical details of structural responses, 2D and 3D elements are required. One possible way that engineers use to treat this type of problem is by using coupled element approaches, however, to achieve this, it is important to be able to couple the element types that conform to the governing equations of the problem. As presented in the literature [12], three different methods are provided to couple different types of elements (beam-solid, beam-shell and shell-solid) with the mathematical development that can be implemented in Abaqus as a command.

Moreover, in [13] it is referred that for a global model made of shell elements, solid elements can replace the shells in the area of interest and be coupled to the surrounding shell elements either by applying the Mindlin-Reissner kinematic assumption or using a similar formulation like the one presented in [13] that allows considering the stretching of the shell thickness. An illustrative example of coupling for local mesh refinement can be seen in Figure 2.6 a).

Although the coupling method can be effective, the complexity of the element combination in the same model appears since there are mathematical difficulties in the connections between the different elements due to the incompatibility in terms of degrees of freedom and the appearance of artificial stresses at the intersected boundaries, compromising the reliability of this method if not done correctly.

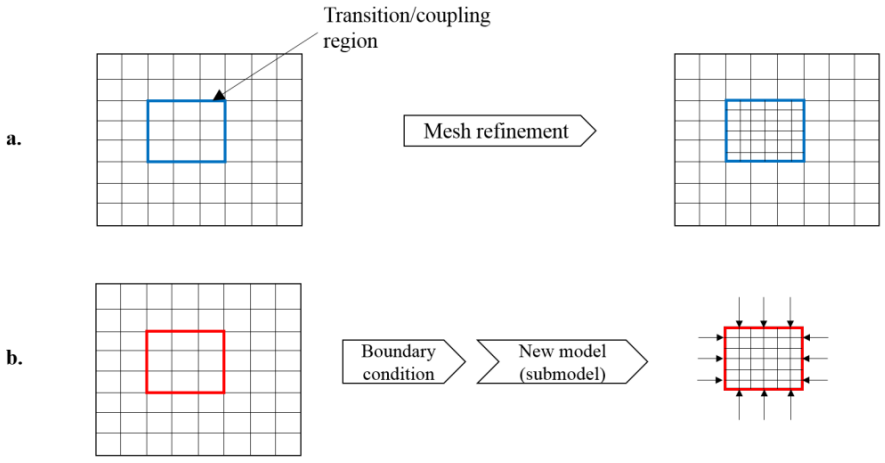

Figure 2.6: Two different methods to merge scales in FEA. [13]

The necessity of having accurate analysis to assist the design process with a more practical method-

ology encouraged to consider the sub modelling technique in Finite Element Analysis in this dissertation, to study the structural behaviour of a sailing yacht. This technique comes in great hands since it allows to make a refined analysis for critical areas of structures. It can be employed in a variety of challenging tasks such as stress concentration, 3D crack propagation, contact analysis, fatigue analysis and others. In the case of a structure as a carbon fibre rigging system of a yacht, it can provide details about stress concentration in mast holes, contact regions between stays and spreaders, secondary bending effects and even in a more profound manner, such as analysing the material's response considering the composite lay-up, to evaluate shear stress in and along ply drop-off boundaries.

The usage of sub models eliminates the necessity of connector elements or regions in the same model by recurring to the creation of local sub models. It consists in using the solution of a coarse mesh model (global model) to provide boundary conditions for a local and more refined analysis in a secondary model (submodel), giving more accurate results for a specific region of interest (Figure 2.6 b)).

The concept of sub modelling is sustained by St.Venant's principle that states "The difference between the effects of two different but statically equivalent loads become very small at sufficiently large distances from the load". This concept implies that with the application of a coarse mesh in a global model and its respective response, a very refined local model can be made for the region of interest to get an accurate and refined response, as long as the boundary conditions are transferred sufficiently far away from the region of interest to ensure that these are not affected by the coarse mesh model inaccuracy in that region.

As referred in [14], despite the benefits that the sub modelling techniques can bring to reduce the computational burden of finely meshing a global model, this can add other sources of error if not performed correctly. Any deficiencies that exist in the global model will be propagated and transferred to the submodel. For example, if the cut boundary is established in a region with high stress gradients, this can lead to a bad definition of the boundary conditions for the submodel. Therefore, the application of the submodel boundary in an adequate region becomes a crucial task to avoid this type of mistake.

The aforementioned study aims to define the effect that the submodel boundary location has on the convergence of the submodel solution defining firstly, the theory used to interpolate displacements from the global model onto the submodel and followed by a case study of a cantilever beam with a hole loaded on the tip to prove the hypothesis.

Sub modelling has been well established in several research studies as a good method to obtain a very accurate analysis. For example, in [15] it is presented a proposal for exploiting the potentiality of the sub modelling technique, applied to the simulation of wear and numerical validation for a pin-on-disc wear test. Different sub modelling techniques were implemented and compared, differing by the quantity that was transferred from the global model to the local one, alternating between nodal forces, displacements and a combination of both. Furthermore, it was emphasized the utility of sub modelling in FE wear predictions since laboratory tests do not always reproduce the effective working conditions and normal numerical wear predictions can take a lot of time since it requires to combining iteratively nonlinear contact analysis and the update of the geometry and mesh after material removal.

Also, in the field of ship structures, it was applied the sub modelling method effectively to the analysis of a large ship structure [16] and according to the numerical analysis, the method of using superconvergent patch recovery improved the stresses along the sub modelling boundary and the presented sub modelling technique provided accurate solutions.

Additionally, in [17] it is proposed a hybrid data + model-based sub modelling (HDMS) method to estimate a refined response distribution near critical locations of structures including the nonlinearities that could appear in the response. The HDMS method uses a sensor measurement on the preselected boundaries of a region of interest in a structure to drive the submodel by applying force-based sub modelling procedure, allowing to avoid the creation of both global and local models once the measurements were coincident with the submodel boundaries, thus only recurring to the creation of the submodel.

In summary, the sub modelling simulations developed in this study were implemented with the loads measured at the cut boundaries with strain gauges and DIC to interpolate in the respective nodes of the FE models, resulting in a reliable and versatile method.

As for the different techniques implemented in sub modelling, the following are the most dominant and present in commercial software:

- **Displacement-based sub modelling** – consists in extracting the displacements from the solution of the global model, interpolate them and apply on the local model. As the most used approach, it is claimed to give the most accurate results with less risk of numerical issues such as rigid-body motions.

- **Stress-based sub modelling** - also known as surface-based sub modelling, in this technique the global stress field is interpolated onto the submodel integration points on the driven element-based surface facets. This technique is recommended when displacement-based sub modelling is not suitable.

Note that, as performed in [15], different techniques can be implemented simultaneously, obtaining a hybrid type of sub modelling that can be advantageous in some cases. For this specific case of study, from the comparison between different methods, the combination between equivalent nodal forces (obtained from an extra routine added to Ansys Workbench) and displacement transferring from the global model to the submodel resulted in the best method. It is also carried out in this research another alternative of sub modelling which consists in transferring displacements as an initial step to assess the reaction forces in the submodel's boundary and apply afterwards the reaction forces to obtain a final analysis.

Moreover, as a general guide selecting a sub modelling technique, in the Abaqus User's Guide [18] it is suggested several factors that must be considered:

- **The technique applied depends on the element used** - The Stress-based technique is only available for solid-to-solid sub modelling and the displacement-based technique applies to all types of elements.

- **The similitude between models' stiffness** - When the stiffness is comparable, displacement-based sub modelling will provide a better response regarding rigid-body modes. On the other hand, if the stiffness between models differs, the stress-based technique provides more accurate stress results.

- **The presence of large deformations or rotations** - Displacement-based technique guarantees a more accurate transmission of results.

- **The type of output of interest** - Displacement-based sub modelling provides better results for the transmission of displacement fields. In contrast, stress-based sub modelling transmits better the stress field and determination of reaction forces in the submodel.

It is also noted that, if necessary, it can be implemented both techniques mentioned in the last topics in Abaqus. Having reviewed the literature referenced throughout the elaboration of this project, it was opted to use the software Abaqus to proceed with the simulations developed with the purpose of practicality. Furthermore, the displacement-based technique was applied since the stress-based is only available for solid-to-solid sub modelling (global model and submodel constituted by solid elements) and, for the masts structural analysis, the usage of shell elements is of great interest to model the structure globally.

2.5.1 Theoretical Development of sub modelling

If a global model is considered, by having the displacement values at the nodal degrees of freedom, it is possible to estimate displacement or stress solutions in the vicinity of the nodes that are known from the global model using interpolation. Since the mesh of a submodel will not contain the same nodes as the global model, it is necessary to use the displacement values at nodal degrees of freedom from the global model in the submodel, this premise ends up being the base of sub modelling.

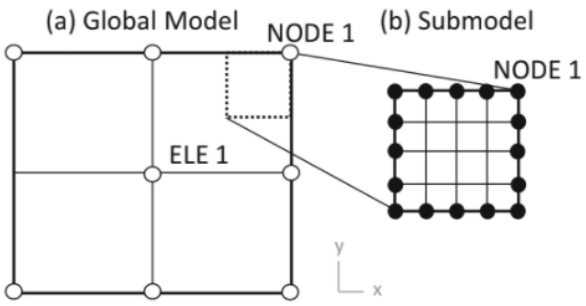

Figure 2.7: Example of sub modelling – global to local model. [14]

The Figure above illustrates an example of a global model and the submodel in the right upper corner where both of them only share one node.

By having the geometric location nodes of the submodel boundary X_S where d_S is the submodel boundary vector, one can say that X_S is a subset of the geometric coordinate space which can be called

X'_G. The geometric coordinate space X'_G is circumscribed by the boundaries of the elements in e'_G which is as subset of the global model element set e_G.

Thus, the following equations can be written:

$$X_S \subset X'_G \tag{2.1}$$

$$e'_G \subset e_G \tag{2.2}$$

Being X_S the matrix of xyz-coordinates for each node in the submodel boundary node vector d_S (e.g. the boundary nodes represented in Figure 2.7 b) and X'_G the xyz-coordinate space of the elements in e'_G.

Using the sub modelling analysis procedure, the global model must be solved:

$$K_G d_G = f_G \tag{2.3}$$

Where d_G is a column vector of nodal displacement solutions, K_G is the global model stiffness matrix, resultant from the element matrices assembly, and f_G is a column vector of the loads applied on the global model.

As for the submodel, driven by the global model response at the cut-boundary, it can be defined as follows:

$$K_S d_S = f_S \tag{2.4}$$

Where K_S is the submodel stiffness matrix, resultant from the element matrices assembly, f_S is a column vector of the loads applied on the submodel and d_S is a column vector of nodal displacement solutions for the submodel. With the global model displacements calculated, to determine the submodel boundary condition displacement d_S, it can be used shape functions that define the elements in e'_G. These shape functions can be found already implemented in software such as Ansys and Abaqus, provided by sub modelling commands. In alternative to the shape functions that are implemented in common software, it has been studied in [19] the application of cubic splines to interpolate the boundary conditions from the global model to the submodel, comparing the results with those obtained with shape functions, and results quite effective for models with stress concentration and nonlinear contact interfaces. Nevertheless, shape functions become more convenient to apply for the matter of practicality. Furthermore, the displacement field of an element in the global model is computed using a function constituted by a linear combination of products of shape functions and the global model degree of freedom solution:

$$u_j = \sum_{i=1}^{N_{elem}} N_i(X) d^j_{(G,i)} \tag{2.5}$$

Where u_j is the estimated displacement field of the j^{th} element in the global model. N_{elem} is the number of d.o.f for the j^{th} element, $N_i(X)$ is the shape function of the i^{th} d.o.f evaluated at any coordinate X within the element. Finally, $d^j_{G,i}$ is the global model dof solution for the i^{th} dof from the j^{th}

element.

Once the nodal coordinates of the submodel boundary X_S are known, they can be used to estimate the displacement within the boundaries of the elements in e'_G with the following equation:

$$d_{S,k} = \sum_{i=1}^{N_{elem}} N_i(X_{S,k}) d^j_{G,i} \tag{2.6}$$

Where $d_{S,K}$ is the k^{th} d.o.f in the boundary node vector d_S and is desired at the xyz-coordinate $X_{S,K}$. With all the boundary node d.o.f's estimated, they can be applied to the submodel to find the refined solution in the region of interest.

In the case of the stress-based sub modelling, the interpolation is built from the strain vectors of the global model onto the submodel, containing normal, parallel and shear components of strain, sampled at the global model elements on the cut boundary. As for the process of interpolation in the stress-based method, it is implemented in a similar way as in the displacement-based method.

With the constitutive equation as presented in the matrix equation (2.7) and considering the material properties, the normal, parallel and shear strains that are interpolated to the submodel boundary elements can be transformed to normal and shear stress on the boundary element faces. These values of stress are then used to build the load vector f_S in equation (2.4), by transforming the tractions into forces to apply on the submodel's boundary, leading to the obtention of the submodel refined response.

$$\begin{bmatrix} \sigma_{11} \\ \sigma_{22} \\ \sigma_{33} \\ \tau_{23} \\ \tau_{13} \\ \tau_{12} \end{bmatrix} = \begin{bmatrix} C_{11} & C_{12} & C_{13} & C_{14} & C_{15} & C_{16} \\ & C_{22} & C_{23} & C_{24} & C_{25} & C_{26} \\ & & C_{33} & C_{34} & C_{35} & C_{36} \\ & & & C_{44} & C_{45} & C_{46} \\ & symm & & & C_{55} & C_{56} \\ & & & & & C_{66} \end{bmatrix} \begin{bmatrix} \varepsilon_{11} \\ \varepsilon_{22} \\ \varepsilon_{33} \\ 2\varepsilon_{23} \\ 2\varepsilon_{13} \\ 2\varepsilon_{21} \end{bmatrix} \tag{2.7}$$

In equation (2.7), the vector on the left represents the normal and shear stress, C_{ij} represent values of the stiffness tensor of material properties or Elastic moduli and on the right there is the strain vector.

Chapter 3

Sub Modelling Study Cases

To assess the effectiveness of sub modelling to obtain accurate responses for the structural analysis, a few different study cases were developed in this project considering load cases that are normally present in a rigging system of a sailing yacht. These study cases represent structural components in different circumstances of loading aiming to simulate simplified scenarios that not only are predictable in terms of their structural response thus, making the interpretation of the results easier, but also allowing to verify the applicability of the sub modelling technique for more complex cases in rigging systems structural analysis, as it will be developed further in this dissertation.

As it has been mentioned before, the complexity present in the loading of a large mast is a result of the most distinct load contributions, leading to a response that is not easy to be directly interpreted, especially when a detailed Finite Element model is considered for local analysis. Thus, to obtain a reliable interaction between a global and local analysis, a good knowledge of what is behind the sub modelling computations is crucial. The following study cases that are presented are focused on that.

3.1 Study Case 1 - Flat Plate under tensile load

As the simplest of the study cases developed in this chapter due to the load case considered, this study case allowed to conclude about the effectiveness of applying displacement-based sub modelling as well as proving the effect of the considerations that must be taken in this type of analysis such as submodel boundary allocation and global model results convergence.

The flat plate that was analysed had the dimensions and material properties shown in the tables below:

Table 3.1: Plate dimensions.

Length	1	[m]
Width	0.4	[m]
Thickness	0.05	[m]

Table 3.2: Material Properties.

E	70×10^9	[Pa]
ν	0.35	-

The plate material was considered isotropic with the same elastic modulus (E) and Poisson ratio (ν) as Aluminium.

The finite element analysis mesh was constituted by shell elements S4R for all the analyses executed. At the first stage of the study case, a global model was created with an element size of 0.05 m and two submodels, submodel 1 and submodel 2 with an element size of 0.02 m and 0.01m respectively.

Afterwards, a global model mesh refinement was elaborated to assess its impact on the response of a submodel made from the refined global model, since by principle that can influence the submodel results. Relative deviation results were estimated to interpret the results. Lastly, a submodel was created for the plate tip to assess the influence of the submodel allocation.

As for the boundary conditions, the plate was subjected to a constraint on the translation degrees of freedom in one extremity, as shown in Figure 3.1 (on the left), and a tensile load of 1000 N in the opposite extremity.

Regarding the type of analysis in this study case, all the simulations were executed as static linear analysis due to the simplicity of the load case and considerably low displacements.

From the global model, it was not expected a smooth transition of stress in regions where high stress gradients are present due to the coarseness of the mesh. However, it was expected that by selecting an adequate region to define the submodel boundaries, the global model would still provide accurately results to analyse a more refined response on the submodel.

In Figure 3.2, there is the normal stress distribution (on the left) and the axial displacement (on the right) for the global model. Results were taken along the longitudinal centreline of the plate to compare with those obtained for the submodels.

The submodels were created representing a portion of the plate where the cut boundaries were allocated longitudinally at 0.3 m and 0.7 m relatively to the global model as shown in the scheme in the Figure below.

From the simulations, results for displacement and normal stress in the longitudinal direction were

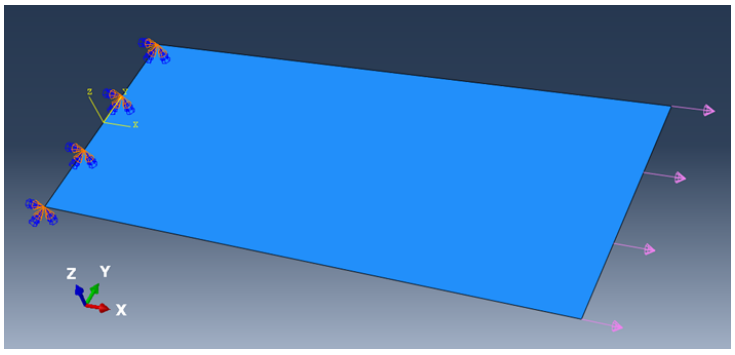

Figure 3.1: Study Case 1 - Loads and boundary conditions applied on the plate.

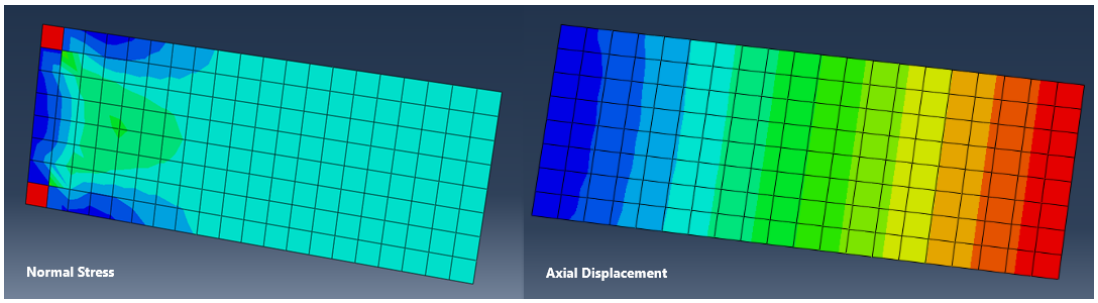

Figure 3.2: Study Case 1 - Global Model response.

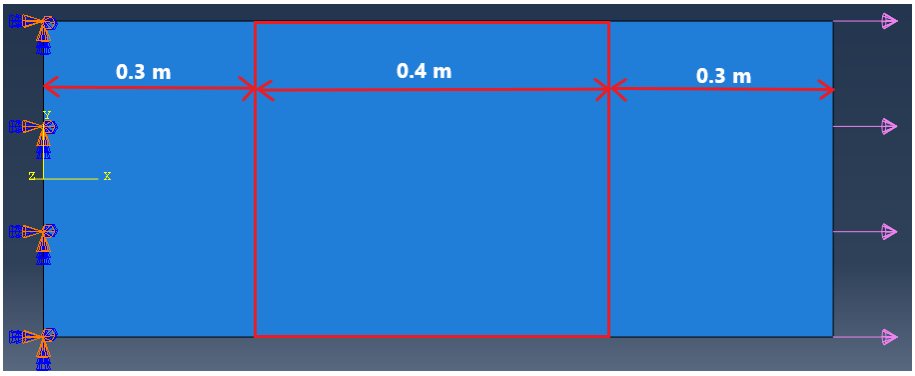

Figure 3.3: Study Case 1 - Submodel location schematization.

taken since those are the most significant results in this study case due to the nature of the loading.

The results shown in the graphs below correspond to the coarse global model and the two submodels that were computed at the first stage of the study case.

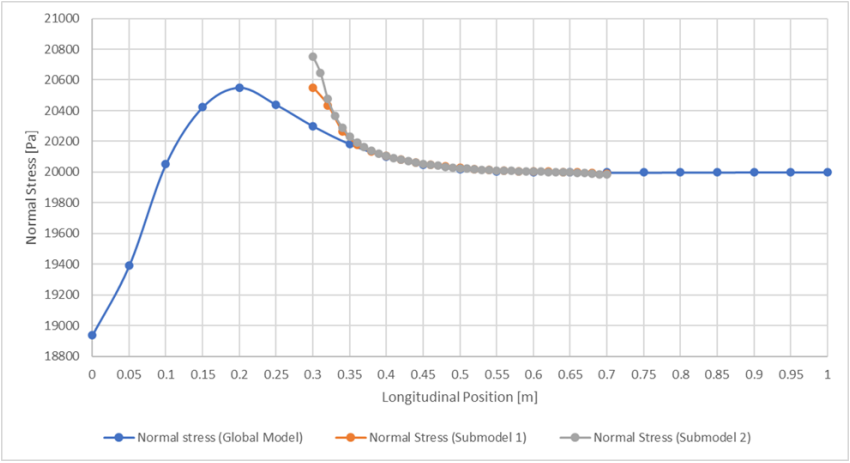

Figure 3.4: Study Case 1 - Normal stress longitudinal distribution.

As visible in the normal stress results (Figure 3.4), both submodels slightly deviate from the global model close to the submodels boundary at longitudinal position x=0.3 m, achieving deviation values of 1.23 % and 2.22 % in submodel 1 and submodel 2 respectively. This deviation was calculated relative to the global model at the nodes situated at x=0.3m. Although the results were consided good, it was opted to obtain a response for a global model with the same element size as submodel 1 (element size of 0.02 m) to calculate the relative deviation of the submodel. This allows to obtaining the nodal positions in the

plate at the same coordinates for both models, making them comparable.

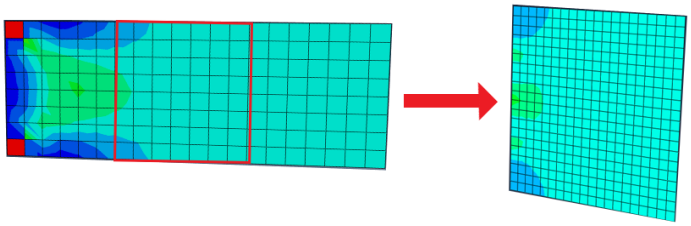

Figure 3.5: Study Case 1 - Normal stress response in global model and refined submodel 1.

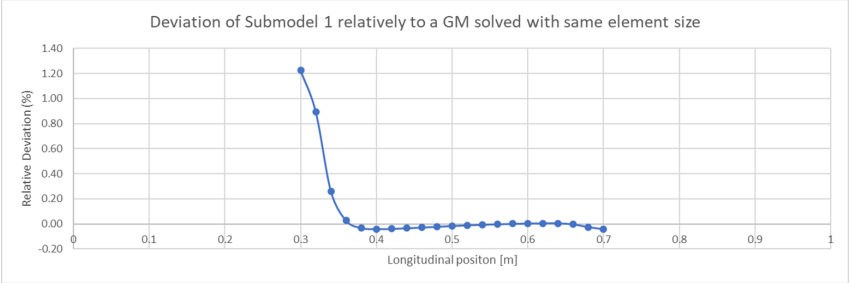

Figure 3.6: Study Case 1 - Submodel 1 relative deviation.

From the relative deviation graph shown above (Figure 3.6), it can be observed that the stress results in the submodel rapidly become very similar to the global model when the longitudinal coordinate increases which is related to the fact that the results transferred to the submodel boundary with the lowest longitudinal coordinate are located in a region with a higher stress gradient making the computation of stress response slightly less accurate. This leads to the remark that the location of the submodel has an important contribution to the stress response of the submodel, verifying what has been seen in the literature mentioned before. It can be also noted that despite the existence of this deviation, the results are still acceptable.

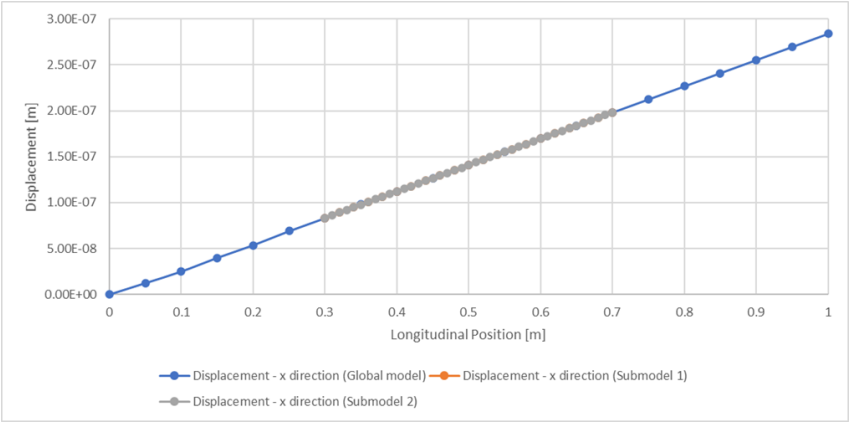

Figure 3.7: Study Case 1 - Axial displacement distribution along the longitudinal centreline.

In the case of the displacement response (Figure 3.7), the results are even more accurate when transferred to the submodels, obtaining a similar displacement distribution as in the global model. This

puts in evidence the potential of displacement-based sub modelling in transferring displacements very accurately as referred earlier.

In a second stage of the study case, a global model mesh refinement was carried on, reducing the element size to 0.025 m and 0.02 m. In the following graph (Figure 3.8) it can be visible the normal stress distribution along the plate centreline in the three different global models.

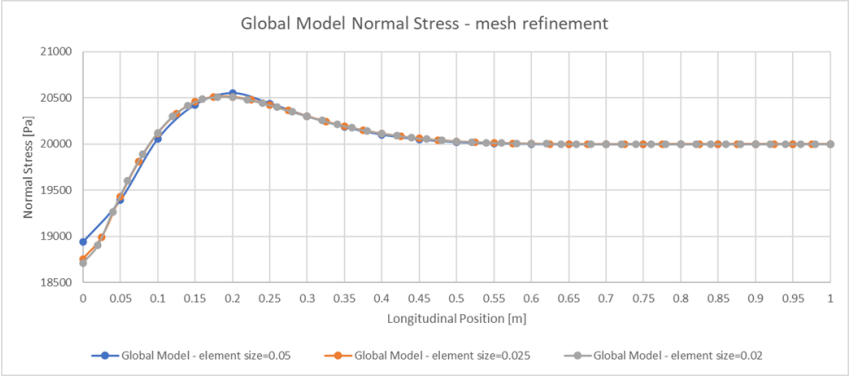

Figure 3.8: Study Case 1 - Global Model mesh refinement.

It can be observed a slight difference in the stress results although it's not very significant. However, when a submodel analysis is performed by transferring the results from a more refined global model, the accuracy should improve. To prove it, the global model with an element size equal to 0.025 m was selected to run a submodel with an element size of 0.01 m.

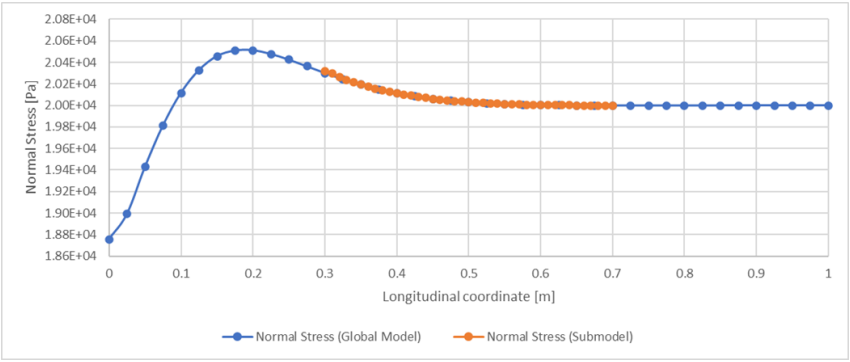

Figure 3.9: Study Case 1 - Normal stress longitudinal distribution after global model mesh refinement.

While the displacements remained accurate, as happened in the previous step of this study case, the normal stress results improved, achieving a very similar response as in the global model. The relative deviation on the node located at $x = 0.3\,m$ was reduced to 0.09%, which is a significant improvement when compared to the result observed in Figure 3.6. This led to the conclusion that global model refinement has a positive impact on the submodel stress results.

For the last stage of this study case, it was created a submodel on a different region of the plate using a coarse global model. From the response observed earlier, it was clear that as the longitudinal coordinate increased, the stress stabilizes, achieving a uniform distribution while the displacement was linear throughout the hole plate. The hypothesis that's to be proved is that by defining the submodel in a region with a more uniform stress distribution, the submodel response should improve concerning the

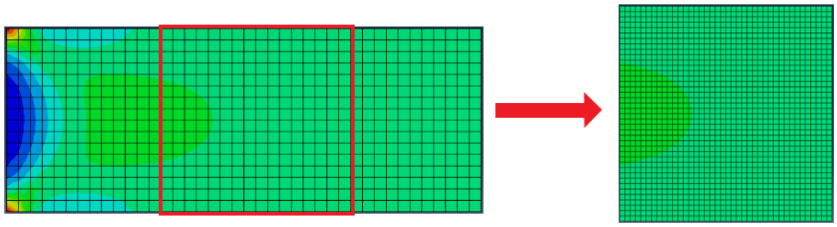

Figure 3.10: Study Case 1 - Normal stress response after global model mesh refinement.

global model.

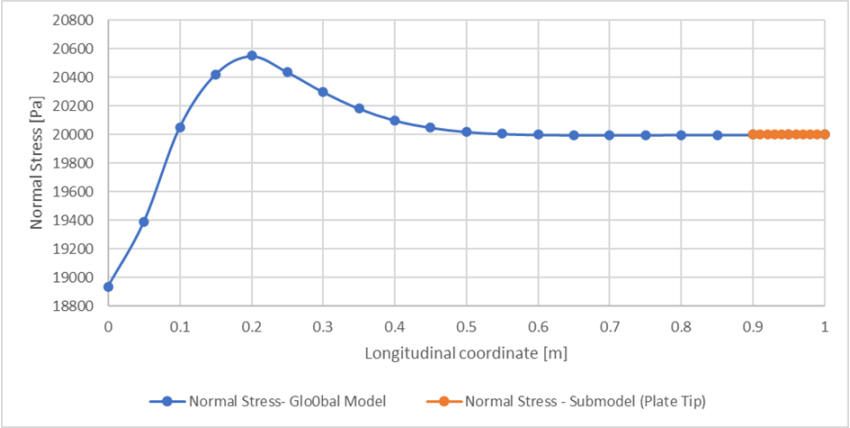

Figure 3.11: Study Case 1 - Normal stress distribution with submodel allocated on the plate tip.

With a submodel created for the last 10 cm of the plate, with an element size of 0.02 m, it can be observed from the stress distribution shown above (Figure 3.11) that the submodel stress results match perfectly those obtained in the global model but in a more refined way. In conclusion, it can be remarked from this study case that by using the technique of displacement-based sub modelling, it must be taken into consideration the allocation of the submodel boundary since it can affect the accuracy of the results, as well as the global model mesh refinement. While displacement results easily match accurate results, the stress response can be conditioned by those two factors, principally near the boundaries of the submodel.

3.2 Study Case 2 - Plate with a hole in compression

Being holes a common geometric feature on masts for diverse purposes, the study of a submodel created around a hole of a structural component under compression is an interesting topic for the engineering field studied in this dissertation. These features can be seen in locations such as the connection between mast and spreaders, as well as for the shrouds and stays, or even for the halyards. In a realistic situation, a mast can be loaded in a more complex way indeed, suffering bending and torsion loads, however, the compression load is the most persistent and dominant in all load cases.

The present study case focused on a plate with the same dimensions as in study case 1 (table (3.1)) as well as material properties (table (3.2)), with the difference of a hole situated in the geometric centre

of the plate with a radius of 0.02 m.

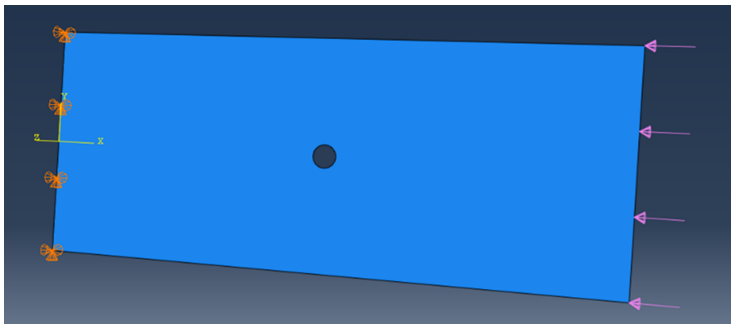

Figure 3.12: Study Case 2 - Loads and boundary conditions applied on the plate.

Once again, the element type used in the FEA was Abaqus shell element S4R. For the global model, an element size of 0.04 m was selected since it fitted the geometry reasonably good for a coarse model. For the submodel, the element size was equal to 7.5 mm to obtain a refined response of stress concentration around the hole.

Regarding the boundary conditions, the plate is pinned in one extremity, i.e., translation degrees of freedom constrained, while on the other extremity there is a compressive force of 1000 N applied on the edge of the plate, as visible in Figure 3.12.

The analysis performed on this study case was, once again, static linear analysis. Besides that, for the result analysis and graph representation, the stress and displacement response were analysed in the longitudinal centreline as well as in the transverse midplate section, as represented in Figure 3.13 on the right. These paths were selected since it is there that the highest stress gradients are observed.

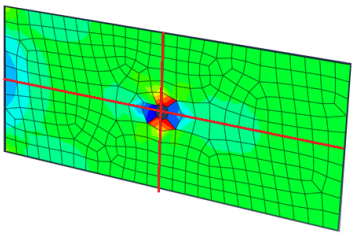

Figure 3.13: Study Case 2 - Global Model paths that were analysed throughout the study case.

The submodel boundaries were selected at a sufficiently high distance from the hole to avoid influencing the stress concentration. The following Figure is a representation of the global model, the selected region of interest and the submodel.

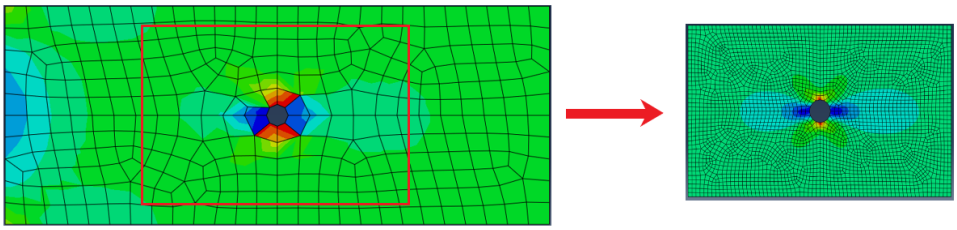

Figure 3.14: Study Case 2 - Von Mises stress response in global model and submodel.

The submodel has a length and width of 0.5 m and 0.3 m respectively and was allocated with the plate hole as the centroid.

In Figure 3.14, showing the Von Mises equivalent stress in both the global model and submodel, it can be noted the difference in the smoothness of stress transition between the two models, revealing

the capacity of sub modelling to represent a more accurate and sensitive stress pattern.

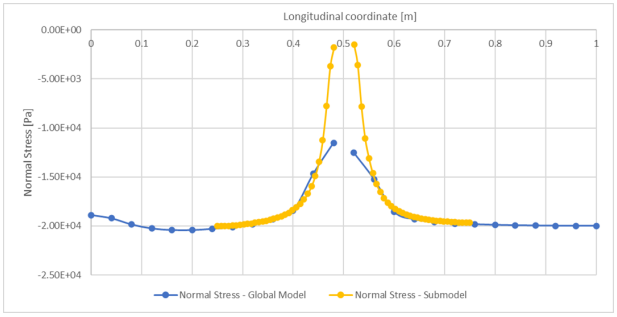

Figure 3.15: Study Case 2 - Normal Stress longitudinal distribution.

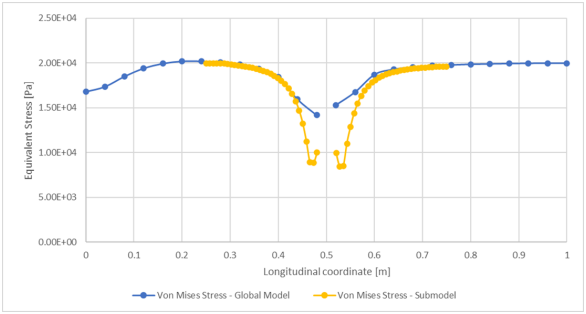

Figure 3.16: Study Case 2 - Von Mises stress longitudinal distribution.

The two graphs above show normal stress and Von Mises equivalent stress, respectively. Both show the stress distribution along the longitudinal centreline. In yellow, the submodel stress distributions match with the stress response of the global model in the submodel boundary (at $x = 0.25m$ and $x = 0.75m$), meaning that the response was transferred with accuracy. Additionally, near the hole it is visible how the submodel stress distribution follows a smoother path thanks to the refined mesh reaching higher values of stress in magnitude. Moreover, in the Von Mises stress distribution in Figure 3.16, it can be seen that near the hole there is a different behaviour compared to the normal stress, obtaining higher values of stress (in magnitude) in that region which is a result of the shear stress presence.

In the case of the transverse stress distribution along the midplate section, the behaviour of both normal and Von Mises stress is very similar, reaching values of around 40 kPa in the hole's edge.

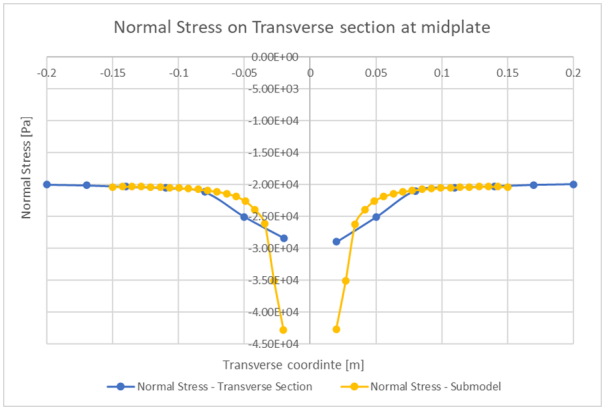

Figure 3.17: Study Case 2 - Normal Stress transverse distribution.

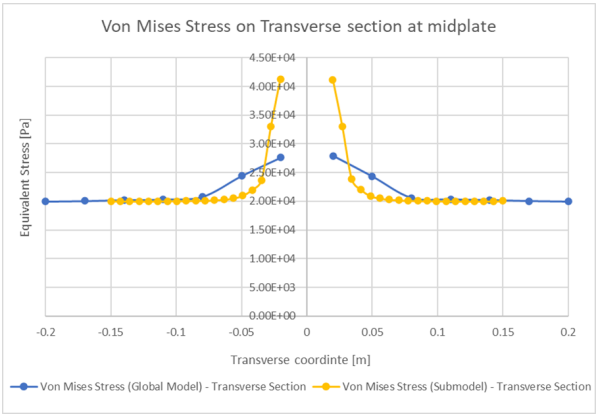

Figure 3.18: Study Case 2 - Von Mises stress transverse distribution.

The application of sub modelling in this analysis also allowed to verify the under estimation of the stress state near the hole in the global model due to the coarse mesh. The usage of a refined mesh provides a more accurate response in terms of the stress distribution and magnitude of the obtained stress state.

Regarding the displacement, it can be seen in Figure 3.19 that displacements, although very small

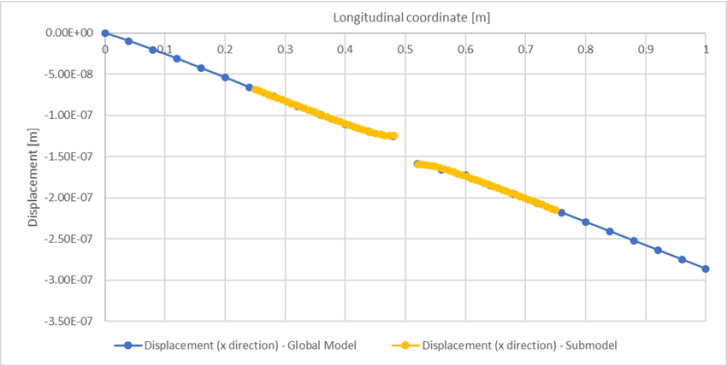

Figure 3.19: Study Case 2 - Displacement longitudinal distribution.

due to the nature of the load case, match precisely with those obtained in the global model since these are not as dependent on the mesh refinement to converge as the stress but still shows the efficiency of sub modelling.

Once again, the stress and displacement results presented in this study case represent the advantage of using sub modelling to assess the response of a certain region of interest for the capability of achieving an accurate and refined response.

3.3 Study Case 3 - Plate with change in geometry

Having the last study case present for comparison, the third study case was developed to assess the effectiveness of applying sub modelling to a structural component that has suffered a geometry change from the global model to the submodel. This concept is sustained in the usage of a simplified global model that's solved with a coarse mesh to obtain a global response and afterwards, use that global response to apply to the region of interest with a more detailed 3D modelling to optimize the structure or elaborate a local analysis.

From the design point of view, this type of sub modelling implementation becomes very useful since it allows the creation of a simplified global model in terms of geometry, improving the computations in terms of modelling and the meshing process since having small geometry details in a coarse global model can create mesh issues. In the case of masts, which are large structures with a significant number of details such as holes and points of contact, the application of this method can be very beneficial.

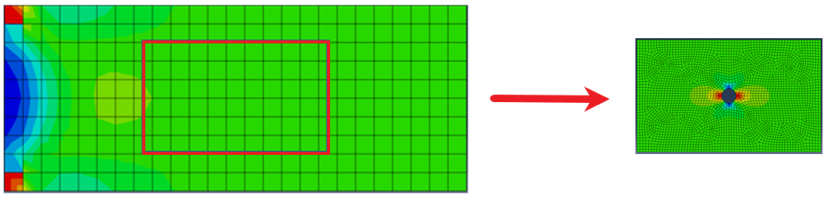

Figure 3.20: Study Case 3 - Von Mises stress response in global model and submodel.

With that said, to elaborate on this study case it was considered the same plate geometry, material

properties, boundary conditions and element size for the global model and submodel as in the former case, with the exception that the global response was obtained from a plate without a hole and only afterwards, in the submodel, the hole was added. In Figure 3.20 shows the Von Mises stress response for both global and local models.

As in the former study case, longitudinal and transverse stress responses were extracted from the analysis to compare the results. For both normal and Von Mises stress, the response was very similar to the one obtained in the previous study case as visible in the graphs shown in Figures 3.21 and 3.22.

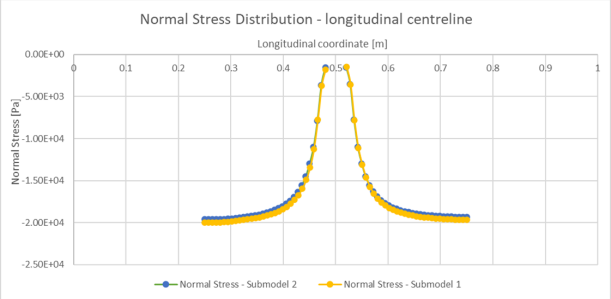

Figure 3.21: Study case 3 - Normal Stress longitudinal distribution.

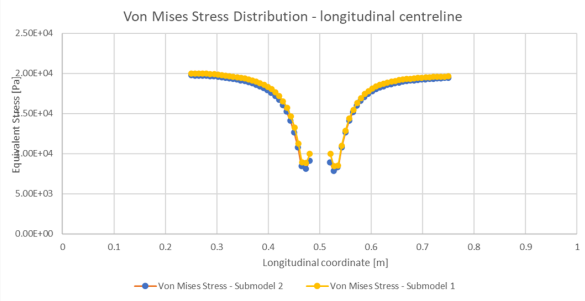

Figure 3.22: Study case 3 - Von Mises stress longitudinal distribution.

Note that in the graphs shown in this section, submodel 1 represents the submodel obtained in the previous study case and submodel 2 represents the one obtained in the present study case.

To have a more precise comparison of the results, a relative deviation was calculated for submodel 2 concerning the results obtained in study case 2.

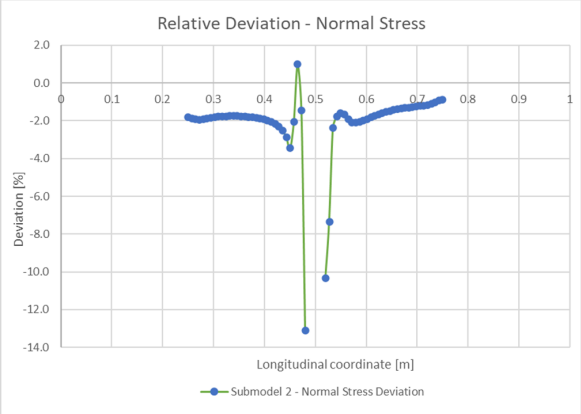

Figure 3.23: Study case 3 - Normal Stress relative deviation.

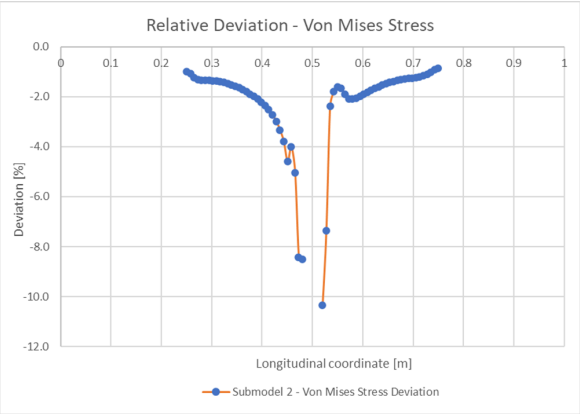

Figure 3.24: Study case 3 - Von Mises stress relative deviation

From these relative deviation results, it is clear that near the plate's hole, the deviation is increased reaching maximum values of approximately -13% in normal stress and -10% in Von Mises stress. Although these results are considered acceptable for the stress response estimation, it was also noted that the node locations in the present submodel do not coincide exactly with the nodes of the study case 2 submodel, varying by a few millimetres, the resultant deviation may be affected by this since in high

stress gradient regions, the stress values can vary significantly in a small length of the material.

In fact, the values where the stress deviation is higher (near the hole) coincide with the node locations that differ the most in the mesh generated by Abaqus.

Concerning the transverse stress response, a similar behaviour was also observed when the two submodels were compared.

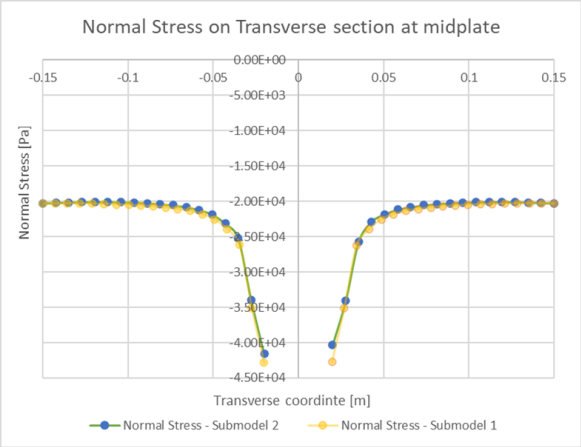

Figure 3.25: Study case 3 - Normal Stress distribution in transverse section.

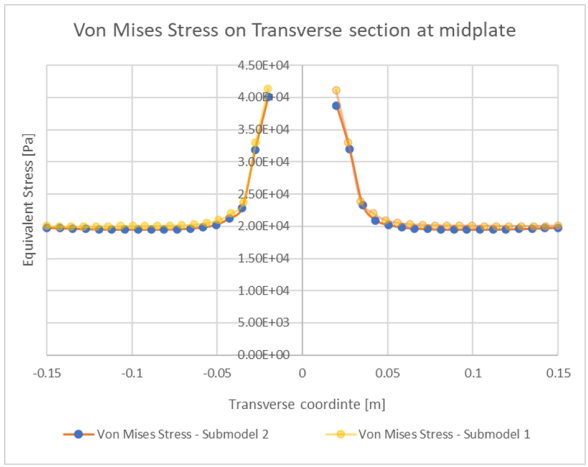

Figure 3.26: Study case 3 - Von Mises stress distribution in transverse section.

In the transverse section studied, situated in the mid plate, where stresses reached the highest results, it was noted a slight under estimation of the stress response, reaching its maximum value at the node situated in the hole's edge, as visible in the graphs presented in Figures 3.25 and 3.26. The relative deviations for those two nodes were the following:

Table 3.3: Relative deviation at the hole's edge

	Normal Stress Relative Deviation [%]	Von Mises Relative Deviation [%]
Lower node	-2.638	-2.717
Upper node	-5.879	-6.139

Note that in the midplate transverse section Abaqus generated two more nodes in the transverse direction for this submodel, making the node locations vary significantly from one submodel to the other. Thus, the relative deviation became meaningless if calculated node by node in this case.

In conclusion, the results, although very close, are slightly underestimated when this technique is employed. However, this underestimation is not worrying when the change in geometry is considerably small as the one implemented and proved by the relative deviation calculations.

Chapter 4

Mast Structural Analysis

As the main goal of this dissertation, a structural analysis of a sailing yacht mast was elaborated making use of sub modelling techniques in FEA software Abaqus. As a result of the work developed with Rondal, a global model (GM) of a mast was developed including its standing rigs and spreaders according to the design and structural configuration conceived by the company. Moreover, submodels were designed with a parametric variation in the patch reinforcement to create a local and more detailed analysis at the forestay-mast connection, the region of interest where the forestay lug is located. The load condition consists in applying pre-tension on the mast and the maximum allowable backstay load, of this rig system in particular, since it is the load that generates the most critical load state on the region being studied with the submodels.

4.1 Problem Description

Due to the complexity in the geometry of the mast and its components, it is computationally expensive to model a detailed geometry with all the features present in a mast and rig system since the length of the mast is much higher than its other dimensions, creating difficulties to generate a finite element mesh that provides detailed results for the whole structure in an efficient way.

As mentioned before in this dissertation, a way of avoiding that situation is using the sub modelling technique where the global model should be simplified in its geometry details and result in a coarse mesh simulation to obtain a global response. Followed to that, submodels are created, extracting results from the global response to apply within the submodel's boundaries. These submodels contain the geometry details that provide a detailed response in specific regions of the mast with a refined mesh and can be attached to the global model and simulated considerably quickly to increase the simulation efficiency.

The aforementioned argument allowed to formulate the following objectives. As a global objective, this type of modelling permitted obtaining an accurate analysis of a local detail of the mast to assess the effectiveness of different design solutions in a region where stresses are concentrated, without having to constantly simulate the mast global model, permitting to study a region of interest as one independent

model that is indirectly coupled to the global model. Added to that, other particular objectives were achieved such as assessing the stress response generated by the different arrangements created for the ply drop-off in the reinforcement patch of the forestay lug and the usage of different element types in the submodels to compare the results of its application.

4.2 Finite Element Models

To develop the Finite Element Analysis present in this dissertation, several methodologies were considered to elaborate on this type of structural analysis, based on the knowledge and experience present in this company, existing studies and the orientation of the thesis supervisors. Added to that, several simplifications and assumptions were taken to create a realistic response to the structure and keep the scope of the project on the application of sub modelling techniques for local stress analysis whilst ensuring, as might be expected, an accurate behaviour of the structure for every analysis.

As referred to at the beginning of this chapter, it was developed a global model including a shell element mast tube that was assembled afterwards with the other structural components that connect to the mast and interact with it, that includes the longitudinal stays, vertical and diagonal shrouds and four spreaders on each side of the mast, all modelled with beam elements. As for the submodels, these were specially modelled to include the reinforcement patches. In addition, each one of the three reinforcement patches was simulated in both shell and solid elements, requiring different three-dimensional modelling for each element type. As a result of that, a total of six submodels were created, two for each mast segment and its respective reinforcement patch.

The following sections concern to a detailed description of the aspects previously mentioned and are structured according to the most relevant steps followed to obtain the FEA results.

4.2.1 3D Models

Since the geometries presented in this structural analysis vary in their characteristics, two 3D modelling software were used, Rhinoceros to create the global model of the mast and shell submodels, and Solidworks to create the solid submodels. This decision was taken to consider the requirements of each geometry. Rhinoceros, on one hand, is advantageous to handle surfaces, thus, better to create the surfaces of the mast global model and submodels that would be modelled with shell elements subsequently. On the other hand, Solidworks allows the creation of solid parts, making it beneficial to design the submodels that were to be analysed using solid elements.

From technical drawings provided by Rondal, the mast was designed and three-dimensionally represented by its mid surface considering the tapering present near the top and the geometrical allocations of the relevant fittings such as the spreaders, longitudinal rigs, shrouds and deck level for its posterior assembly, a topic that will be presented further in this chapter.

For confidentiality reasons, not all the technical drawings that were used to design the mast model are presented in this dissertation. However, in Appendix A, details of the cross-section and lug are

presented.

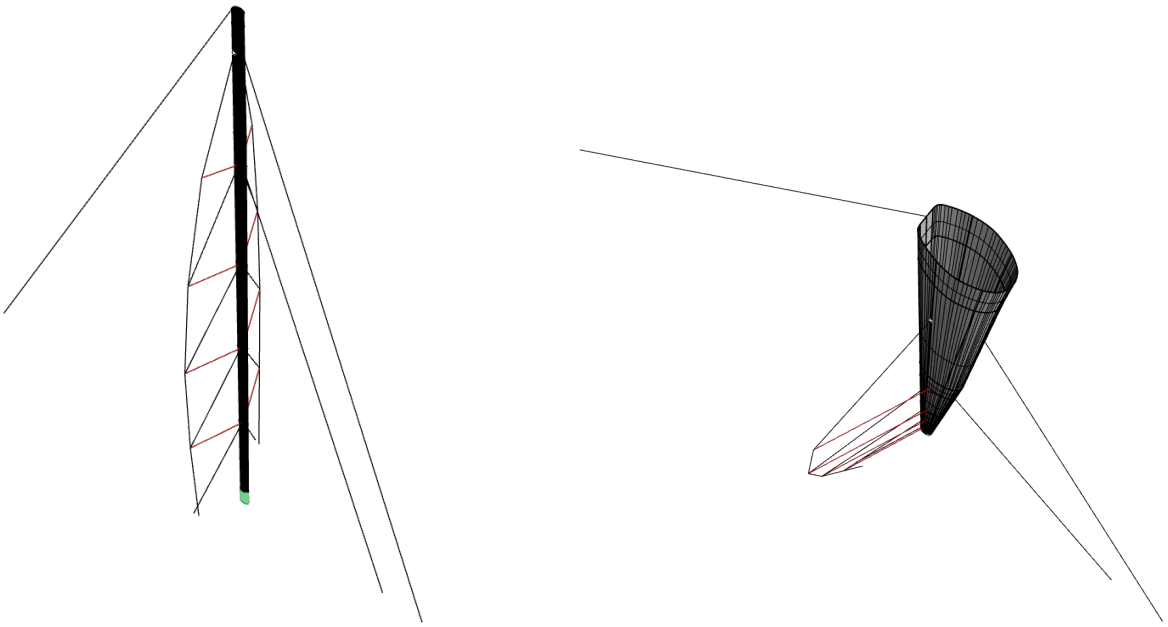

(a) GM modelled in Rhinoceros (b) Forestay-Mast connection

Figure 4.1: Global Model - Mast surface with rig system scheme.

As for the submodels, a more detailed procedure had to be followed. Since the geometry considered for the submodels consists of a fraction of the mast near the mast-forestay connection, the geometry was fragmented relatively to the point of intersection between the forestay and the mast. Two horizontal planes at a distance of 1500 mm from the forestay-mast connection point define the longitudinal extremities of the submodels while the other extremities are defined by a plane offset from the back face of the mast at a distance of 250 mm. These extremities constitute the submodels' boundaries.

Note that, although in reality the forestay does not have a physical connection with the mast since these are connected by the lug, the forestay-mast connection point represents the intersection between the mast and the line of action of the forestay (as represented in the global model, visible in Figure 4.1 b)).

Added to that, the reinforcement patches were designed as rectangular surfaces of different sizes, representing stacked plies of carbon fibre (also called blocks) that are laid upon the inner surface of the mast. For the different submodels, different configurations of ply-stacking and ply drop-off were considered.

From the practical point of view, an interesting point of this project to evaluate different ways to stack the carbon plies for the reinforcement patches and how the ply drop-off can be employed on the mast tube to optimize the stress distribution and increase the strength.

Thus, three different patch arrangements were considered:

- **Submodel 1 (SM1)** - Submodel with a reinforcement patch with 5 blocks of 10 layers, with a ply drop-off spacing of 30 mm in the cross-sectional direction and 60 mm in the longitudinal direction.

- **Submodel 2 (SM2)** - Submodel with a reinforcement patch with 10 blocks of 5 layers, with a ply drop-off spacing of 30 mm in the cross-sectional direction and 60 mm in the longitudinal direction.
- **Submodel 3 (SM3)** - Submodel with a reinforcement patch with 10 blocks of 5 layers, with a ply drop-off spacing of 15 mm in the cross-sectional direction and 30 mm in the longitudinal direction.

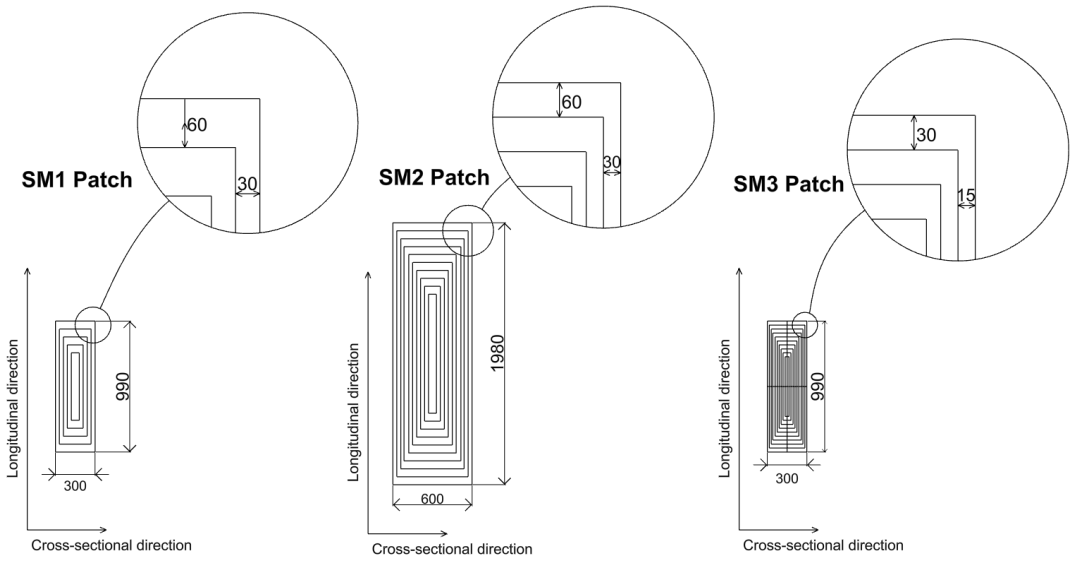

Figure 4.2: Submodels patch arrangement.

In summary, each patch ends up having the same thickness if all the layers are summed, but with different geometrical dispositions and covering different areas of the interior surface of the mast in the region of interest. It is also worth mentioning that this was designed considering that each layer of carbon has a thickness of 0.3 mm.

The design of the patches of each of the submodels listed above was performed for both shell and solid submodels, resulting in a total of six submodels for the subsequent analysis. Thus, henceforward the submodels will be referred to as their element type followed by the initials enumerated above, i.e., Shell SM1, Shell SM2 and Shell SM3 for the submodels to be analysed with shell elements and Solid SM1, Solid SM2 and Solid SM3 for the submodels to be analysed with solid elements (Figure 4.3).

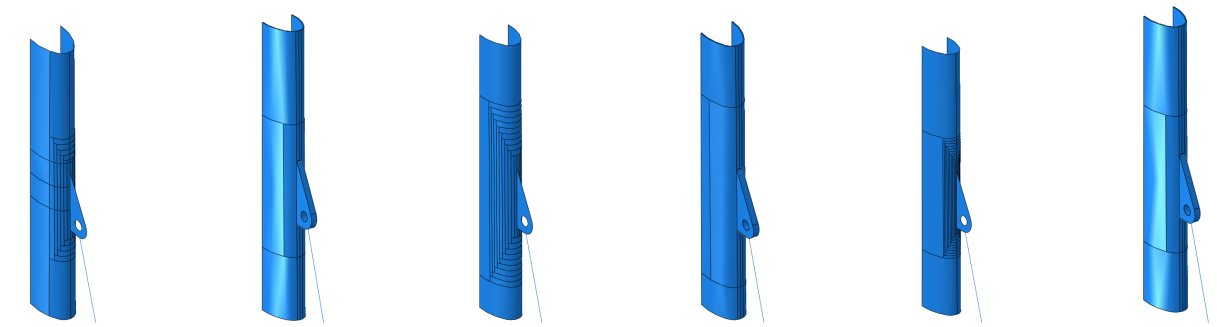

(a) Shell SM1 (b) Solid SM1 (c) Shell SM2 (d) Solid SM2 (e) Shell SM3 (f) Solid SM3

Figure 4.3: Submodels.

4.3 Material Properties

As in many super yachts, the mast being analysed in this project was designed in carbon fibre. As a material for this type of structure, it brings numerous advantages in terms of strength, performance and weight saving. The laminate lay-up that is required to build this type of structure is of high complexity and involves the application of a great number of carbon fibre plies as part of the production process, in specific orientations to optimize its strength capabilities and ability to meet the sail design and shape requirements.

Since one of the most predominant loads that the mast faces its in the longitudinal direction, the mechanical properties should fulfil this condition.

As previously mentioned, the complexity of the composite lay-up lead to the decision of defining the mechanical properties of the mast as an anisotropic material, based on common values of carbon fibre reinforced plastic (CFRP) used in the industry with the characteristics shown in Table 4.1.

Table 4.1: Material Properties.

Property	Mast CFRP	Rigs Solid Carbon	Unit
E_{xx}	125×10^9	180×10^9	Pa
E_{yy}	25×10^9	10×10^9	Pa
E_{zz}	25×10^9	10×10^9	Pa
ν_{12}	0.3	0.3	-
ν_{13}	0.3	0.3	-
ν_{23}	0.04	0.04	-
G_{12}	6×10^9	6×10^9	Pa
G_{13}	6×10^9	6×10^9	Pa
G_{23}	5×10^9	5×10^9	Pa

It is worth noting that the same material properties were defined for the mast components and spreaders (Mast CFRP in Table 4.1) while for the rigs that constitute the rest of the structure, the material Rigs Solid Carbon was attributed.

4.4 Assembly

In this stage, all the components of the global model and submodels were assembled and geometrically allocated in their respective position, considering the arrangement in the technical drawings. Several aspects such as the spreader angle, rigs length, mast rake angle and chainplates position were considered in to allocate the rigs correctly. It's worth noting that the rig's length were calculated in terms of its mast connection points and the chainplates position. Table 4.2 shows the rig's characteristics.

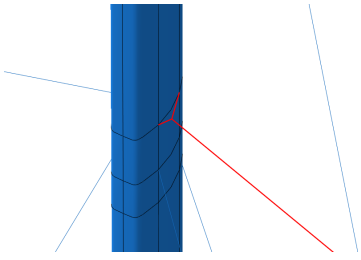

Figure 4.4: Spreader connectors.

In the case of the spreaders, since these have a oval cross-

Table 4.2: Rigs specifications.

Rig	Length [mm]	Diametre [mm]
Forestay	56821.4	24.6
Inner Forestay	46437.7	20.8
Backstay	62583.9	18.7
Babystay	35512.1	16
V1	13424.5	36.4
V2	11699.7	30.1
V3	10557.0	26.6
V4	10185.5	23.9
D1	13255.5	19.8
D2	11636.7	16.1
D3	10492.0	14
D4	9799.6	13.7
D5	8935.4	23.9

section varying through its length, a simplification was done based on the real spreader characteristics and were finally defined as circular beams with a pipe profile, having a radius equal to 290 mm and 10 mm thickness. Additionally, two connector beams were created in each mast-spreader connection with the same characteristics, forming a bifurcation of the spreader beam to prevent the rotation of the spreaders around the vertical axis, making the spreaders to be connected to the mast in two points as in reality (Figure 4.4).

Using the assembly tools in Abaqus, the entire rig system was put together.

4.5 Interactions and Boundary Conditions

To obtain an accurate behaviour of the global model, interactions were introduced to connect the structural elements that constitute the model. Added to that, boundary conditions were introduced in such a way that it simulates the attachment of the rigs and mast to the deck of the yacht as well as the mast pre-tension and backstay load as part of the load case being studied. In the case of the submodels, the respective boundary conditions were applied to transfer the loads obtained from the global model.

4.5.1 Interactions

Global Model

In respect of the interactions and starting on the rigs, these are not meant to support bending loads, therefore it was important to connect them to the spreaders and mast in such a way a that it wasn't being transferred that type of loading.

Hence, kinematic coupling constraints were applied to the locations where the shrouds and stays are connected to the mast and spreaders. This type of coupling constrains the motion of the coupling nodes to the rigid body motion of the reference node. The constraint can be applied in specified degrees of

freedom at the coupling nodes. In this case, the coupling was applied only for the translation degrees of freedom, allowing the rigs to rotate freely. This created the connection between the components without transferring bending moments or rotation to the rigs, preventing them to suffer from bending.

Regarding the interactions between the spreader and mast, Multi-Point Constraints (MPC) were applied , more precisely Beam MPC. This provides a rigid beam between the nodes to constrain the displacement and rotation at the first node to the displacement and rotation at the second node, as if there was a rigid beam between the two nodes.

This constraint was applied for each spreader beam and its connectors (visible in Figure 4.4) as well as in the connections to the mast surface. This imposes the connections between the mast and spreaders maintaining the spreader angles initially defined as in the technical drawings.

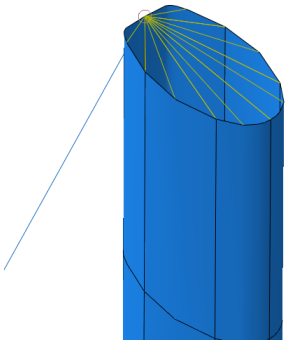

Figure 4.5: Backstay-Mast connection.

Finally, on the top of the mast, the backstay was coupled to the entire cross-section of the mast head (Figure 4.5), simulating the effect that the mast crane creates and avoiding the backstay load to be transferred at only one nodal location since that would generate a big stress concentration.

Submodels

Being the submodels, a fraction of the mast, another type of interaction had to be imposed. In the case of the shell submodels, the mast with the reinforcement and lug had to be connected with the forestay through a Multi Point Constraint, applied on the circular edge of the lug and the extremity of the forestay, the place where the end fitting of the stay is pinned on the lug in reality. This interaction provides a pinned rigid link between the nodes to keep its distance constant while the rotations are not involved.

For the solid submodels, additional interactions had to be introduced. These submodels were partitioned into three parts, the mast tube, the patch reinforcement and the lug for meshing purposes thus, tie constraints had to be applied to the contact surfaces of the parts. This constraint allows tying two separate surfaces together so that there is no relative motion between them, fusing two regions even though the meshes created on the surfaces of the regions may be dissimilar.

4.5.2 Boundary Conditions

Global Model

The boundary conditions applied on the structure, as referred to before, simulate the attachment of the structure to the yacht's deck as well as creating the load condition of the mast facing the backstay maximum allowable load.

As mentioned in a previous chapter, these structures must have a pre-tension state to ensure structural stability and safety, also for performance reasons. Since the pretension process is quite extensive and iterative, in this particular project a simplification was introduced, by attaching the shrouds (V1 and D1) and forestays at their respective deck level location, simulating the chain plates with Pin displacement constraint as a boundary condition. These constraints the translation degrees of freedom on the rigs extremities but allow the rigs' to rotate freely. This was done in alternative to the application of tension in the rigs. The tension in these components would be brought as a consequence of the vertical displacement applied in the mast-step.

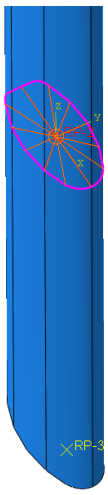

Figure 4.6: Deck-Mast connection.

An additional boundary condition imposed was the deck displacement constraint representing the hole in the deck that constitutes a support point of the mast. Using a coupling constraint, the cross-section of the mast at the deck level was coupled to a reference point in the centre of the cross-section where the translations were constraint in the longitudinal and transverse directions, (x and y-axis in the coordinate system shown in Figure 4.6). The rotational degree of freedom around the vertical axis was also a constraint (z in the coordinate system shown in Figure 4.6).

In addition, it was imposed a vertical displacement on the mast-step with a magnitude of 200 mm, pushing the mast upwards as a way of simulating the hydraulic mast jack. This boundary condition was imposed similarly as the deck-mast connection, by coupling the cross-section to a reference point (RP-3 in Figure 4.6) to apply the displacement.

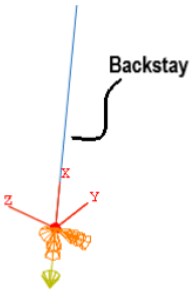

Figure 4.7: Boundary condition in Backstay.

Another fundamental part of the boundary conditions to generate the load case is the backstay load. Since the submodel's region of interest is situated near the forestay-mast connection, the backstay load is fundamental to analyse it since it generates the most critical load on this region when the tip of the mast is tensioned backwards. This load configuration is often used when the yacht's sailing upwind to improve the sails shape according to the wind and sea conditions. For that reason, the maximum allowable load with a magnitude of 25 tons was applied on the lower end of the backstay. For that reason, the displacement constraints at that point were exceptional. It was created a local coordinate system, allowing the displacement in the axial direction and rotation in the transverse axis (x and y axis

in Figure 4.7 respectively) in the Figure of the backstay and constraining the other degrees of freedom.

Submodels

Regarding the submodels, the submodel boundary conditions were applied in the respective cut-boundaries taking into consideration that shell-to-solid sub modelling requires a special option in Abaqus to be applied on the analysis when selecting the model from which the response is extracted. An important requirement for these boundary conditions to be correctly applied in the software was to allocate the submodel geometry in the same geometrical position as the global model.

4.6 Finite Element Mesh

As a topic with big significance for finite element analysis, this step of the modelling had to be meticulously executed, creating the required conditions for the mesh to be created the most efficiently. That included the creation of partitions in the geometries, the selection of the element size and the seeding of critical regions of the parts to ensure nodal allocations in desired places. Obtaining a good arrangement of the elements in the most uniform way with appropriate aspect ratios is crucial to achieve accurate results in FEA and can also affect the efficiency of the analysis in terms of computational costs.

The principal goal of these analyses was to implement sub modelling, thus the global model mesh was defined with a considerably coarse element size. It is defined by 14 shell elements (S4R - 4 node shell element) around the cross-section and an approximate element length of 900 mm, varying exceptionally on the regions where partitions were defined for the assembly and to extract results at specific nodal locations (near the submodel boundaries).

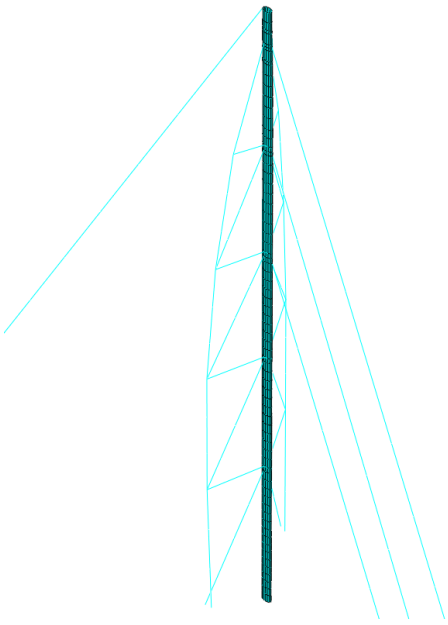

Figure 4.8: Global Model mesh.

Concerning the shrouds, stays and spreaders, these were meshed with beam elements. Although the solid carbon rigs are not meant to support compressive and bending loads as beams do, these still have a certain bending and compressive strength and are similar to a beam even so they have a large traction strength when compared to another type of loads.

Regardless of that, the loading condition and the interactions defined for the structural components do not allow to transfer bending moments. In addition, the nature of the load case, the rigs tend to be tractioned with exception of the D5 (uppermost rig connected to the mast and spreader 4) due to the backstay loading. For that reason, in the material properties of these elements, ”No Compression” property was selected, preventing the elements to transfer compressive loads onto the mast. In numerical terms, this property results in a null stress for a negative strain In practice, this would result in the slacken of the D5 shroud.

The beam element size was defined in terms of the desired elements per rig. In the case of the stays, which are larger in length, the beams were divided into 8 elements, while the shrouds were divided in 4 elements and the spreaders in 3 elements.

In the case of the submodels, a more refined mesh was implemented. For the shell submodels, the element used was the same as in the global model (S4R) with an element size that varied depending on the submodel to ensure enough node locations along the ply drop-off of the reinforcement since it would make the result analysis more accurate.

The following list shows the approximate element size of the shell submodels:

- Shell SM1 - 15 mm.
- Shell SM2 - 15 mm.
- Shell SM3 - 15 mm in the tube mast and 7.5 mm in the patch reinforcement.

The solid element submodels, on the other hand, required special attention in terms of nodal seeds allocation. In Shell-to-Solid sub modelling it is of extreme relevance that the nodes are in the submodel's cut boundary nodes are located at a small distance from the nodal locations of the global model for the interpolation of the nodal response to be more accurate, requiring a lower tolerance to transfer the displacements from the global model to the submodel. For that matter, it was pertinent to ensure that there were nodes positioned throughout the middle of the mast tube thickness, in other words, approximate to the global model's nodal positions that are geometrically defined by the mast mid surface.

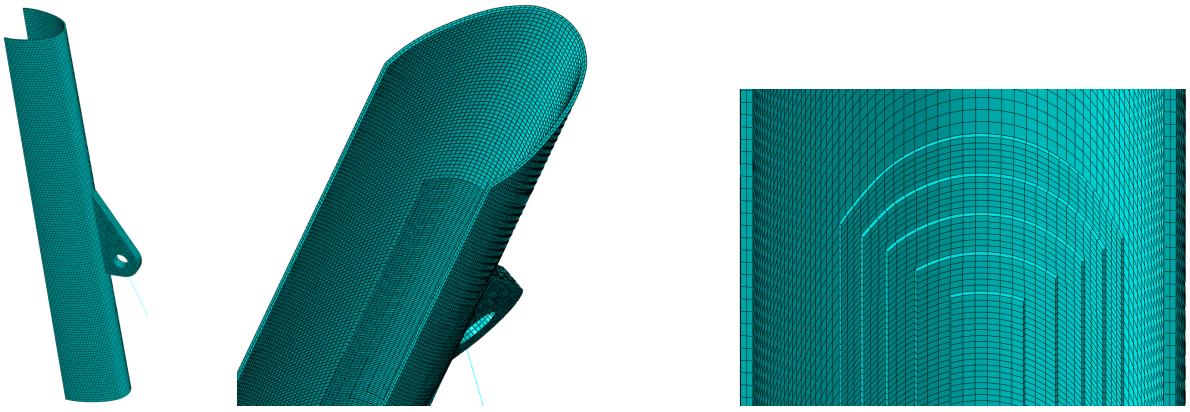

(a) (b) (c)

Figure 4.9: Solid SM1 Mesh.

The element type selected was the hexahedral solid element (C3D8R: An 8-node linear brick, reduced integration), and element size as follows:

- Solid SM1 - 20 mm in the mast tube, 10 mm in the patch reinforcement and lug.
- Solid SM2 - 20 mm in the mast tube, 7.5 mm in the patch reinforcement and 10 mm in the lug.
- Solid SM3 - 20 mm in the mast tube and 7.5 mm in the patch reinforcement and 10 mm in the lug.

Table 4.3: Solid submodels mesh aspect ratio.

Submodel	Part	Average Aspect Ratio	Worst Aspect Ratio
Solid SM1	Mast Tube	4.15	4.33
	Patch	3.17	3.79
	Lug	1.55	4.13
Solid SM2	Mast Tube	4.07	4.28
	Patch	5.55	8.67
	Lug	1.34	2.45
Solid SM3	Mast Tube	4.15	4.33
	Patch	5.63	7.25
	Lug	2.19	4.85

As presented in table 4.3, the elements aspect ratio of the submodels is increased in the patch reinforcement parts of Solid SM2 and Solid SM3 since these are composed of thinner carbon blocks (stacked layers of carbon) when compared to Solid SM1. Notwithstanding, all the values obtained for the presented mesh quality criteria are in a satisfactory range.

4.7 Results

The post processing consisted in the extraction of results with the to assess a variety of aspects such as the global model structural behaviour, the correlation between the global model and submodels, submodels stress distribution in the most critical regions to analyse the different stress components throughout the reinforcement patch and the evaluation of the parametric variation.

After running the analysis, results were extracted in the global model and each one of the submodels, using node paths that were located longitudinally and along different cross-sections. This allowed obtaining a detailed understanding of the stress distribution in components as normal and shear stress.

4.7.1 Global Model

Considering the global behaviour, as it depends on the contribution of many structural elements, the response is the result of a complex interaction between all of its components. However, there is an expected behaviour based on practical knowledge and the arrangement of the rigs that support the mast. Given the load case, it was expected that the mast was subjected to compression due to its connection to the shrouds, that are attached to the deck, while the spreaders should bend the mast backwards due to its angle and connection to diagonal shrouds. Added to that, the stays should balance the longitudinal deformation. Another aspect that's fundamental to the global response, as previously mentioned, is the tension that can be applied on the shrouds, which in this case was only achieved uniquely by the mast displacement boundary condition.

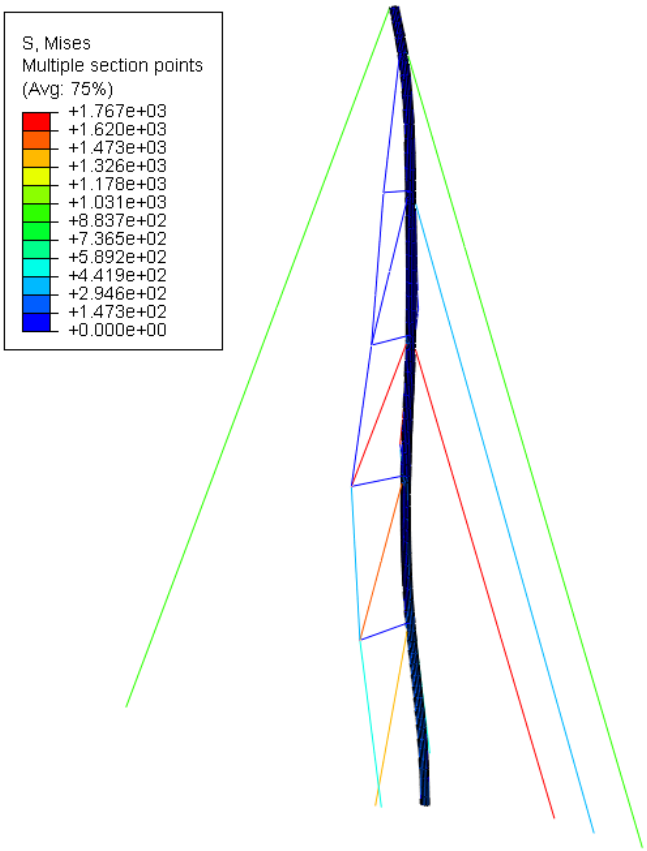

Figure 4.10: Von Mises Stress on Global Model

Although in reality, the desirable deformation of the mast would be with a slight backward deformation, in this case, it wasn't entirely achieved due to the simplification mentioned in section 4.5.1, which led to a slight forward deformation near the baby stay. Most certainly, the application of multiple predefined tensions on the upper diagonal and vertical shrouds simultaneously with the displacement of the mast step would lead to the desired response. However, this solution would require an iterative process to verify the loads achieved for the desired curvature and the total compressive load on the mast step, which is normally used as an empiric reference.

Despite that, the global model exhibited an accurate behaviour of the structure, where the vertical displacement on the mast generates tension on the rigs, components the higher stresses of the structure are observed. Added to that, the load generated by the backstay, pushing the tip of the mast to the aft, clearly created a bending effect on the higher part of the mast, generating tension in the forward face of the mast and compression in the back face of the mast which is a proper behaviour given the load condition and stress results, reaching the a highest of approximately 1.8 GPa produced by the tensile load in the baby stay an D3 shrouds , being in the allowable range given the fact that High Modulus Carbon present in the composite industry can go up to 2.8 GPa in tensile strength.

In Figure 4.10, it is visible the Von Mises Stress result for the global model response and the curvature obtained from the mast.

To validate the displacement results, nodal displacements were extracted at the same location in the

global model and submodels. To do this, it was considered two cross-sections of reference to extract the results in the different models. This led to conclude if the stiffness of the global model and submodel correlated. For that matter, the cross-sections aforementioned were allocated at a distance of 300 mm from the submodel's boundary and its corresponding location in the global model.

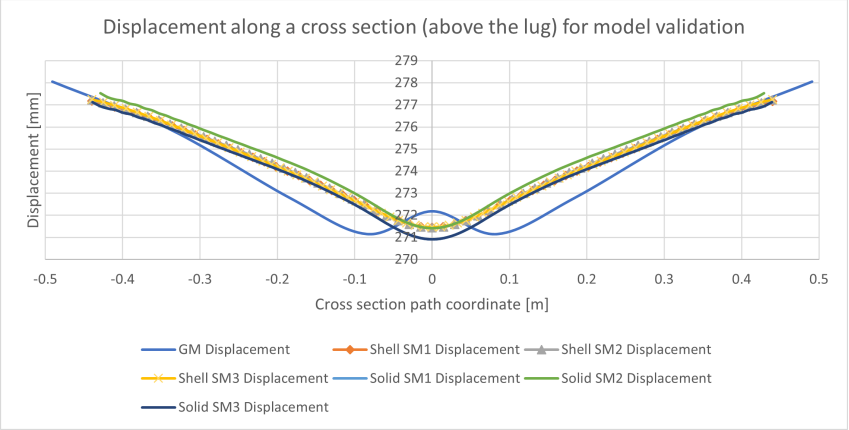

Figure 4.11: Cross-sectional displacements for model validation: Cross-section above the lug (near the highest submodel boundary).

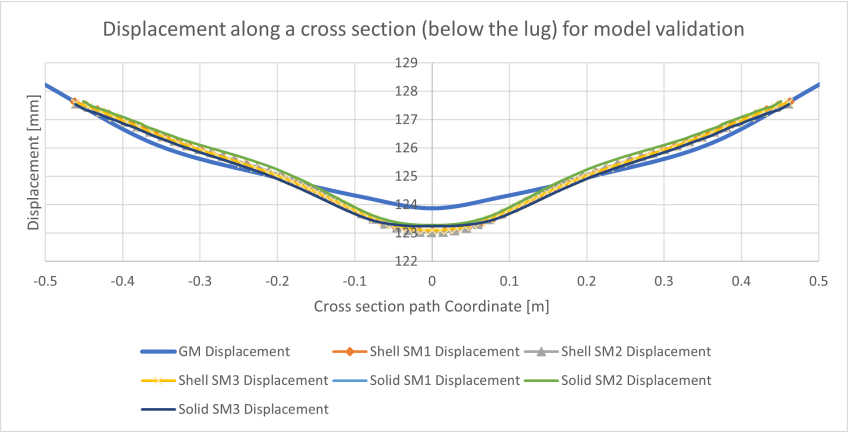

Figure 4.12: Cross-sectional displacements for model validation: Cross-section above the lug (near the lowest submodel boundary).

From the displacement results (Figures 4.11 and 4.12), it can be observed that the submodels results in the same region as in the global model correspond to similar responses, having a maximum deviation of 0.8% and 0.7% in graphs a) and b), respectively. It's relevant to note that the displacement presented is the magnitude displacement resulting from the contribution of its three components.

4.7.2 Submodels

After verifying the obtention of proper results for the global model and its correlation with the submodels, stress results were extracted in different components to achieve a detailed stress analysis of the structure in the reinforcement patches. The results were post-processed in such a way to make visible the most critical regions of the structure considering different stress components. It was important to

observe the stress distribution along the submodel's length (longitudinal) as well as in the cross-sections that intersect with the patch in different regions, allowing to create a very detailed representation of results. For that matter, multiple paths were created to represent the results for every cross-section that intersected a different combination of ply drop-off blocks, i.e., consecutive cross-sectional paths were generated including each one of the carbon blocks that constitute the patch reinforcement. This allowed to analyse the stress distribution along the cross-sections positioned in the different 'steps' of the ply drop-off.

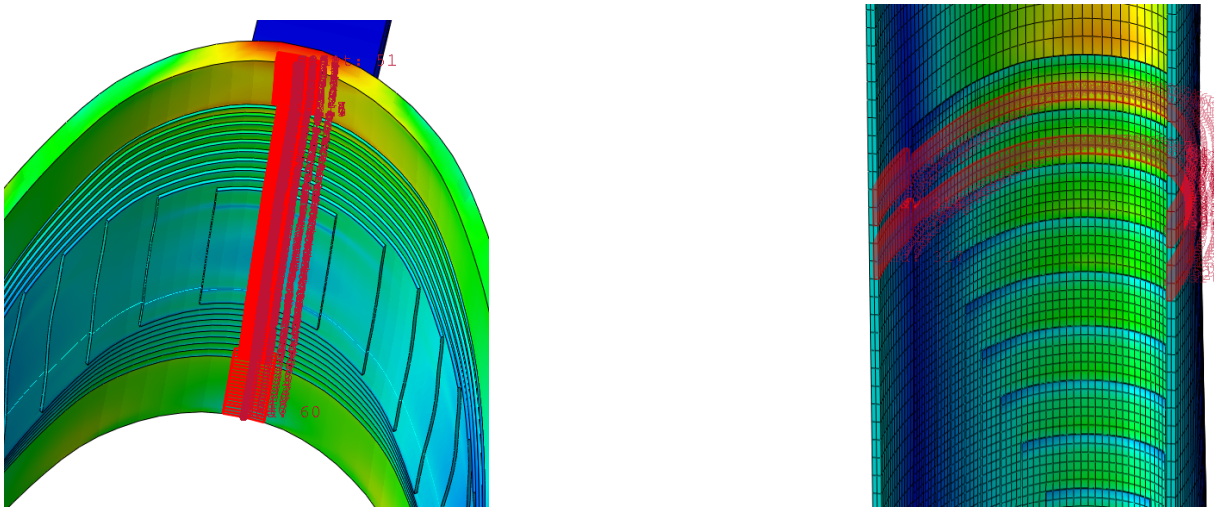

(a) Longitudinal path on Solid SM2.

(b) Example of cross-section paths in Solid SM2.

Figure 4.13: Examples of paths created for submodels' result analysis.

Figures 4.13 represents an example of the paths created to post-process submodels' results. Not all the cross-section paths are graphically represented in (b), the figure shows just a representation for a better understanding. For each one of the drops in reinforcement thickness, there is a cross-section path.

It is important to note that the response of the submodels was extracted at similar locations in both shell and solid submodels for comparison. In the Figure presented (4.13), a solid submodel was presented as an example and it is visible that the results were extracted in the inner surface of the mast tube and patch reinforcement since that region is of most interest for the designed parametric variation. In the case of shell submodels, the surface nodes were selected for this purpose, since their thickness is represented relative to the mid surface or an offset reference surface (as modelled in the reinforcement patches to imply the thickness drop-off).

Lastly, it should be mentioned that the region of the submodel used to analyse the results was the part of the reinforcements situated above the lug since it is where the highest stress values were achieved and, the paths introduced in the last paragraphs allowed to assess stress components as Normal Stress, Von Mises Stress and In-plane Shear stress.

In the following sections, results will be presented and subdivided according to the submodel's reinforcement patch in question with a comparison between the element type used for each design solution (solid and shell). Moreover, only the most relevant cross-section paths were presented to help the visu-

alization. In Appendixes B, C and D it will be possible to observe all the remaining results in graphs for a more detailed observation.

Submodel 1

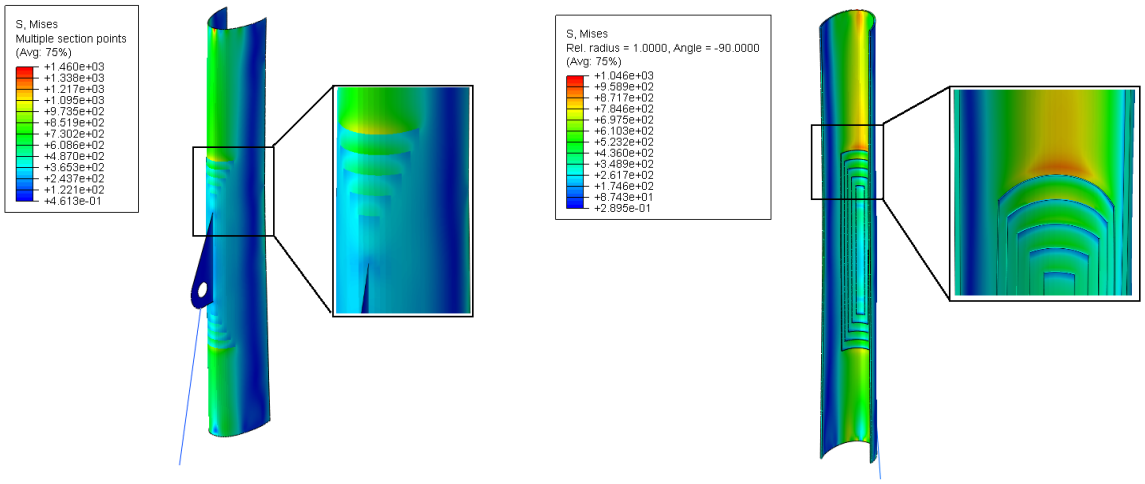

(a) Von Mises Stress in Shell SM1.

(b) Von Mises Stress in Solid SM1.

Figure 4.14: Von Mises Stress results in MPa for Submodel 1 (Shell and Solid elements).

This is the submodel with the highest drops in thickness throughout the reinforcement patch. Being constituted by 5 blocks of 10 layers of carbon each, it results in a drop in thickness of 3 mm at each block present in the patch. To make a global analysis of the stress state, the Von Mises Stress as an equivalent stress represents a good overview, considering all stress components despite not considering its directions (Figures 4.14 and 4.15).

To analyse better the stress distribution, the normal stress was represented in graphs for different locations of the submodel.

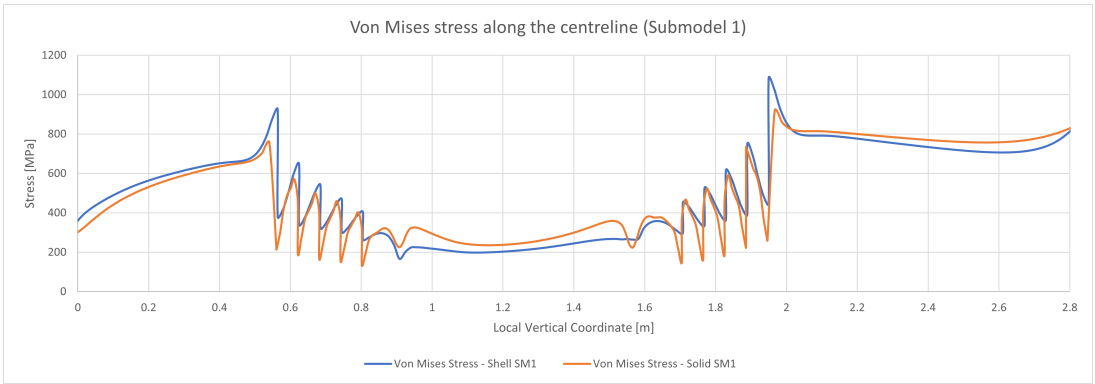

Figure 4.15: Von Mises Stress along longitudinal path of Submodel 1.

From the response of the submodel, it was concluded that the main component in the resultant stress state comes from the normal stress generated by the backstay load. It is also visible that the reinforcements generate a decrease in the stress as the ply drop off thickness increases as was expected and a

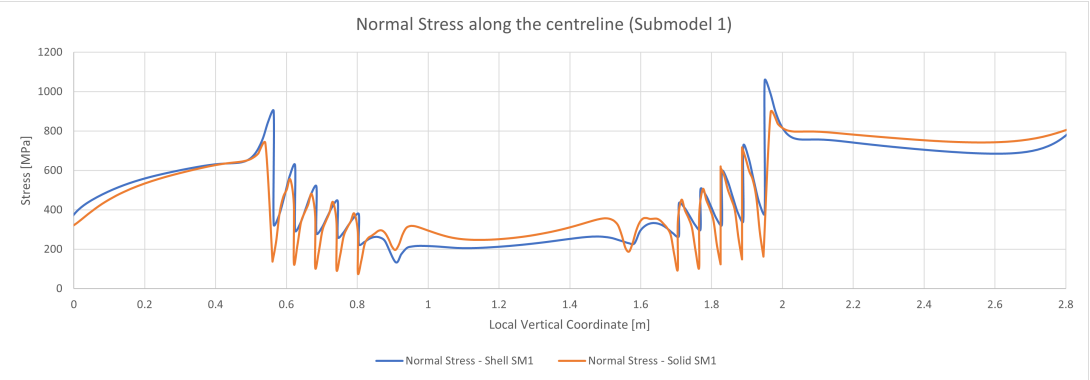

Figure 4.16: Normal Stress along longitudinal path of Submodel 1.

low stabilized stress value in the region of the lug since it is where the highest thickness is present. The longitudinal stress distribution in Figures 4.15 and 4.16 show, very explicitly, the role of the reinforcement and how it can drastically decrease the stress value in a short distance.

When comparing the results obtained from the shell element submodel and solid element submodel, it can be seen that, although the behaviour is very similar, the solid elements compute a drop in the stress value considerably higher than the shell submodel. That is observed only in the lower peaks of the stress values, in the maximum values of stress results are similar.

This sumbodel showed a maximum normal stress drop (variation) of approximately -668 MPa for the shell submodel and -733 MPa for the solid submodel at the local vertical coordinate of 1.95 m, the location of the highest extremity of the reinforcement patch. This is a tremendous decrease in stress due to the reinforcement, resulting in a relevant increase of strength for the structure in this region. On the other ply drop-off steps it is also visible that the drops in stress decrease in amplitude.

To visualize the normal stress distribution along the cross-sections, the most relevant cross-section results were selected. More precisely, it was selected a cross-section situated on the inner surface of the mast tube, close to the reinforcement patch. The second cross-section selected intersects with the first block of the reinforcement patch. These two cross-sections are situated in the region where the highest stresses are observed and are located at approximately 70 mm apart. Lastly, a third cross-section was selected at a location that intersects with all the blocks of the ply drop-offs.

It is visible in both graphs of Figure 4.17 that the stress transition along the cross-section is not as abrupt as in the longitudinal path shown before. This is related to the nature of the loading condition since the mast is being pulled backwards by the backstay load. This generates maximum normal stress in the zone that's furthest away from the cross-section neutral axis. Meanwhile, in the extremities of the graph, which represent a region of the cross-section that's situated closer to the back face of the mast, it can be seen that the normal stress is reduced, reaching zero at the neutral axis and becomes negative, indicating the compression on the other part of the cross-section.

Analysing this submodel more specifically, it can be observed that in the first graph of Figure 4.17 there is a considerable gap between two cross-sections that are 70 mm apart from each other and it is maintained throughout the width of the patch reinforcement (interval of [-0.15,0.15]), emphasising the utility of the reinforcement. The visible gap takes a maximum value of approximately -340 MPa and -290

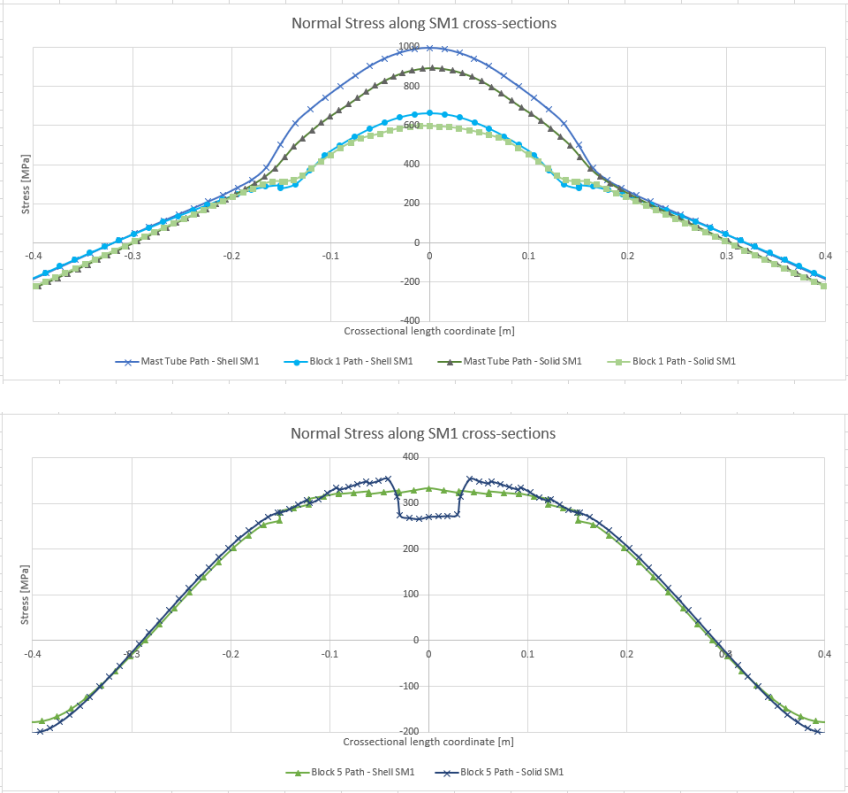

Figure 4.17: Normal Stress in selected cross-sections of Submodel 1.

MPa in the shell element and solid element submodels, respectively, showing the reduction of stress that the reinforcement can bring to the structure.

Although in general there is a similitude between the two element type submodels, it is clear that the shell submodel presents higher stress values. Furthermore, in the centre of the second graph of Figure 4.17, there is a considerable drop in stress for the solid element submodel, a region where the reinforcement thickness at the location of that cross-section is maximum. Similar gaps can be observed in the other normal stress results presented in Appendix B. In contrast, this is not captured by the shell element submodel.

As for the in-plane shear stress analysis, it was used the same cross-section paths as in the normal stress to represent the results.

The Shear Stress graphs show how the reinforcement not only affects the normal stress components but also the shearing, creating peaks in the shear stress distribution. These sudden peaks are found principally in the locations where the thickness varies.

It is notable in Figure 4.18, that the values with higher magnitude are achieved in different regions of the cross-section. In the case of the first graph, both cross-sections achieve the biggest peaks at the location where the edge of the reinforcement is situated, indicating also that the change in the thickness due to the reinforcement patch also affects the shear stress distribution in its surroundings as visible in the mast tube cross-section. On the other hand, the cross-section situated near the lug, that intersects all the reinforcement blocks has its peaks located near the centre of the cross-section.

Comparing the element types used, it is evident that the solid element submodel computes higher

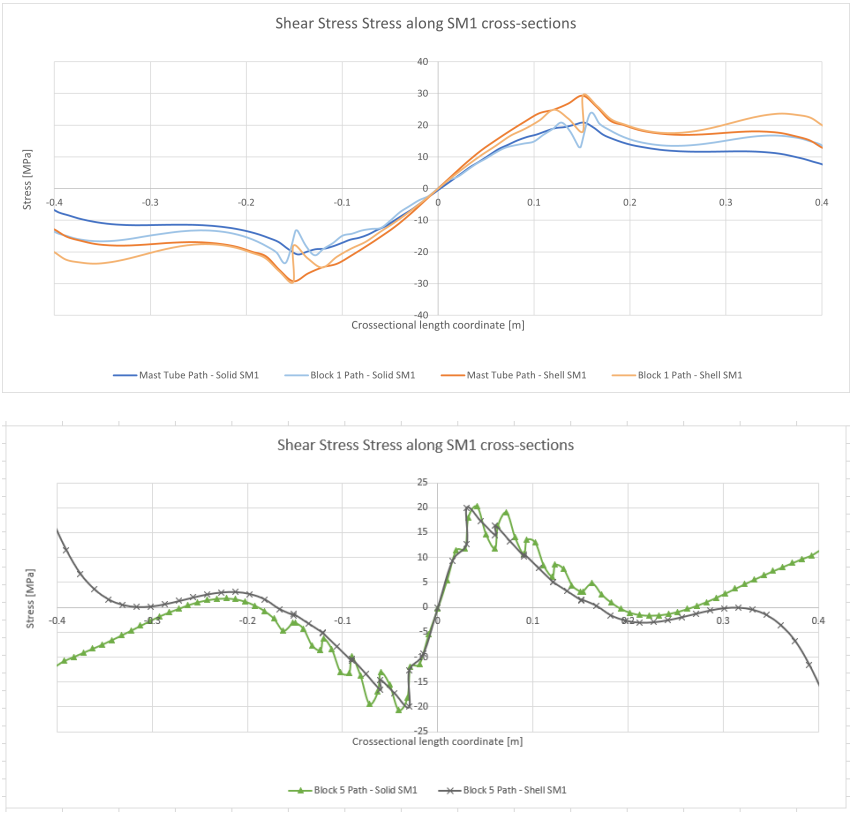

Figure 4.18: In-plane Shear Stress in selected cross-sections of Submodel 1.

variations in the stress values when the thickness changes.

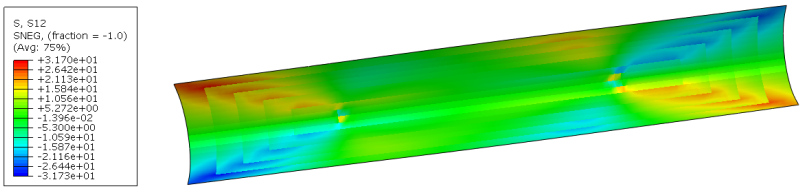

(a) Shell reinforcement patch (SM1).

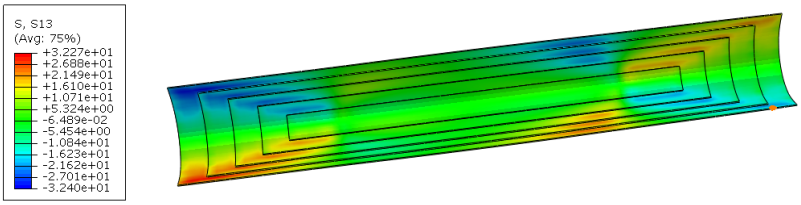

(b) Solid reinforcement patch (SM1).

Figure 4.19: In-plane Shear Stress pattern in MPa in reinforcement patch (SM1).

In Figure 4.19 it can be visualized with more detail the shear stress pattern in the reinforcement patch isolated. Although in the two submodels the results have inverted signals, this is only due to the local coordinate system, which has the surface tangent axis in opposite directions, thus the response has a similar behaviour in both submodels and that was taken into consideration when presenting the results.

Moreover, the divergence visible near the extremities of the path in the second graph of Figure 4.18,

was caused by the shear stress pattern present in the mast tube, near the submodels' boundaries. In the free-edges of that region, there is a stress gradient that has a change in the stress signal in a small area, and since the paths defined for result analysis depend on the nodal locations of the meshes, it is extremely difficult to obtain nodes at the same location for submodels created with different element types. Although the mesh is refined in the submodels and the paths were defined as close as possible to represent a similar cross-section of the mast in the shell submodel and solid submodel, the aforementioned event leads to the obtention of cross-sectional paths with a slight deviation.

Consequently, the shear stress results diverge in the region near the submodels boundaries due to this sensitive stress results region of the submodels. Figure 4.20 shows how a slight change in the cross-section allocation can create a difference in the path results for this region.

However, the singularity observed in this region is not representative of the rest of the submodels' behaviour, in both shell and solid cases. The patch reinforcement response corresponds in both submodels and its behaviour resulted as expected.

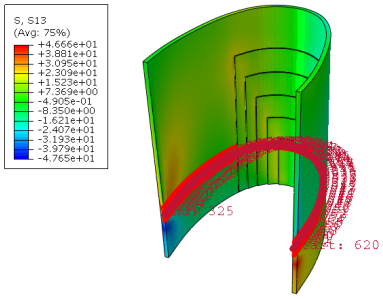

Figure 4.20: Detail of mast tube stress pattern in MPa (SM1).

In addition, a study of the peel stress (via the normal stress component in the perpendicular direction of the surface) was created to assess this stress component that is very frequently a topic of study in composite components, principally in components that are built separately and are bonded during the assembly process. In the case of the mast detail studied in this thesis, the components are indeed assembled and the carbon plies that constitute the patch reinforcement are applied and bonded to the inner surface of the mast. Figure 4.21 shows the results obtained on the edges of the reinforcement patch plies:

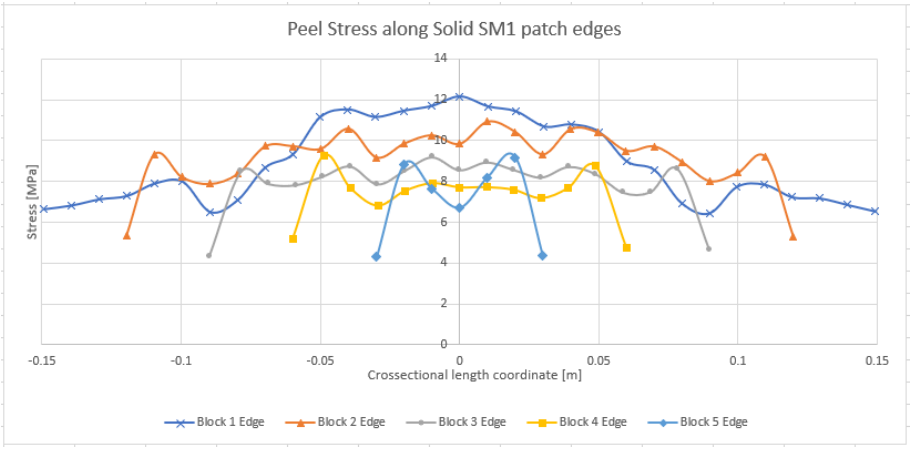

Figure 4.21: Peel Stress distribution in patch plies edges (SM1).

The edges of the reinforcement plies that were selected to represent the results belong to the uppermost extremity of the reinforcement patch (above the lug), more precisely, in the leading edges of the

ply drop-off, a region of interest to assess peel stress due to the importance obtaining a good bonding between components (Figure 4.22).

In the graph presented in Figure 4.21, the peel stress results present positive values through all the lengths of the edges, meaning that the stress state creates an effect of 'pulling' the plies of carbon in the edges due to the load condition of the mast, reaching a maximum of approximately 12.2 MPa for the outermost carbon ply. This is the ply that is is directly bonded to the mast tube. As for the other plies, it can be observed a decrease of stress as the thickness of the reinforcement patch increases.

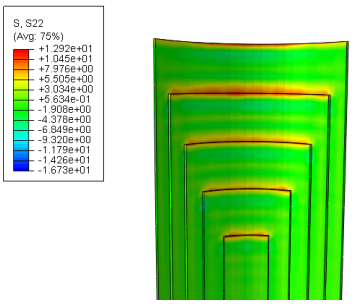

Figure 4.22: Peel stress in ply drop-off in MPa (SM1).

Note that in this last paragraph, it is referred to as 'ply, to the reinforcement patch that in practice are constituted by stacked individual laminate plies of carbon with the same dimensions to create the thickness drop-off, these group of stacked plies are first introduced as 'blocks' at the beginning of Section 4.2.1.

It should be also noted that, besides the analysis of peel stresses the ply drop-off, it was noticed that in the area of the lug-reinforcement connection, peel stress results reach the highest values, achieving a maximum of 54.9 MPa in the upper extremity of the lug as shown in Figure 4.23. This is naturally caused by the tension generated in the forestay as a consequence of the load applied in the backstay, pulling the lug downwards.

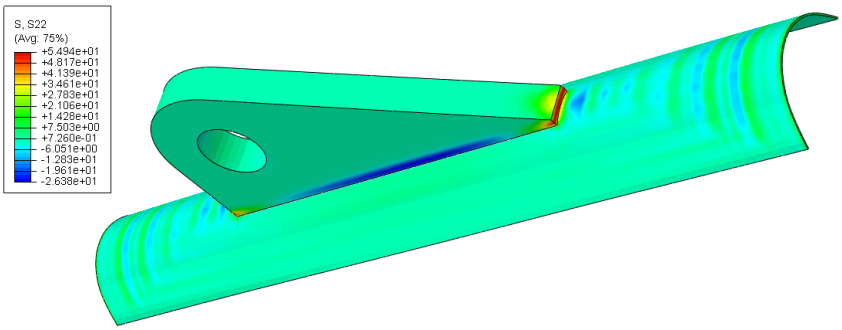

Figure 4.23: Peel Stress in lug-reinforcement connection in MPa (SM1).

Submodel 2

This submodel resulted in a design with the reinforcement patch that covers the biggest area of the mast's inner surface, when compared to the other two submodels. The idea was based on maintaining the same spacing between the ply drop-off as in Submodel 1 but applying thinner blocks of stacked carbon layers. In this case, the reinforcement is composed of 10 blocks of 5 layers each, having a drop-off thickness of 1.5 mm at each block. The drop-off spacing remained at 30 mm in the cross-sectional direction and 60 mm in the longitudinal direction of the submodel as visible in Figure 4.2.

As expected, the present submodel in Figure 4.24 has a similar behaviour as the latter submodel

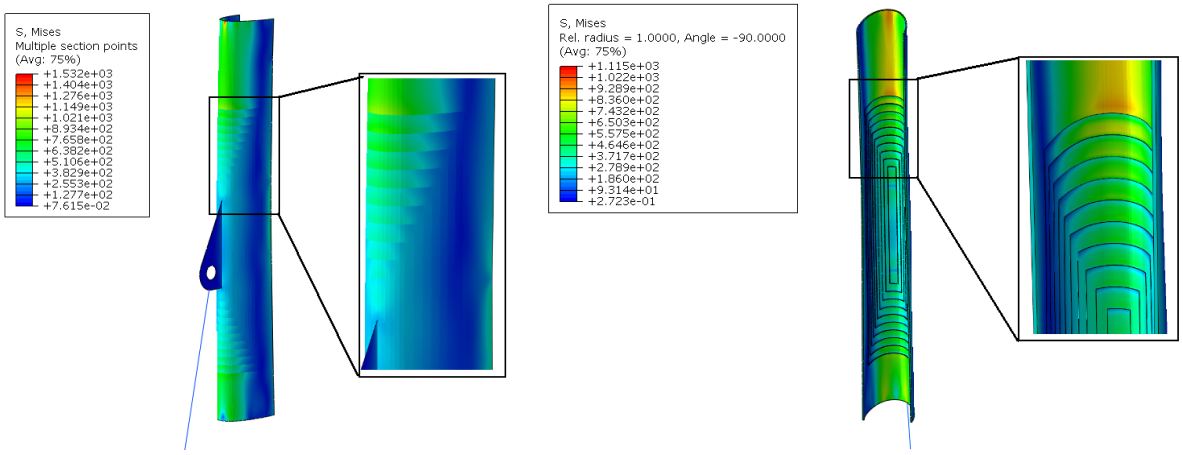

(a) Von Mises Stress in Shell SM2.

(b) Von Mises Stress in Solid SM2.

Figure 4.24: Von Mises Stress results in MPa for Submodel 1 (Shell and Solid elements).

analysed but with more reinforcement blocks, as visible in the images. In addition, the effect of the reinforcement is visible on the stress state of the submodel, principally in the solid submodel, where there is a significant reduction of the stress, in the region of the cross-section positioned most forward. This behaviour can be analysed in more detail in the following graphs.

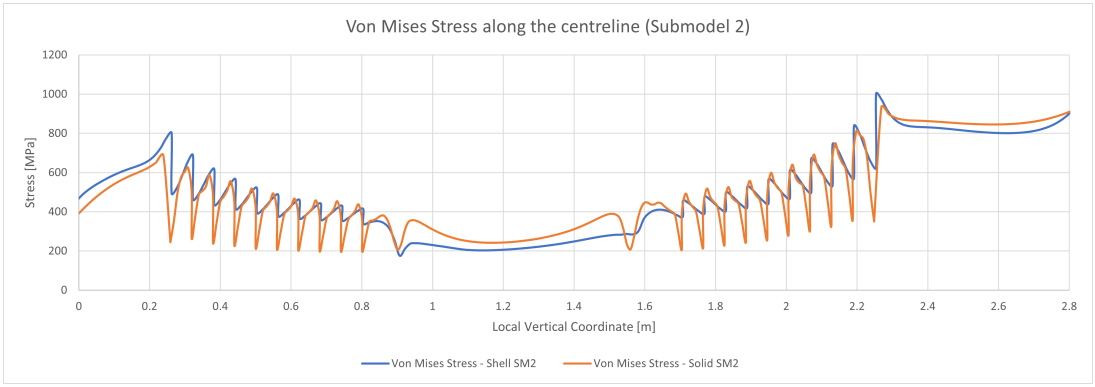

Figure 4.25: Von Mises Stress along longitudinal path of Submodel 2.

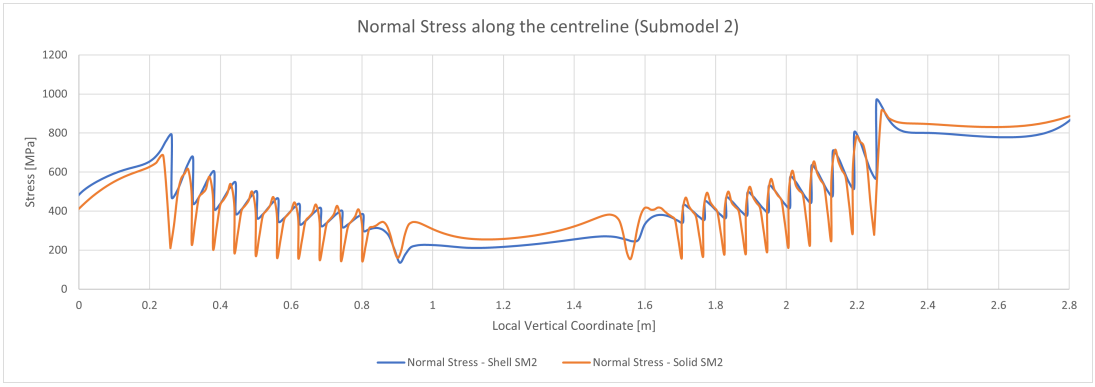

Figure 4.26: Normal Stress along longitudinal path of Submodel 2.

Once again, in similarity with the results obtained for the longitudinal distribution of Normal Stress and

Von Mises Stress in Submodel 1, the stress peaks generated by the reinforcement change in thickness are visible in Submodel 2 (Figures 4.25 and 4.26). Once again, it was verified that the shell element submodel computed slightly higher stress values than the solid element submodel. Moreover, higher amplitude of stress drops was encountered for the solid element submodel due to the reinforcement drop-offs. The maximum amplitude observed for the normal stress drop was -368 MPa and -598 MPa in the shell and solid submodels, respectively. These stress variations are located in the uppermost extremity of the patch reinforcement. Comparing these results with those observed in Submodel 1, it can be seen that the amplitude of the stress peaks is considerably smaller and the decreasing of the stress is more distributed through a bigger length since the path is bigger in area.

As for the results measured in the cross-sections, a similar methodology was applied as in Submodel 1. Several cross-section paths were created, intersecting with the different patch blocks in the upper part (above de lug) of the reinforcement since it is in that region where the higher stress values were achieved.

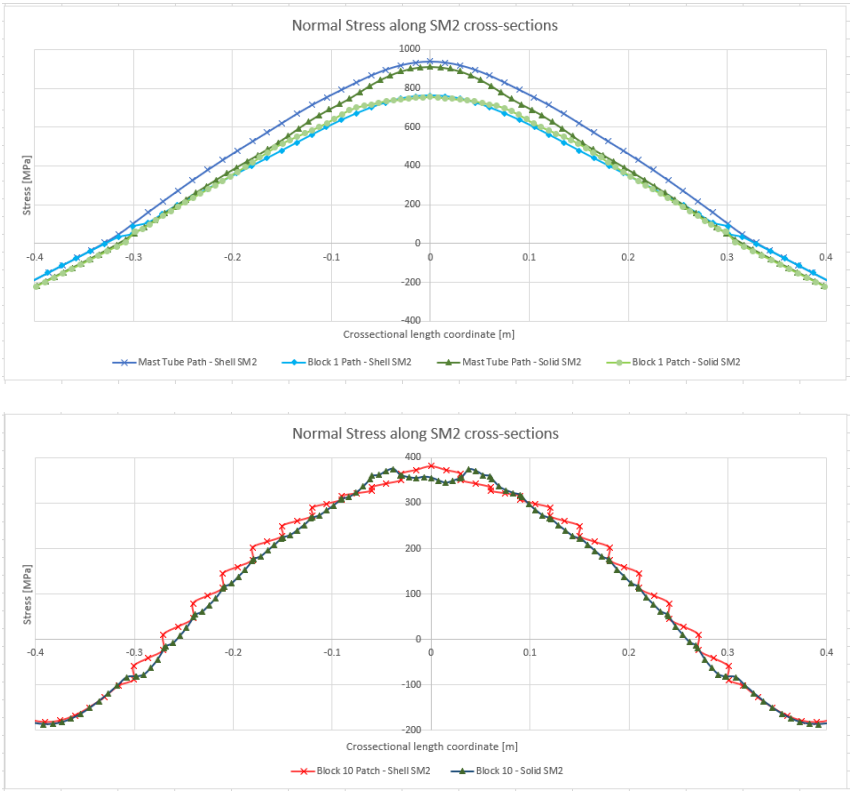

Figure 4.27: Normal Stress in selected cross-sections of Submodel 2.

To visualize the normal stress distribution along the cross-sections, the most relevant cross-section results were selected. More precisely, it was selected a cross-section situated on the inner surface of the mast tube, close to the reinforcement patch. The second cross-section selected intersects with the first block of the reinforcement patch. These two cross-sections are situated in the region where the highest stresses are observed and are located approximately 60 mm apart. Lastly, a third cross-section was selected at a location that intersects with all the blocks of the ply drop-offs.

It should also be mentioned that the cross-sections in all submodels were selected in both shell and

solid element models in such a way that these represent a very similar cross-section of the submodel. This depends, of course, on the node locations that result from the mesh, which creates a diminutive difference in the allocation of the cross-sections. This difference has been minimized as much as possible to obtain results that can be correlated.

Analysing the first normal stress graph in Figure 4.27, it is notable that there is a smoother transition of the normal stress, compared to the Submodel 1 (figure 4.17) since the patch is more extended through the cross-section length. In the second graph, similar behaviour is observed comparing to Submodel 1 in terms of the stress interval in which the results were obtained. However, more pronounced variations are observed in the locations where there is a thickness variation in the reinforcement patch, principally in the shell submodel.

Regarding the shear stress in the cross-sections, the same cross-sections were selected for its analysis.

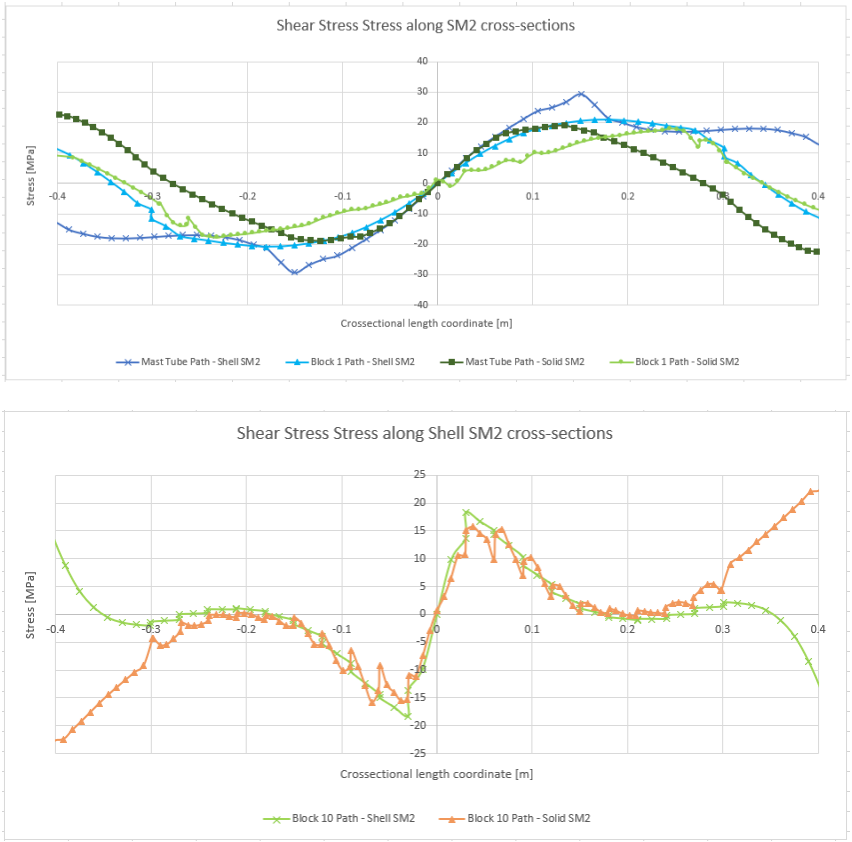

Figure 4.28: In-plane Shear Stress in selected cross-sections of Submodel 2.

From the results obtained from the In-plane Shear Stress it can be observed once again the influence that the reinforcement patch has on this stress component. Just as in the case of the normal stress, in the graphs of Figure 4.28, it can be observed that the usage of thinner carbon blocks decreases the variation of shear stress. Furthermore, the cross-sectional coordinate (horizontal axis on the graph) where the maximum magnitude of shear stress is achieved resembles to those observed in Submodel 1.

Considering Submodels 1 and Submodel 2, their reinforcement patches have similitude in geometry,

however, the first graph of Figure 4.28 presents the results for the outermost block of the reinforcement and is located in a different region of the mast when compared to the outermost block of the Submodel 1 reinforcement since the latter one has half the area of the former. This leads to conclude that not only the nature of the load case has an influence on the shear stress response but also the geometry of the reinforcement patch has its contributes to the stress pattern that is obtained. In Figure 4.29 it is visible the shear stress pattern of Submodel 2 that has similitude to the one obtained for Submodel 1. Plus, the magnitude of the highest peaks of shear stress are similar in both submodels (about 30 MPa).

In the second graph of Figure 4.28, it is clear that the solid element type computed peaks with higher amplitudes than the shell element type, in the ply drop-off locations. It can also be seen that the amplitudes of these sudden changes in stress value are lower than those observed in Submodel 1 since, in general, the stress is distributed through a larger area. This comparison is made considering the results observed in Figure 4.18.

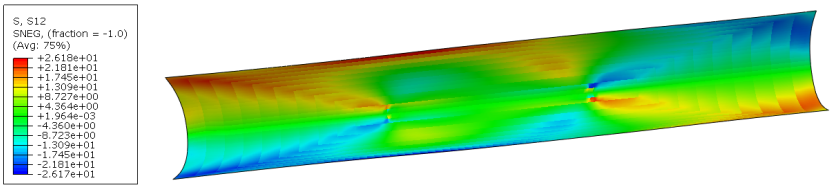

(a) Shell reinforcement patch (SM2).

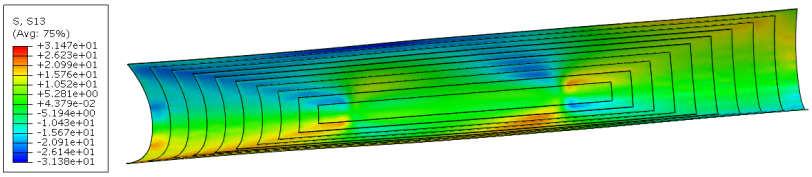

(b) Solid reinforcement patch (SM2).

Figure 4.29: In-plane Shear Stress pattern in MPa in reinforcement patch (SM2).

Once again, the results shown in Figure 4.29 inverted signals, this is only due to the local coordinate system, which has the surface tangent axis in opposite directions, thus the response has similar behaviour in both submodels and that was taken into consideration when presenting the results shown in the graphs. Plus, the divergence observed in extremities of the cross-section, in the second graph of Figure 4.28, was caused by the same event explained in the final three paragraphs of the previous section, as it was expected given the similitude in the behaviour of the submodels.

Similarly to the previous submodel, a study of the peel stress was created to assess the eventual stress concentration and can affect the bonding of the laminate. As mentioned in the previously, the edges of the reinforcement plies that were selected to represent the results belong to the uppermost extremity of the reinforcement patch (above the lug), more precisely, in the leading edges of the ply drop-off, a region of interest to assess peel stress.

In the graph present in Figure 4.30, the peel stress results present positive values through the length of the edges that were selected as verified in the previous submodel and reaching a maximum of 7 MPa in the edge of Block 2 (blocks are enumerated from the outside to the inside of the reinforcement). In

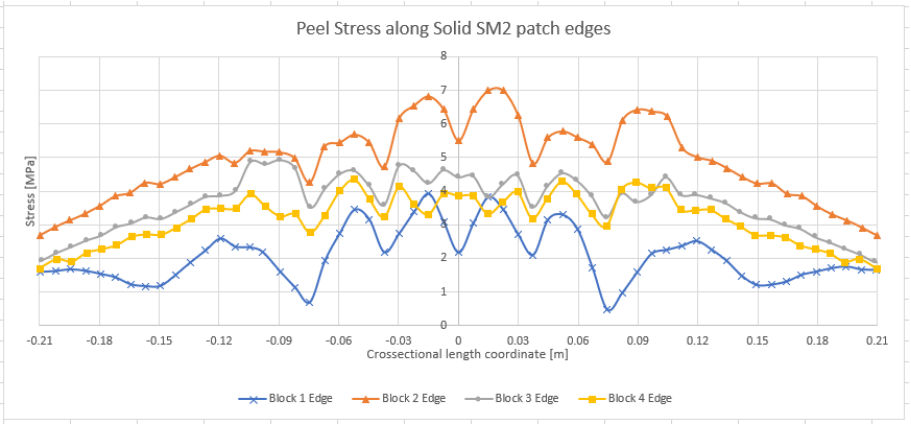

Figure 4.30: Peel Stress distribution in patch plies edges (SM2).

Figure 4.31, it is possible to observe the region where the peel stress increases, presenting an orange and red colour. In contrast with submodel 1, this submodel presented a considerably lower level of peel stress.

It's relevant to mention that in the graph presented above,it was only represented four of the studied edges since these presented the most relevant results and allow to visualize better the graph. The results obtained for the remaining edges whose results were extracted are presented in Appendix C for a more detailed analysis.

Just as it was observed in the former submodel, in the area of the lug-reinforcement connection, peel stress results reach the highest values, achieving a maximum of 82.2 MPa in the upper extremity of the lug as shown in Figure 4.32.

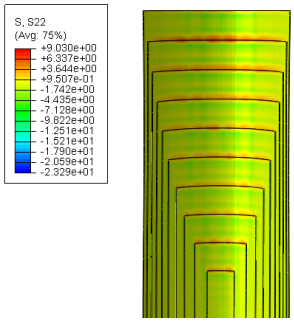

Figure 4.31: Peel stress in ply M2).

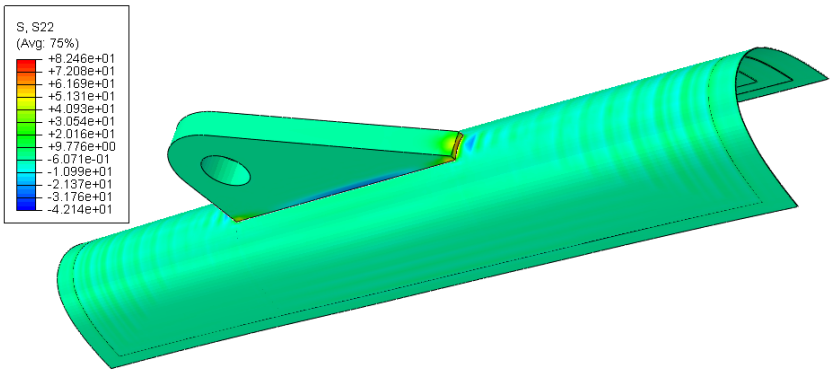

Figure 4.32: Peel Stress in lug-reinforcement connection in MPa (SM2).

Submodel 3

As the final submodel, it was opted to create an arrangement of the patch reinforcement with a smaller spacing in the blocks of the ply drop-off. This decision was sustained given the fact that it was observed some improvement in the results when the block thickness

was reduced.

Just as in the other two submodels, it was only made modifications in the reinforcement patch. The reinforcement of the present submodel is constituted by 10 blocks distributed through the patch with a ply drop-off of 1.5 mm in thickness. The spacing used in this case was of 15 mm in the cross-section length and 30 mm in the longitudinal direction, as visible in Figure 4.2.

In practical terms, the reduction of the spacing parameter would also result in a reduction of material used for the reinforcement patches, which is positive.

The Figure presented below allows obtaining an insight into the submodels stress response by means of the equivalent stress Von Mises:

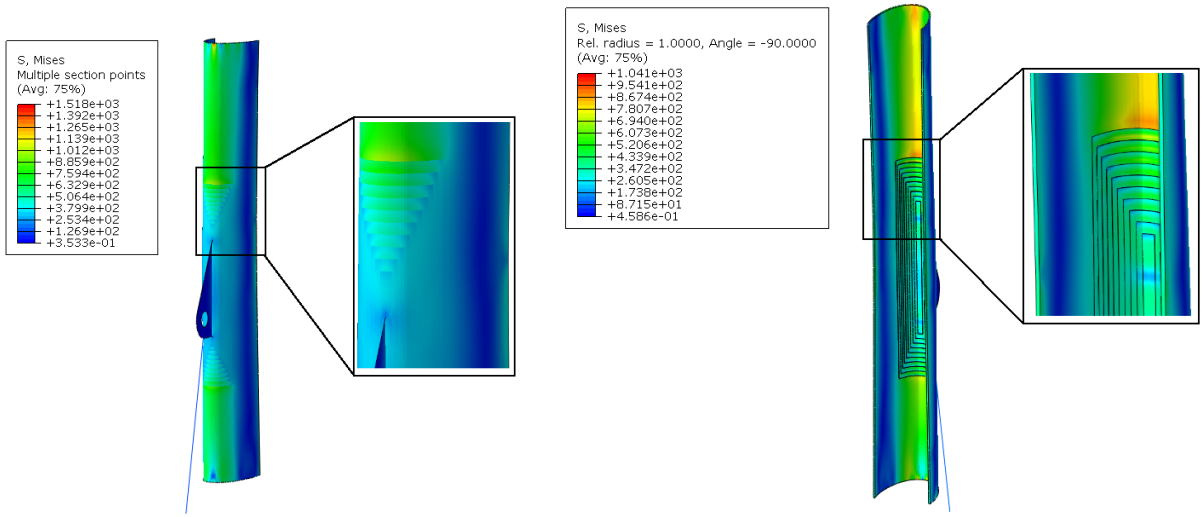

(a) Von Mises Stress in Shell SM3. (b) Von Mises Stress in Solid SM3.

Figure 4.33: Von Mises Stress results in Submodel 1 in MPa (Shell and Solid elements).

Just as in the other two submodels, it is evidenced in the Figure above that the responses have similitude, as it is visible a stress pattern. Once again, the longitudinal and cross-section stress results are presented in this section, to assess the results and compare them with the other submodels.

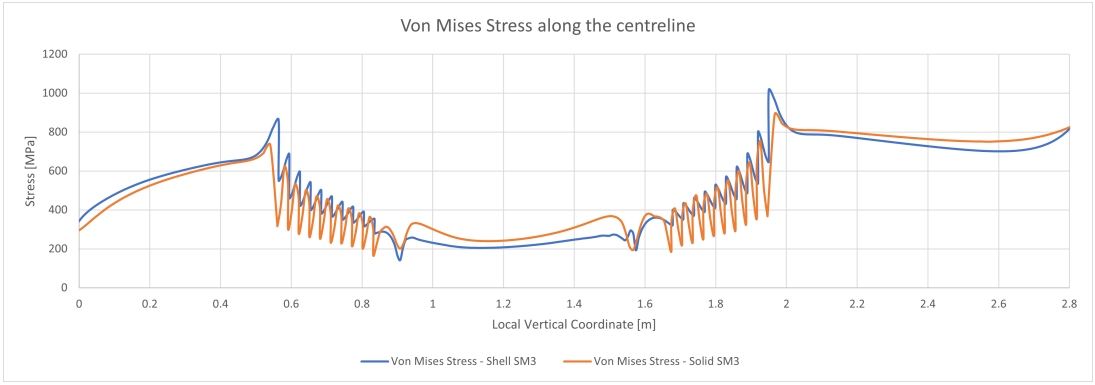

Figure 4.34: Von Mises Stress along longitudinal path of Submodel 3.

As seen in previous submodels, both Von Mises and Normal Stress graphs (Figures 4.35 and 4.34) have a similar distribution along the longitudinal path of the submodel. The successive stress variations

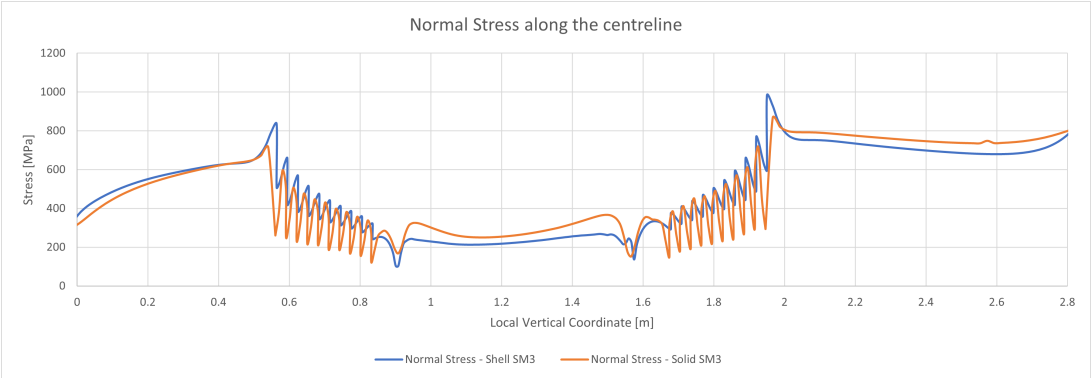

Figure 4.35: Normal Stress along longitudinal path of Submodel 3.

visible on the locations of the ply drop-off are stress changes due to the thickness variation that, on one hand, are distributed through a smaller distance when compared to Submodel 2. On the other hand, the gaps that are observed are smaller in amplitude, achieving a maximum value of -363 MPa and -523 MPa. This is a smaller variation than the one noticed in the submodels previously presented. This leads to conclude that two factors that generate a reduction in the stress variation in the reinforcement patch are the reduction of the thickness drop-off and the reduction of spacing between the different blocks.

The cross-section stress distribution is also presented in this section to evaluate the influence of the reinforcement patch along the cross-section, more precisely in components of normal stress and in-plane shear stress.

To do a selection of the results that were measured in the cross-sections, a similar methodology was applied as in Submodel 1 and Submodel 2. Several cross-section paths were created, intersecting with the different patch blocks in the upper part (above de lug) of the reinforcement since it is in that region were the higher stress values were achieved.

It was selected a cross-section situated on the inner surface of the mast tube, close to the reinforcement patch. The second cross-section selected intersects with the first block of the reinforcement patch. These two cross-sections are situated in the region where the highest stresses are observed and are located approximately 40 mm apart. Lastly, a third cross-section was selected at a location that intersects with all the blocks of the ply drop-offs.

Analysing the normal stress in the presented cross-sections (Figure 4.17), it is observed a behaviour that's significantly similar to the one observed in Submodel 1.The backstay load and other boundary conditions generate maximum normal stress in the zone that's furthest away from the cross-section neutral axis. Meanwhile, in the extremities of the graph, which represent a region of the cross-section that's situated closer to the back face of the mast, it can be seen that the normal stress is reduced, reaching zero at the coordinate that represents the neutral axis and becomes negative, indicating the compression on the other part of the cross-section.

As in submodel 1, it is also observed in the first graph of Figure 4.36, the gap between two cross-sections of -198 MPa and -150 MPa, in the shell and solid submodels, respectively. The aforementioned gap, although it presents a similar behaviour to submodel 1, it has a smaller stress variation if both submodels results are compared.

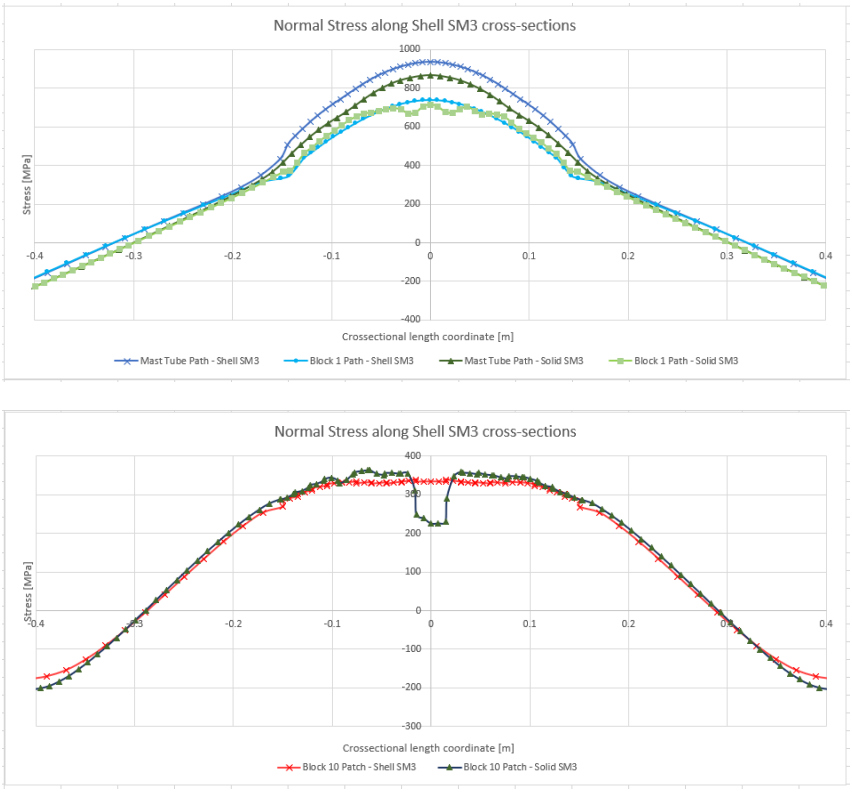

Figure 4.36: Normal Stress in selected cross-sections of Submodel 3.

It was also noticed that in the second graph in Figure 4.36, that represents a cross-section that's located near the lug, there is a drop in normal stress in the solid element submodel, event that is not captured by the shell submodel. Regardless of that, there is a similar general behaviour in both element types used to simulate this submodel.

Moreover, to analyse the shear stress in the cross-sections, the results were plotted in using the same cross-sections referred in the previous paragraphs.

In the shear stress graphs shown in Figure 4.37 it's notable the variation in shear stress due to the reinforcement patch that varies in thickness. The behaviour of the in-plane shear stress is similar to the other submodels as well as the stress pattern. However, it can be observed that the variation of stress through the drop-off are happen more suddenly due to the smaller spacing between each block. Moreover, the peaks of shear stress that are observed using solid elements for this submodel are more pronounced than in the other submodels solved with solid elements, principally in the block that's situated closer to the lug.

As it happened in the other two submodels, the results shown in Figure 4.38 inverted signals, this is only due to the local coordinate system of the reinforcement patch, which has the surface tangent axis in opposite directions in the shell and solid submodels, thus the response has a similar behaviour in both submodels and that was taken into consideration when presenting the results shown in the graphs.

As a final analysis of this project, the peel stress results are presented in the following graphs to compare with the other two submodels.

As previously mentioned, the edges of the reinforcement plies that were selected to represent the

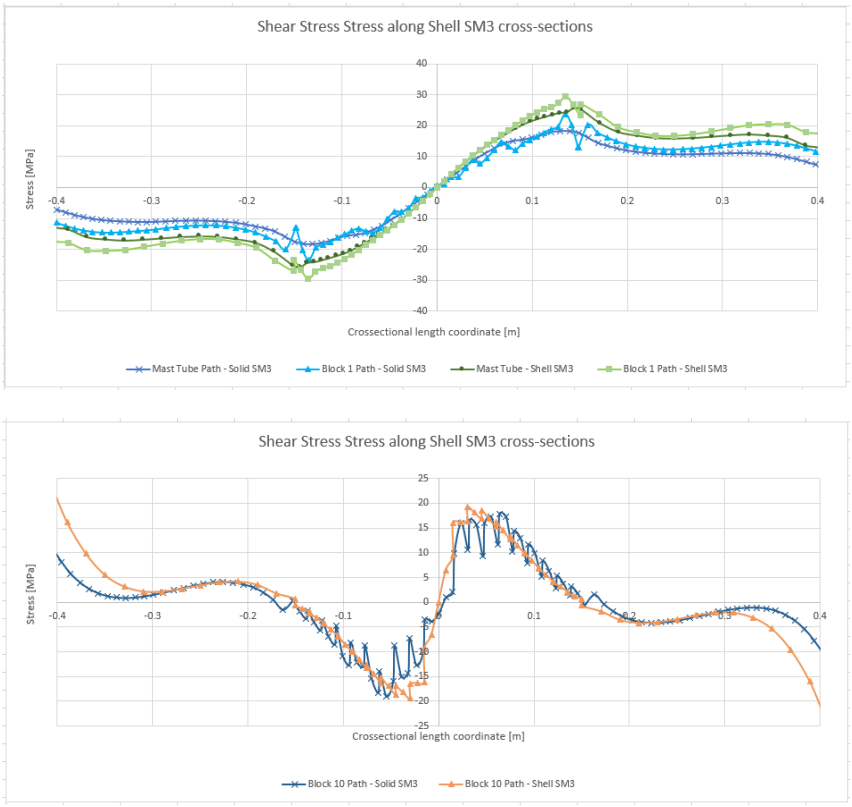

Figure 4.37: In-plane Shear Stress in selected cross-sections of Submodel 3.

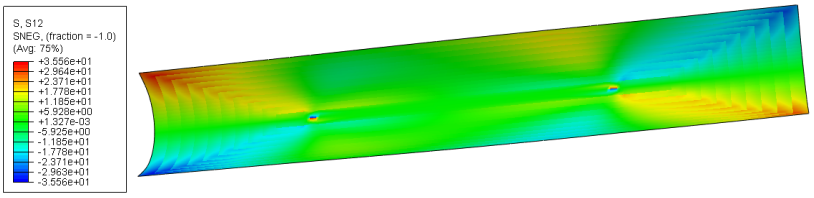

(a) Shell reinforcement patch (SM3).

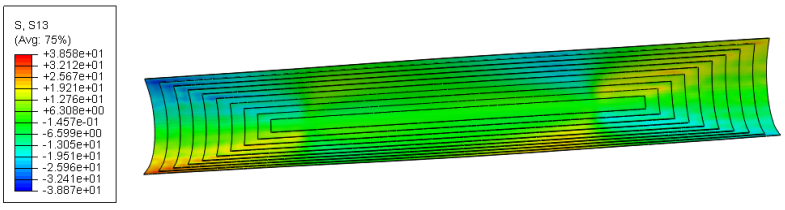

(b) Solid reinforcement patch (SM3).

Figure 4.38: In-plane Shear Stress pattern in reinforcement patch in MPa (SM3).

results were those that belong to the uppermost extremity of the reinforcement patch (above the lug), more precisely, the edges where the two reinforcement blocks make contact and a stress concentration is created, as visible in Figure 4.40. This is a region of interest to assess peel stress for bonding purposes.

In the graph present in Figure 4.39, the peel stress results present positive values through all the lengths of the edges as verified in the previous submodels and reaching a maximum of 11.4 MPa for the outermost ply, i.e., the block that's is directly bonded to the mast tube. In the other plies, a decrease in

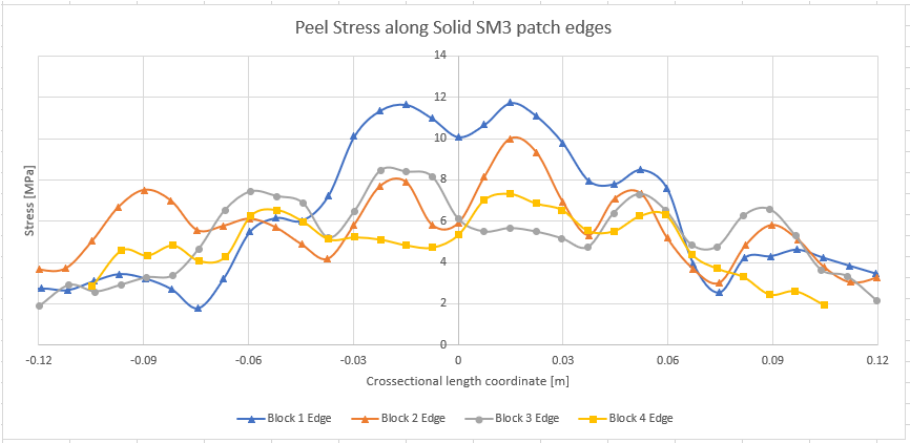

Figure 4.39: Peel Stress distribution in patch plies edges (SM3).

the values of peel stress was observed.

Just as in submodel 2, the results that were presented graph from Figure 4.39 belong to the four more relevant edges. The results obtained for the remaining edges whose results were extracted are presented in Appendix D for a more detailed analysis.

Moreover, in the region of the lug-reinforcement connection, it was verified, once again, the highest results for this stress component, achieving a maximum of 72.2 MPa in the upper extremity of the lug as shown in Figure 4.41. This behaviour, as it has been mentioned before, is caused by the tension generated in the forestay as a consequence of the load applied in the backstay, pulling the lug downwards.

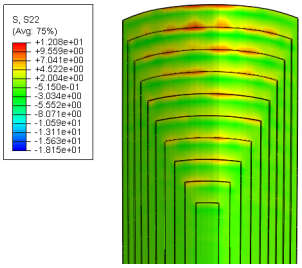

Figure 4.40: Peel stress in ply drop-off in MPa (SM3).

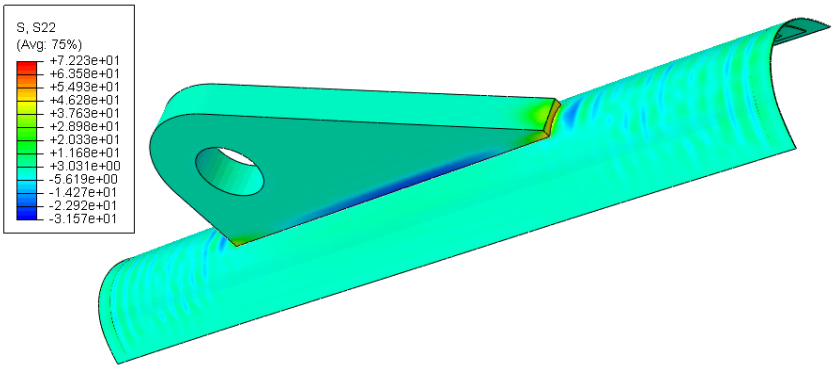

Figure 4.41: Peel Stress in lug-reinforcement connection in MPa (SM3).

From the three peel stress analysis performed, it was observed considerable differences in the results for the three submodels. Submodel 1 and submodel 3, having similitude in the patch reinforcement area resulted similar in terms of the maximum peel stress values obtained in the edge of contact between block 1 and the mast tube. On the other hand, submodel 2 obtained lower values for peel stress in ply drop-off edges.

Moreover, the stress concentration verified in submodel 2 and submodel 3 (maximum of 82.2 MPa and 72.2 MPa respectively) is significantly higher in magnitude than the one observed in submodel 1 (45.9 MPa).

To finalize the present chapter, it is relevant to state a few conclusions that were made from the result analysis. Firstly, a significant difference in normal stress distributions was noticed in the different designs that were produced for the reinforcement patches.

On the other hand, the in-plane shear stress had similar behaviour in the three submodels. Although it was noticed a change in the stress peaks due to the ply drop-off, the global behaviour for shear stress resembled in the three submodels, achieving the maximum values in a similar cross-sectional coordinate regardless of the parameters that were modified and the mast area that was being covered. The latter observation could be better seen in shell element solutions while the solid element solutions allowed to observe with more detail the variation in stress at each ply drop-off.

Finally, the magnitudes of the results obtained for the normal stress in the submodels were considered moderately high and can be allocated above the admissible limit considering the values that are acceptable (up to 800 MPa) by the composite manufacturer of the mast being studied in this thesis. In the case of shear stress, the values obtained are within the acceptable range for these materials. In conclusion, the results are still in the right order of magnitude and allowed us to obtain a good understanding of the structural analysis and the implications of the parametric variation.

Chapter 5

Conclusions

The present Master's Thesis allowed to create an approach for a structural analysis of a sailing yacht mast and its rigs, based on the fundamentals used to design this type of structure and implementing the FEA sub modeling technique to assess the structure locally. This application has great benefits for the initial stage of design for very detailed projects since it allows to implement a number of parametric variations to optimize the design and strength of structures. This way of modelling, creates a rational method to analyse different design solutions and is very engineering oriented, creating opportunity to study more complex topics such as crack propagation, contact wear and many others.

As each submodel can be ran individually, this type of analysis allow to assess a variety of details in a mast and still be indirectly coupled to a global model, generating a complex net of singular models with more detailed geometries and load cases.

From the literature found related to this type of structure, it was concluded that each scientific research presents its challenges due to the singularity of each mast design and loading conditions. In addition, the requirements of Classification Societies are not considered computationally demanding. However, in the industry and from existing scientific research it has been verified the benefits of Finite Element Analysis to design spars and rigging systems, allowing to elaborate reliable analysis to improve components in terms of strength and performance.

5.1 Achievements

The elaboration of this dissertation allowed to obtain a profound understanding of the capabilities of Finite Element Analysis on a variety of study cases, as well as in the methodology employed in sub modelling techniques. Moreover, it proceeded to the application of that technique in the structural analysis of a sailing yacht mast to create a local analysis of a region of interest and evaluate the results of a parametric variation in the design of the reinforcement patch of the lug.

Added to that, a vast amount of knowledge was acquired regarding the modelling of this type of structure, principally using the type of finite element implemented for the analysis, which is not commonly found in available literature regarding this topic.

This research was elaborated in partnership with the composite and spars design company Rondal and allowed to achieve the goals that were set throughout its elaboration and fulfil the expectations created for the results.

In this project, three design solutions were presented in the submodels, using shell and solid elements to analyse the stress distribution along with the reinforcement patch. Having that as the main focus of analysis, the third solution (Submodel 3) turned out as the one that presented the most reliable solution and presented a smoother stress transition, showing stress peaks with less amplitude and allowing to save production materials. It was also verified that the usage of thinner layers of carbon in the reinforcement to define the ply drop-off is beneficial to decrease the high stress gradients.

It is significant to state that, from the practical point of view, it is interesting to assess the best way to stack the carbon plies on the reinforcement patch and how the ply drop-off can be employed on the mast tube to optimize the stress distribution and increase the strength.

5.2 Future Work

The conclusions taken from the present study create opportunities for future work, such as developing submodels for other components present in the structure as a mean of obtaining a detailed analysis for several regions of the mast that are relevant in the load case that was created for the global model.

As additional recommendations, there are a few subjects of interest for future research such as modifying the shape of the reinforcements using curved edges to improve the shear stress concentration and introducing more detail in the pretension process, by applying tension loads in the shrouds through an iterative process.

Furthermore, alternative solutions to this structural detailed analysis could be made such as the application of shell-to-solid coupling, using mixed-dimensional elements in the same model, or implementing adaptive mesh refinement tools. Additionally, other type of sub modelling boundary conditions could be also applied, in alternative to the displacement-based boundary conditions. Depending on the objective of the analysis, the application of other governing parameters could be employed such as stress-based boundary conditions or reaction forces and moments in the submodel boundary.

References

[1] L. Larsson, R. Eliasson, and M. Orych. *Principles of Yacht Design*. Bloomsbury Publishing, 2000.

[2] G. Grabe. The rig of the research sailing yacht "DYNA" measurements of forces and fea. 1^{st} *High Performance Yacht Design Conference*, December 2002.

[3] *Design and Construction of Large Modern Yacht Rigs I*. DNVGL, 2016. Part4, Ch.2, Sec. 1.

[4] *Hints and Advice on rigging and tuning of your Seldén mast*. Seldén, 2020.

[5] P. Ploé. Scantling of sailing yacht mast and sail deformation simulation using finite elements. Master's thesis, University of Liege and Ecole Centrale de Nantes, February 2012.

[6] C. Rizzo and D. Boote. Scantling of mast and rigging of sail boats: a few hints from a test case to develop improved design procedures. *11^{th} International Symposium on Practical Design of Ships and Other Floating Structures*, 2010.

[7] A. Shenoi, R. Beck, D. Boote, P. Davies, A. Hage, D. Hudson, K. Kageyama, J. Keuning, P. Miller, and L. Sutherland. Report of committee v.8, sailing yacht design. In *17^{th} International Ship and Offshore Structures Congress*, volume 2, pages 456–470, 2009.

[8] S. Ghelardi, A. Garavaglia, C. M. Rizzo, and M. Paci. On the rig dock tuning of large sailing yachts. *Ocean Engineering*, pages 384–397, 2019.

[9] M. Gaiotti and C. M. Rizzo. Dynamic buckling of masts of large sail ships. *Ships and Offshore Structures*, 10(3):290–301, 2015. doi: 10.1080/17445302.2014.887175.

[10] *Rules & guidelines I ship technology – part 4, rigging technology*. Germanischer Lloyd, Hamburg (Germany), 2009.

[11] D. Melo. MaRSoft - Automated Yacht Mast and Rigging System Design and Analysis. *Instituto Superior Técnico, Universidade de Lisboa*, 2015.

[12] K. W. Shim, D. J. Monaghan, and C. G. Armstrong. Mixed dimensional coupling in finite element stress analysis. *Engineering with Computers*, pages 241–252, 2002. doi:10.1007/s003660200021.

[13] C. Möller and O. Sundlo. Method for merging scales in finite element analysis. Master's thesis, Chalmers University of Technology, Gothenburg, Sweden, 2017.

[14] M. W. Sracic and W. J. Elke. Effect of boundary conditions on finite element submodeling. In *Nonlinear Dynamics*, volume 1, pages 163–170. Conference Proceedings of the Society for Experimental Mechanics Series, 2019.

[15] C. Curreli, F. D. Puccio, and L. Mattei. Application of the finite element submodeling technique in a single point contact and wear problem. *International Journal for Numerical Methods in Engineering*, 2018. doi:10.1002/nme.5940.

[16] M. Kitamura, H. Ohtsubo, A. Akiyama, and K. Bandoh. Submodeling analysis of ship structure with superconvergent patch recovery. *International Journal of Offshore and Polar Engineering*, 2003.

[17] B. Valeti and S. N. Pakzad. Hybrid data + model-based submodeling method for a refined response estimation at critical locations. *Structural Control and Health Monitoring*, 2020. doi:10.1002/stc.2646.

[18] *Abaqus Analysis User's Guide*. Abaqus (6.14), 2021.

[19] N. Cormier, B. Smallwood, G. Sinclair, and G. Meda. Agressive submodelling of stress concentrations. *International Journal for Numerical Methods in Engineering*, 1999.

Appendix A

Technical Drawings

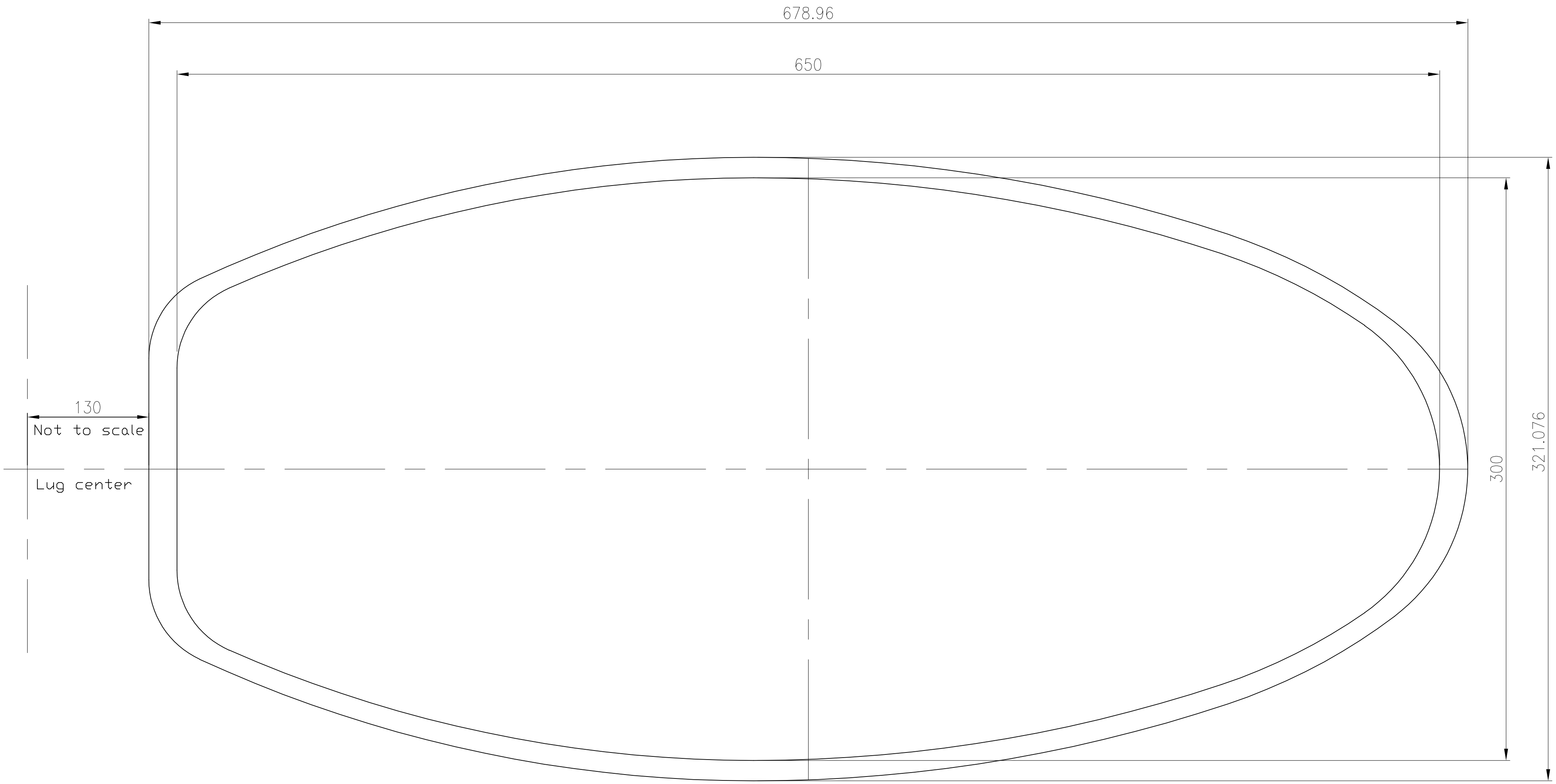

MAST SECTION Project Ingenieursburo				RONDAL Flevoweg 1d P.O. Box 52 8325 ZH Vollenhove Holland Phone: +31 527 243500 Fax: +31 527 243900 www.rondal.com info@rondal.com
Author	JJN	Project	32305	
Created	27-10-2020	Part No.	–	
Status	For information	Sheet	1 of 1	
Appr. by		Scale	1:1	
Approved		Units	mm	Drawing Number: Reference section — Revision:
		Format	A1H	

AutoCAD, C:\Users\mnan\Desktop\Students\section.dwg, 10-02-2021 2:54, MNAN

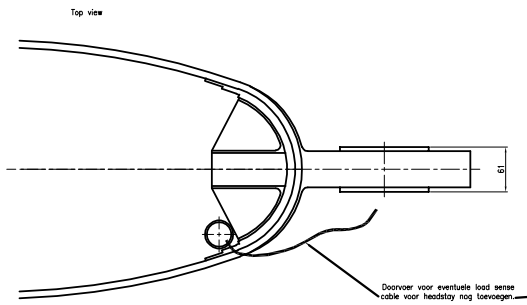

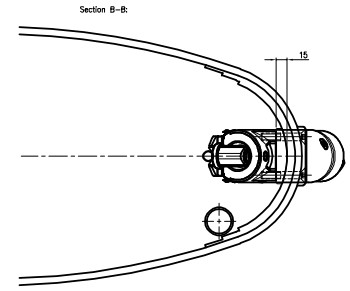

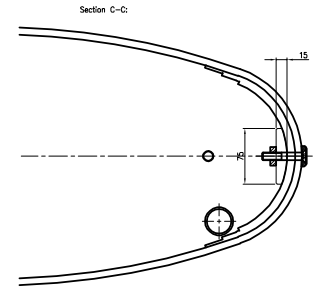

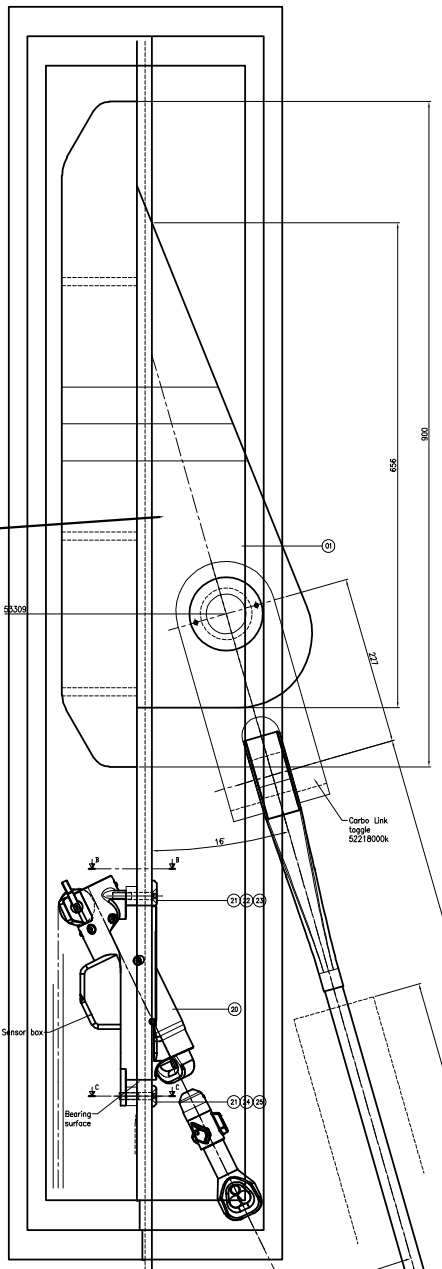

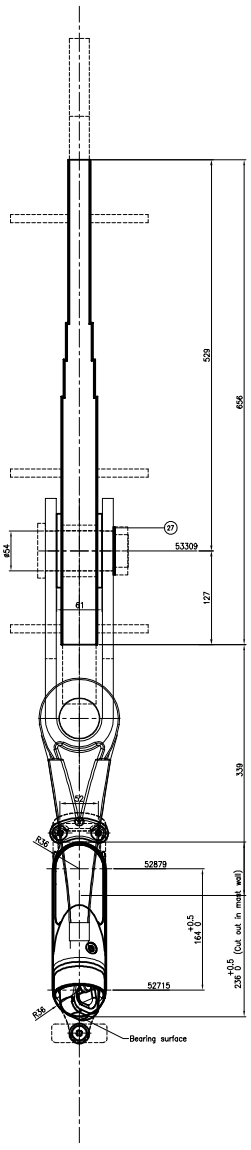

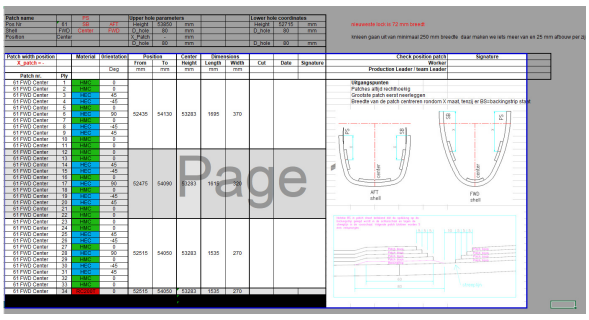

27	1	Washer		HSS 316L (1.4404)		32000-021-027	
26	1	Spacer		Tubal HSSB 3302		32000-021-026	
25	1	Washer		HSS 316L (1.4404)		32000-021-022	
23	1	Spacer		Tubal HSSB 3302		32000-021-023	
22	1	Pole		HSS 316L (1.4404)		32000-021-022	
21	3	Hex. socket countersunk head screw	M10x60	A4-70 (1.4401)			DIN 7991
20	1	Internal halyard lock 137 with sensor					Forner
01	1	Forestay lug		Carbon		32000-021-010	
Pos.	Qty.	Description	Dimension	Material	Part No.	Drawing No.	Remark

FORESTAY LUG AND HALYARD LOCK			
Author	JJN	Project	32000
Created	12-12-2019	Part No.	–
Status	Engineering approved	Sheet	1 of 1
Appr. by		Scale	1:2.5
Approved		Units	mm
		Format	ADV

RONDAL

Flevoweg 14 | Phone: +31 527 243500
P.O. Box 53 | Fax: +31 527 243800
8325 ZH Vollenhove | www.rondal.com
Holland | info@rondal.com

Drawing Number: 32000-021-000 | Revision

Appendix B

Mast Analysis Results - Submodel 1

The following figures regard to the results obtained for Submodel 1 (in shell and solid element) that were not presented previously, throughout the thesis.

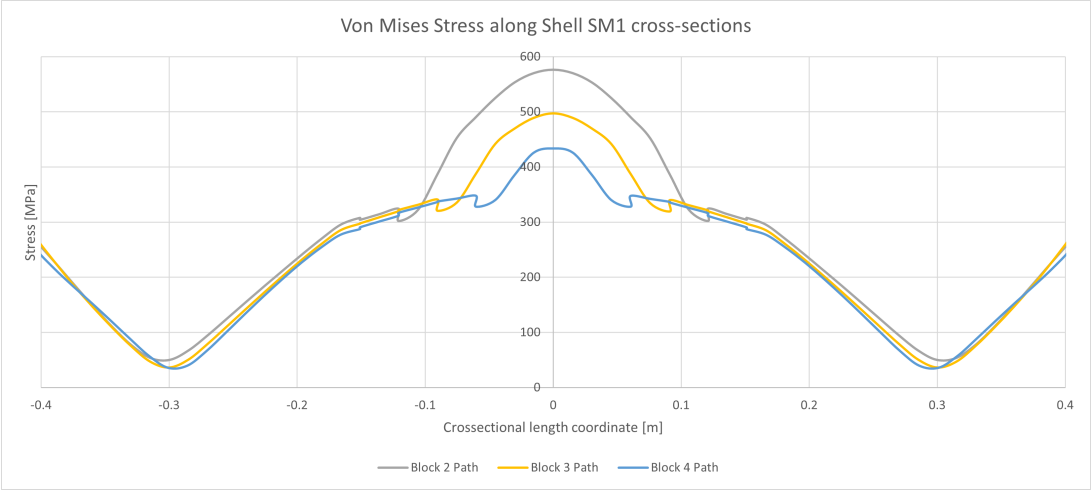

Figure B.1: Normal Stress along Shell SM1 cross sections.

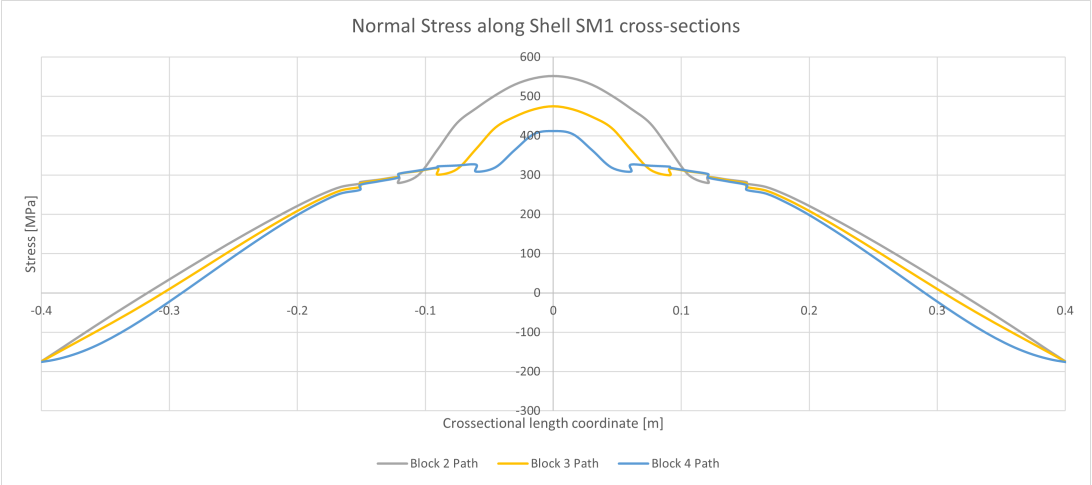

Figure B.2: Von Mises Stress along Shell SM1 cross sections.

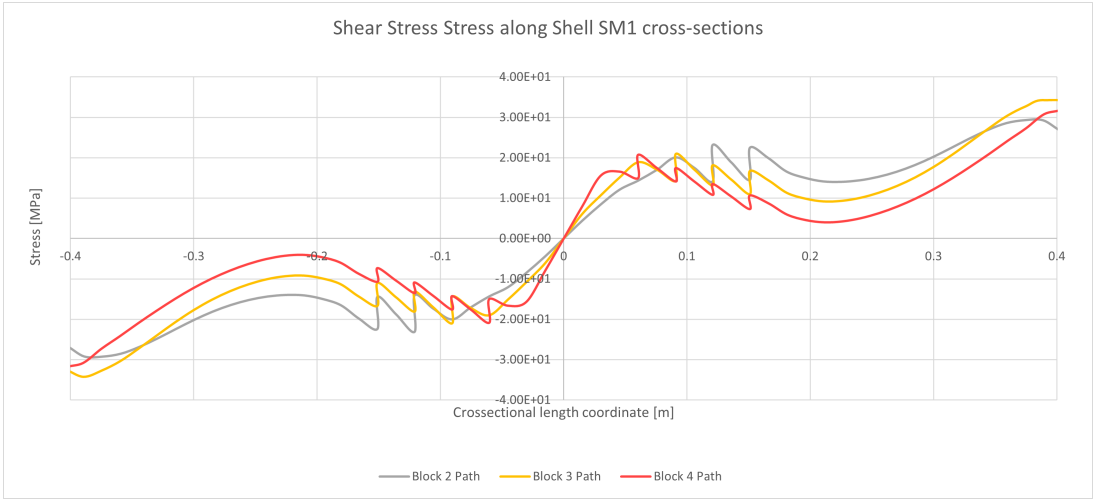

Figure B.3: In-plane Shear Stress along Shell SM1 cross sections.

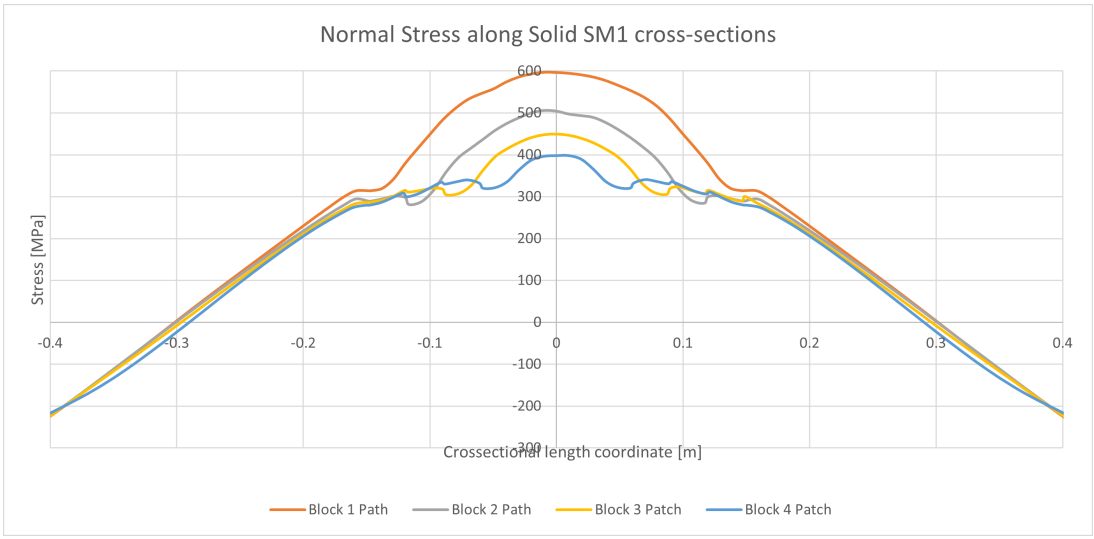

Figure B.4: Normal Stress along Solid SM1 cross sections.

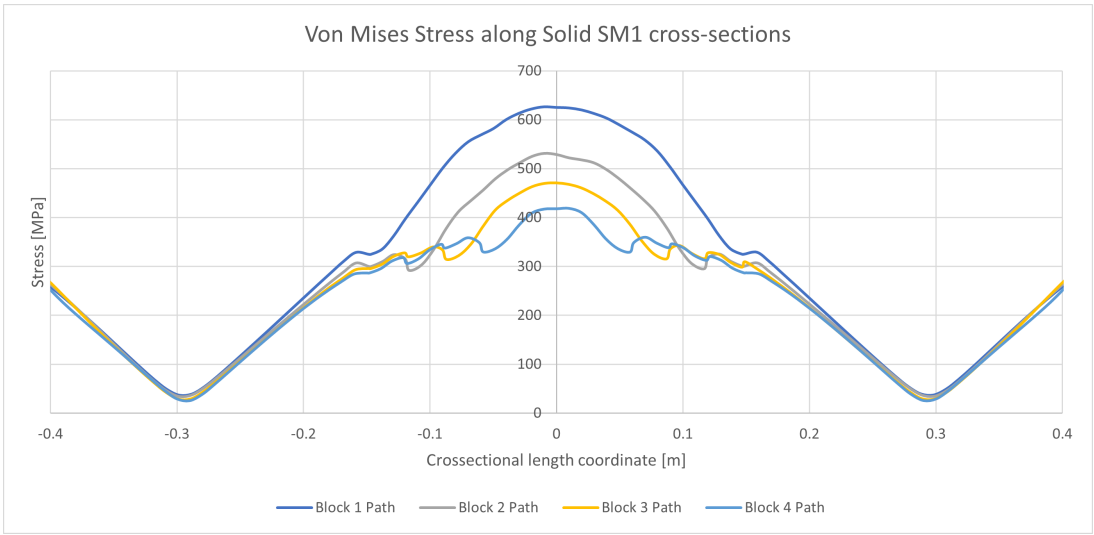

Figure B.5: Von Mises Stress along Solid SM1 cross sections.

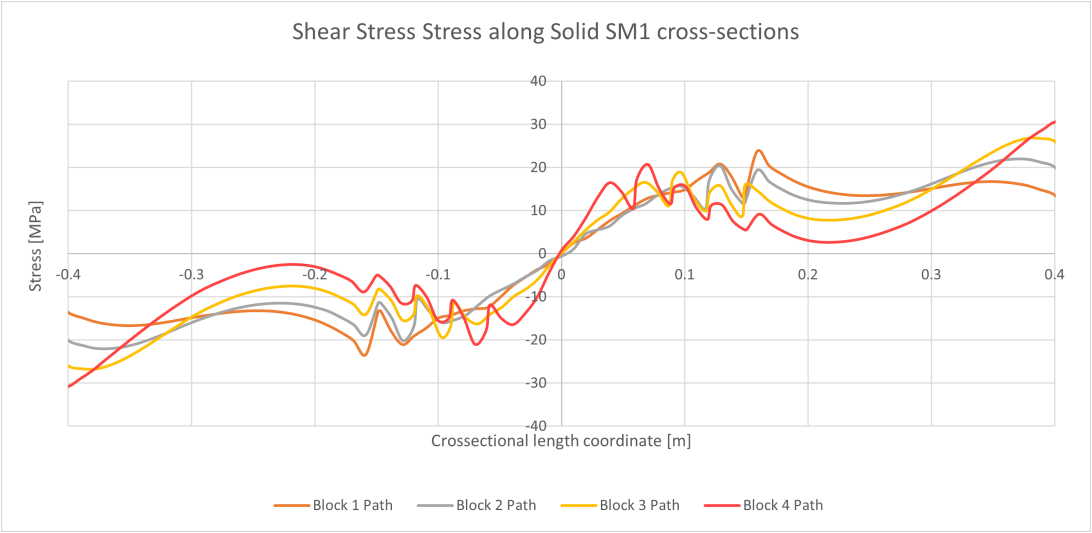

Figure B.6: In-plane Shear Stress along Solid SM1 cross sections.

Appendix C

Mast Analysis Results - Submodel 2

The following figures regard to the results obtained for Submodel 2 (in shell and solid element) that were not presented previously, throughout the thesis.

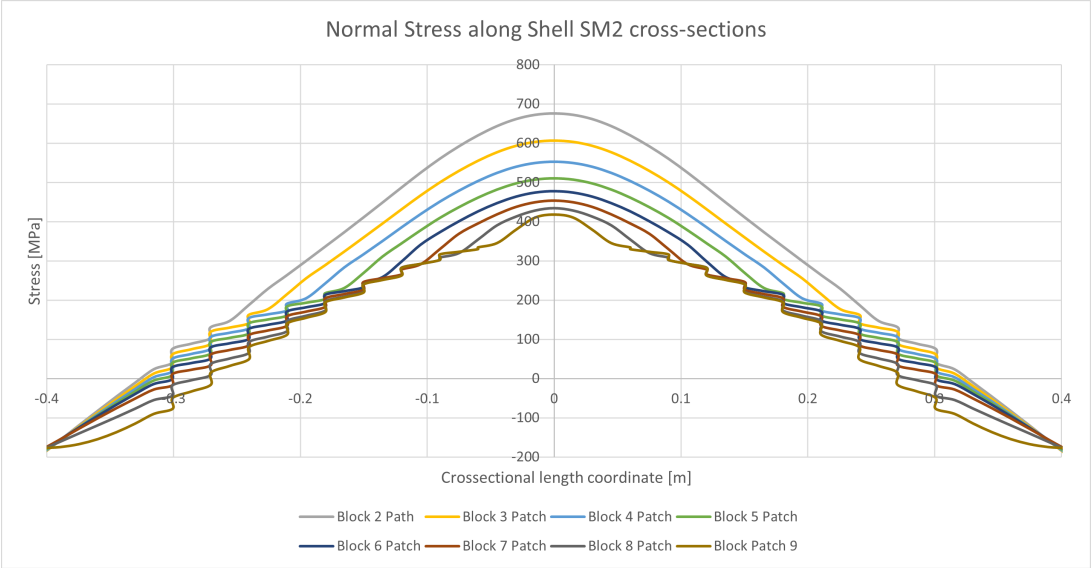

Figure C.1: Normal Stress along Shell SM2 cross sections.

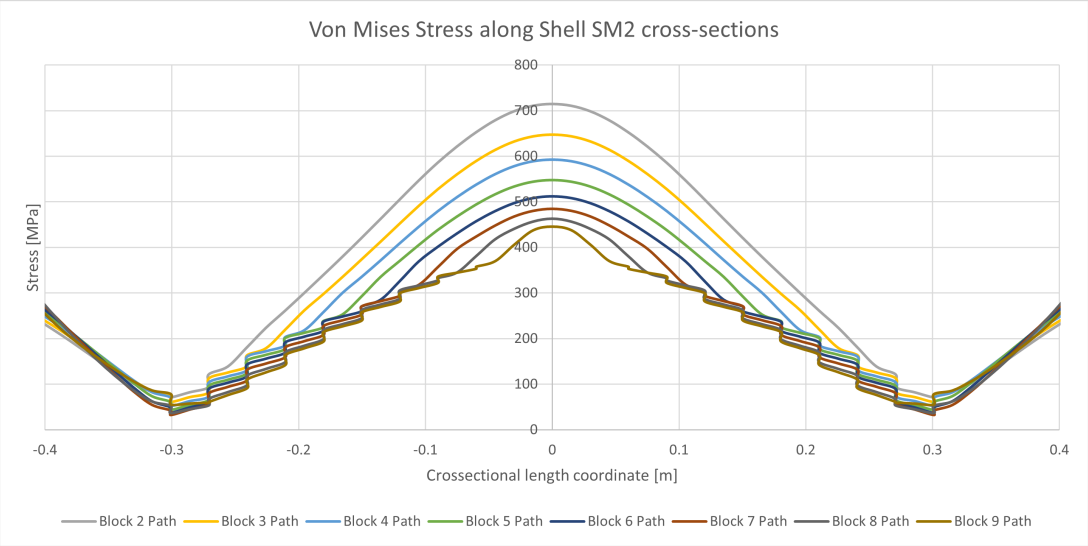

Figure C.2: Von Mises Stress along Shell SM2 cross sections.

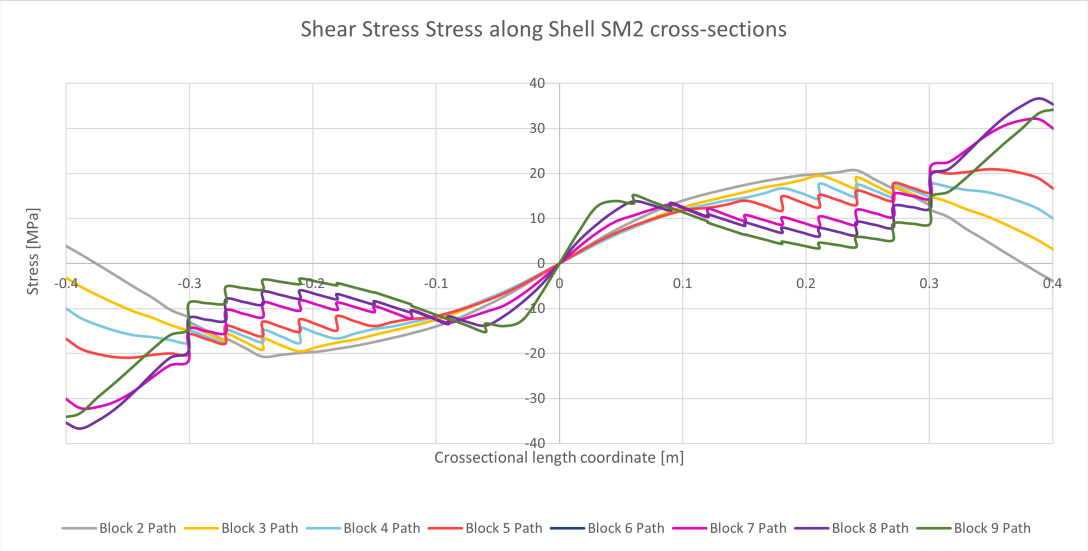

Figure C.3: In-plane Shear Stress along Shell SM2 cross sections.

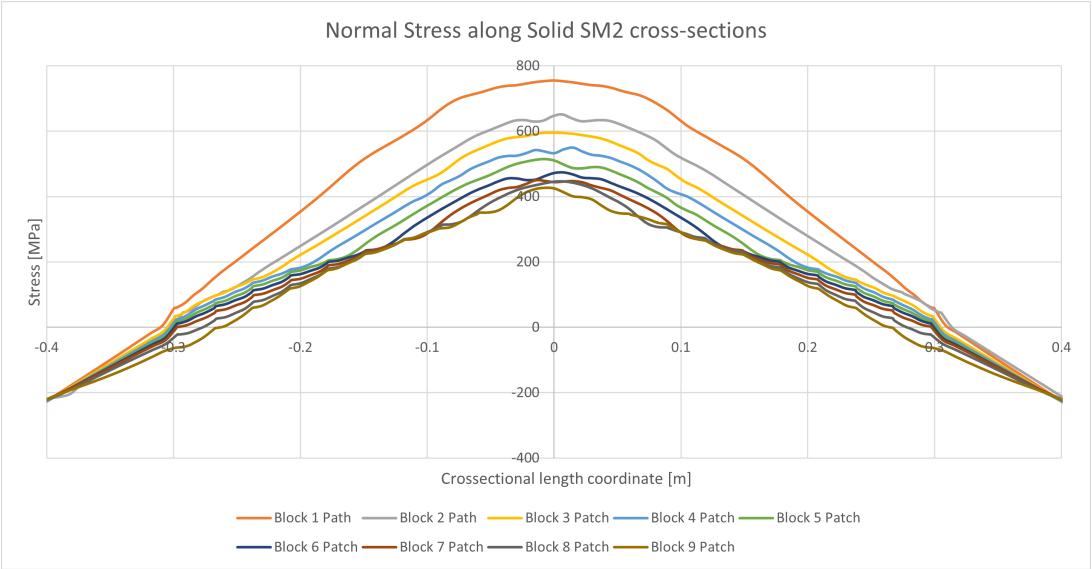

Figure C.4: Normal Stress along Solid SM1 cross sections.

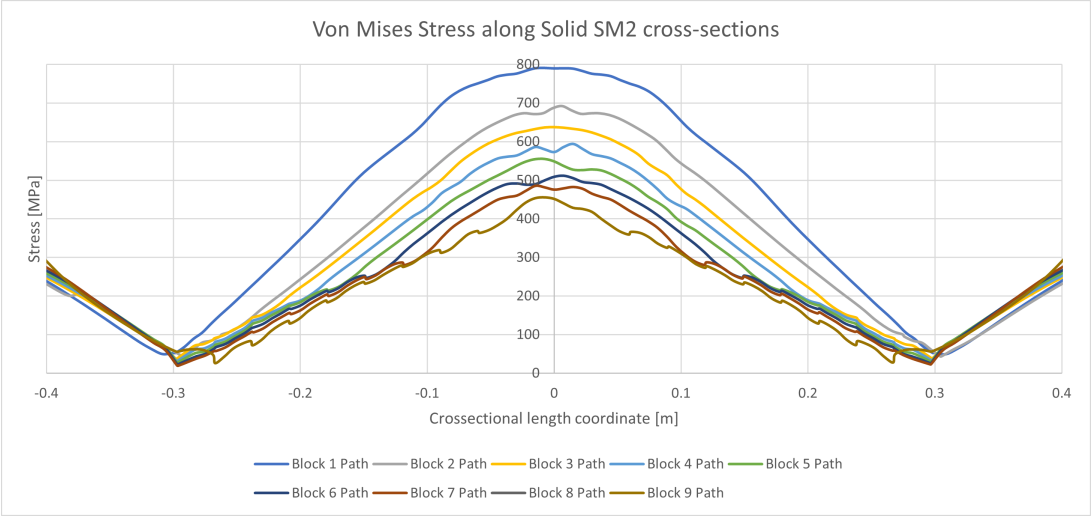

Figure C.5: Von Mises Stress along Solid SM1 cross sections.

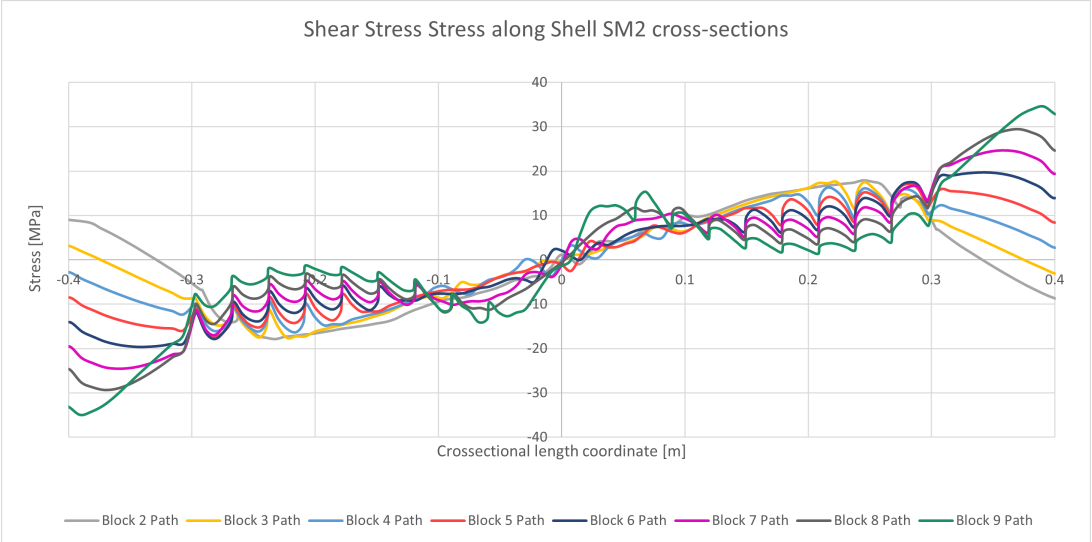

Figure C.6: In-plane Shear Stress along Solid SM2 cross sections.

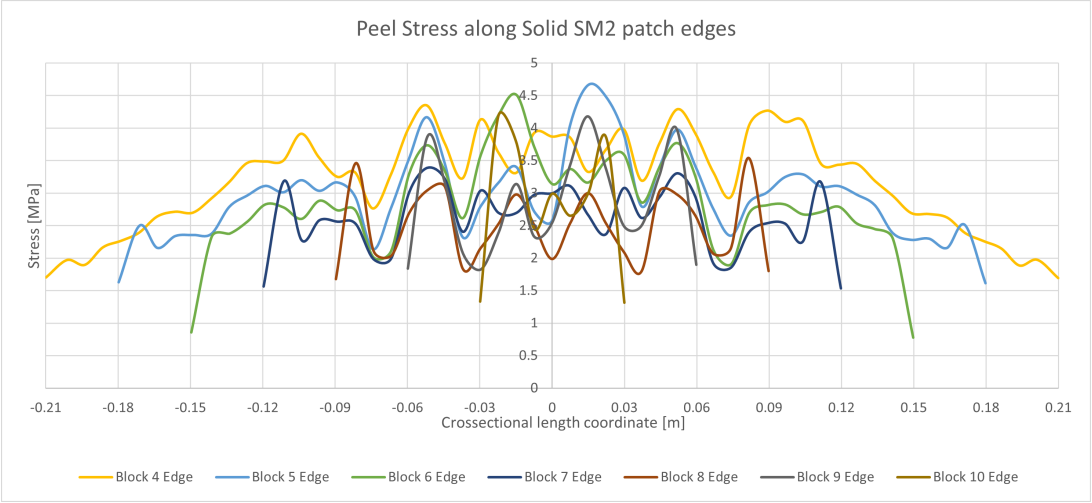

Figure C.7: Peel Stress along Solid SM2 reinforcement patch edges.

Appendix D

Mast Analysis Results - Submodel 3

The following figures regard to the results obtained for Submodel 3 (in shell and solid element) that were not presented previously, throughout the thesis.

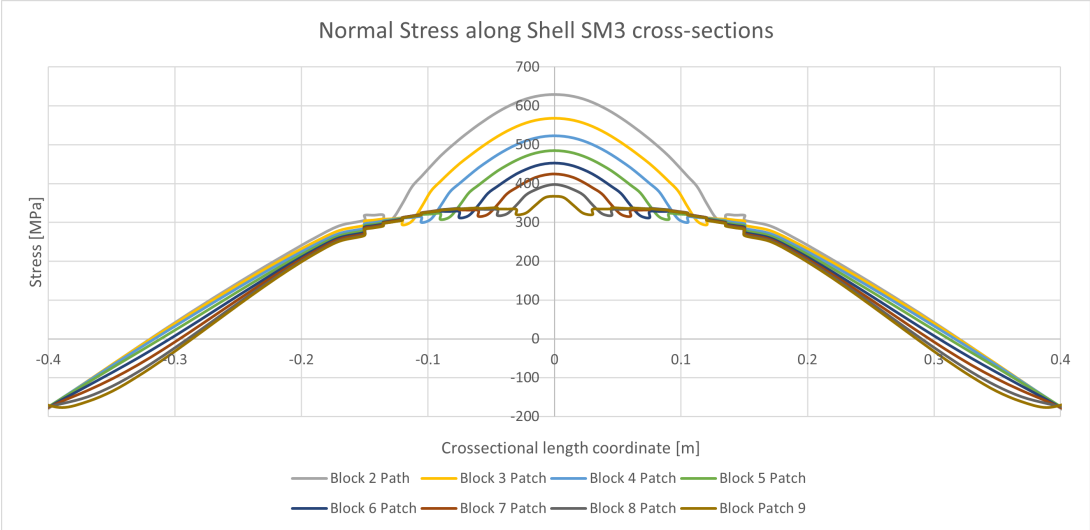

Figure D.1: Normal Stress along Shell SM3 cross sections.

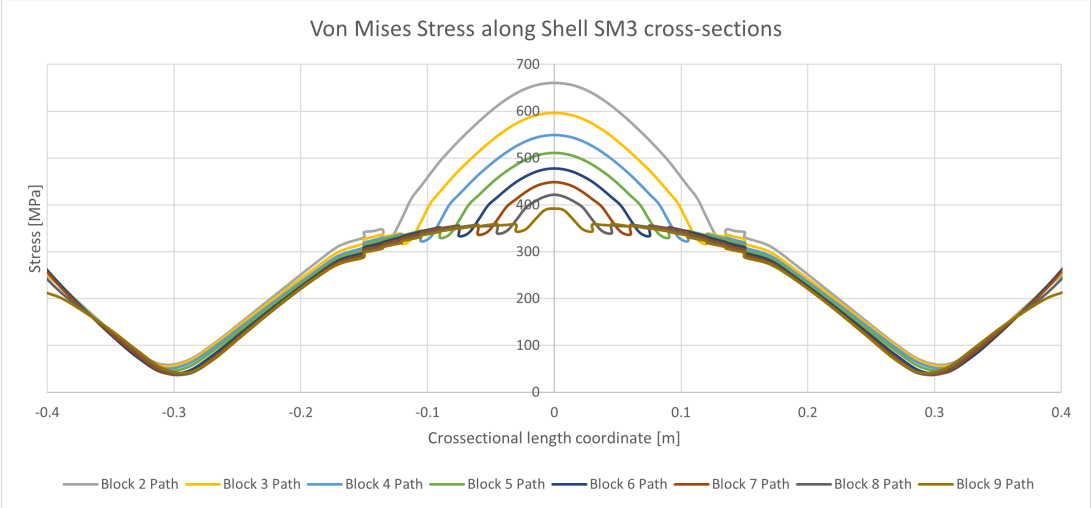

Figure D.2: Von Mises Stress along Shell SM3 cross sections.

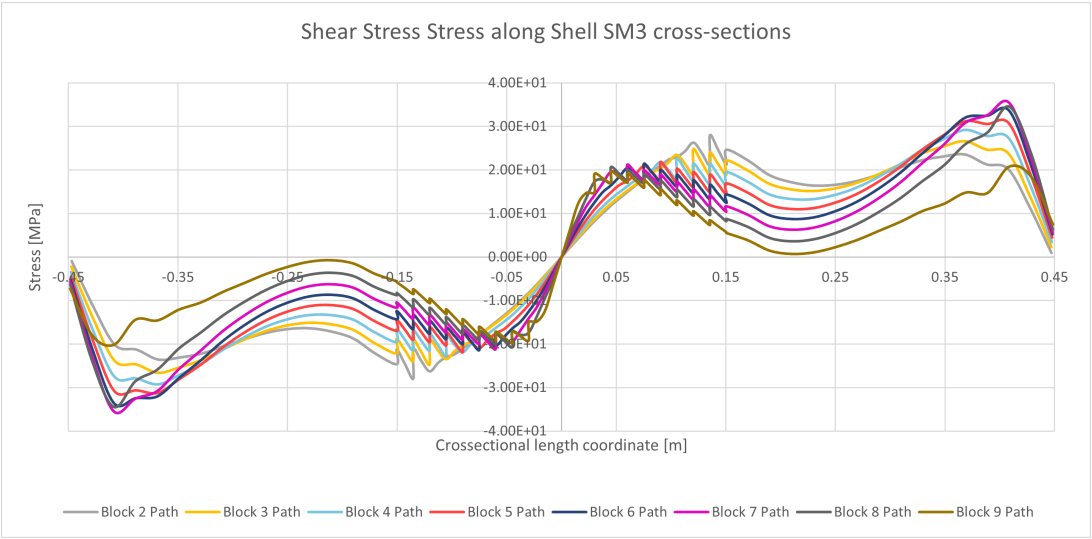

Figure D.3: In-plane Shear Stress along Shell SM3 cross sections.

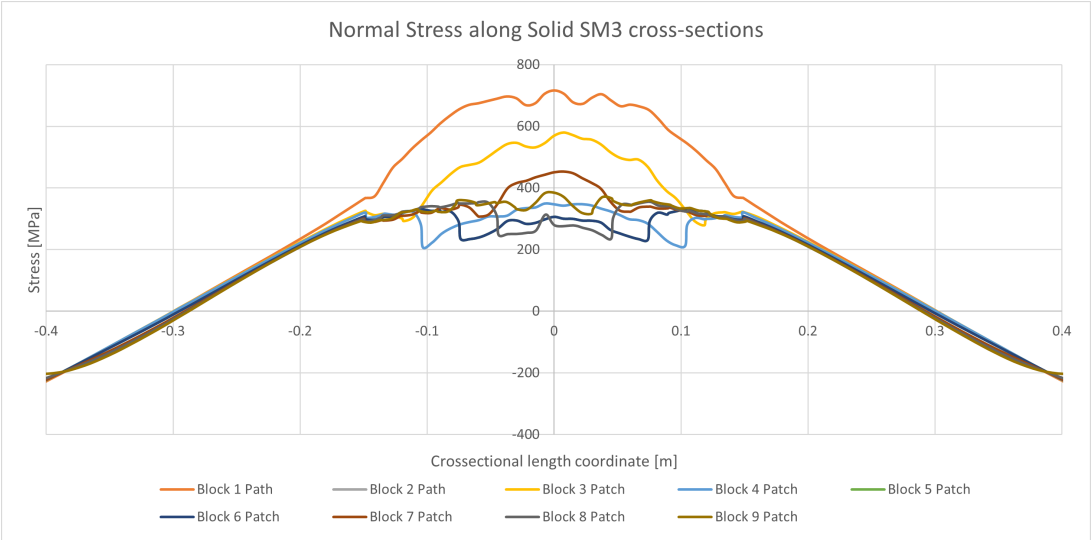

Figure D.4: Normal Stress along Solid SM1 cross sections.

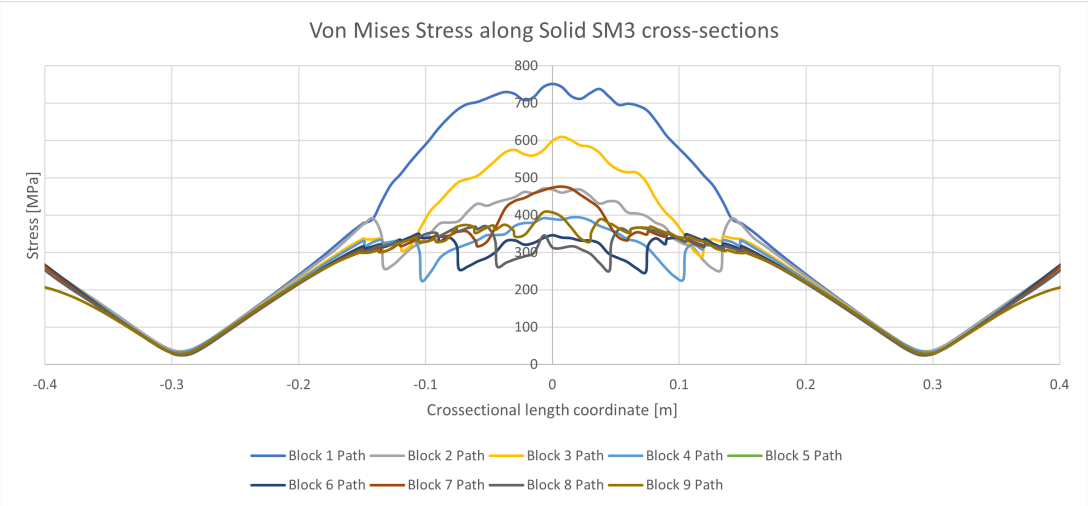

Figure D.5: Von Mises Stress along Solid SM1 cross sections.

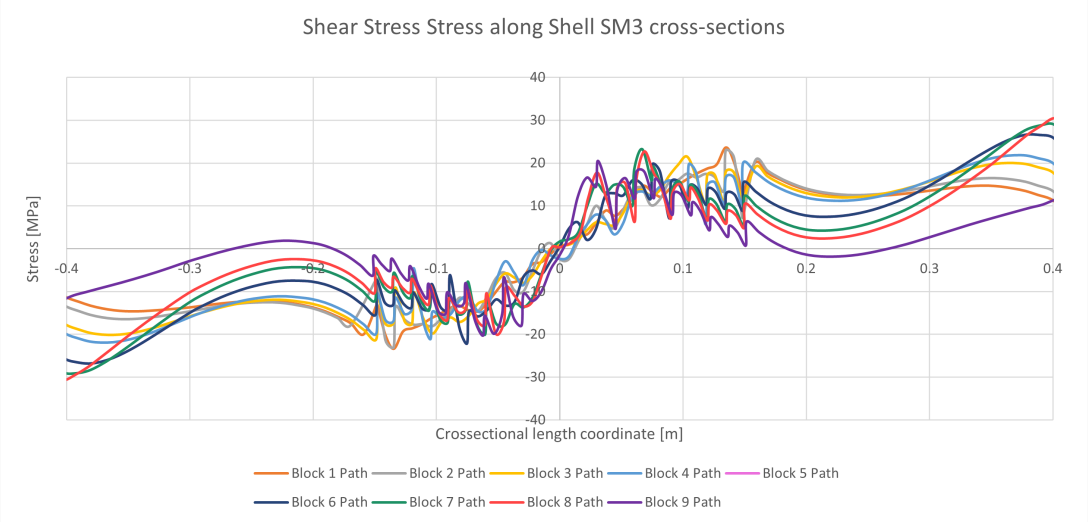

Figure D.6: In-plane Shear Stress along Solid SM3 cross sections.

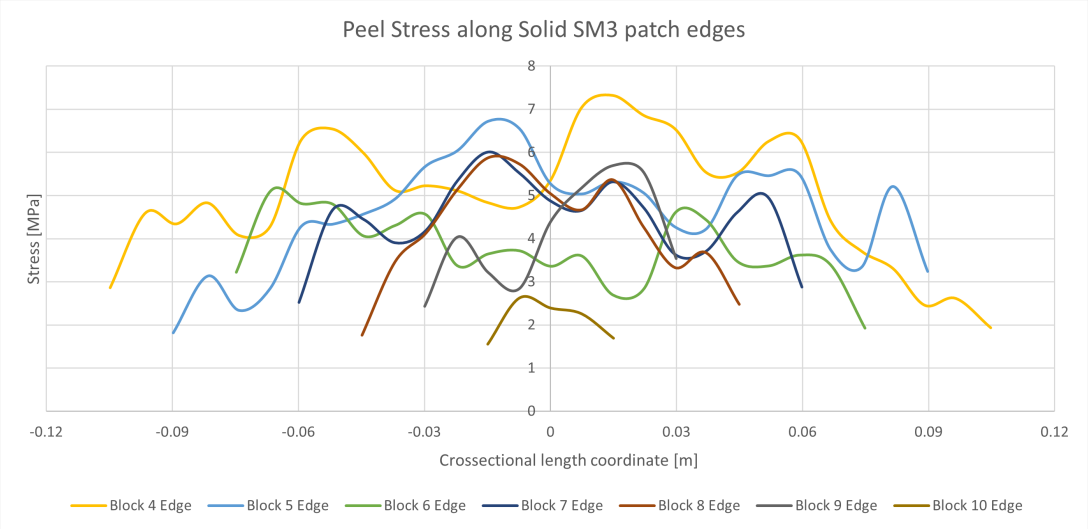

Figure D.7: Peel Stress along Solid SM3 reinforcement patch edges.